STRENGTH OF THIN-WALLED ELLIPTICAL CYLINDERS SUPPORTED AT THE MINOR AXIS

Thesis

by

Walter Lavern Howland

In Partial Fulfillment of the Requirements for the Degree of Doctor of Philosophy

California Institute of Technology

Pasadena, California

1939

SUMMARY

In this investigation it was found that the instability failure of curved sheet is nearly independent of the type of loading and is primarily a function of the maximum stress, radius-thickness ratio and modulus of elasticity. A method of correlating the critical stress of thin sheet under several different types of loading is given. An explanation for the experimental critical stress of thin walled cylinders under bending being greater than that for pure compression is given. The strength of unstiffened thin walled circular nose sections under pure bending was found to be controlled by local instability of the section, rather than a large scale instability. The equation of local instability of curved sheet gives values which are in fair agreement with those found experimentally.

The strength of elliptical cylinders supported at the minor axis under bending plus shear loads is governed primarily by the bending strength, and is little effected by the shear force unless the amount of shear is quite large with respect to the moment. The effect of increasing the amount of ellipticity greatly reduces the bending and shear strength of nose sections. Under torsional loads the stress at

buckling falls off as the ratio of the major to minor axis increases but the failure stress decreases at a slower rate than the buckling stress. The length effect of semi-circular sections under torsion is similar to that of a circular tube, and can be obtained by Donnell's theoretical equation.

ACKNOWLEDGMENT

The author wishes to express his appreciation of the assistance furnished by members of the staff of the Guggenheim Graduate School of Aeronautics at the California Institute of Technology and also of the services rendered by members of the graduate student body. In particular he wishes to thank Doctors Th. von Karman, E. E. Sechler, C. B. Millikan and A. L. Klein, for their helpful suggestions and criticisms.

The author also wishes to express his gratitude to the National Advisory Committee for Aeronautics for its support and sponsorship of the research which has made the preparation of this thesis possible.

TABLE OF CONTENTS

TABLE OF CONTENTS (cont'd)

TABLE OF FIGURES

TABLE OF FIGURES (cont'd)

TABLE OF FIGURES (cont'd)

TABLE OF FIGURES (cont'd)

LIST OF TABLES

LIST OF TABLES (cont'd)

I. INTRODUCTION

Interest in the strength of thin sheet metal in relation to aircraft construction first arose from the substitution of such metal for fabric as a covering material for braced frame structures. This substitution naturally resulted in an increase of weight because the metal was heavier than the fabric. In order to obtain some compensation for this increase, attempts were made to utilize some of the strength of the metal panels by the omission or modification of other structural parts.

One of the first successful endeavors to manufacture all-metal planes was in Germany. The airplane branch of the Zeppelin Works at Lindau, later known as the "Dornier-Metallbauten," which had the advantage of the experience of the Zeppelin Works in the use of the light-weight metal duralumin, built an all-metal plane on entirely new principles of construction under the direction of Professor Junkers. Up to that time essentially the sole purpose of airplane wing coverings was to provide a certain wing shape and also a surface for maintaining the supporting air pressure. Junkers made the external fairing of the wings of metal and, at the same time, combined it with the internal supporting structures so as to form a strong integral supporting body. Thus the increase of weight of the metal fairing over a cloth covering was at least partially compensated for in modified internal structure.

The art of working with thin-sheet metal has progressed greatly since the first all-metal airplane. However, calculations at the present time, pertaining to the strength of modern stressed skin construction, consist of a combination of simplifying assumptions, simplified versions of the complex thin sheet theory, empirical equations from test results, and a disturbing amount of guesswork. The object of this thesis is to attempt to decrease the amount of guesswork required in designing thin curved sheets, by presenting,

a. A theory for correlating the critical stress of curved sheets under various combined loads.

b. A theory for the strength of thin-walled elliptical cylinders supported at the minor axis.

c. Experimental work on the strength of thin-walled elliptical cylinders supported at the minor axis.

This thesis is the direct result of an investigation which started in 1936 at the Guggenheim Aeronautical Laboratory, under the sponsorship and support of the National Advisory Committee for Aeronautics. Many of the ideas presented were developed during the study of existing literature on curved sheets.

II. TOTAL STRESS THEORY

In general, shear stresses can arise in three different manners, First, by direct shear, such as the vertical load on a cantilever beam, second, as an induced shear caused by direct stress or change in direct stress such as the diagonal shear in an element under direct stress, and finally, by pure torsion.

A fuselage or a wing nose section may be, and usually is, subjected to bending and direct shear in either or both of the vertical and horizontal planes. In addition, torsional loads are resisted, especially in the case of the nose section. This means that, in the case of a nose section, the curved sheet may have shear stresses which originate from five different sources, First, direct shear due to lift, second, induced shear due to normal stresses from the bending moment in the vertical plane, third, direct shear due to drag, fourth, induced shear due to normal stresses from the bending moment in the horizontal plane, and fifth, torsion. Some of these stresses may be quite small, but nevertheless are present. One of the interesting loading conditions for the nose section of a single spar wing occurs when the flaps are down, resulting in a large lift, large drag, and large moment.

BENDING

We will start first with pure bending. If it is assumed that the ordinary beam theory applies, then

$$\sigma_x = \frac{My}{I} \qquad \sigma_y = 0 \tag{1}$$

where σ_x = stress in x-direction, lbs./sq.in.,

M = moment, in.-lbs.,

y = distance in y-direction to fiber, in.,

I = moment of inertia, in.^{4}.

Since the maximum value of the unit shearing stress at a point in a stressed body is one-half the algebraic difference of the maximum and minimum principal unit-stresses, that is

τ_{max} = maximum shearing stress = 1/2 ($\sigma_{max} - \sigma_{min}$)

then, (2)

$$\tau = \frac{1}{2}\sigma_x = \frac{1}{2}\frac{My}{I}$$

for a thin-walled circular cylinder, we get

$$y = r \sin\theta \qquad I = \pi r^3 t$$

$$\sigma = \frac{M \sin\theta}{\pi r^2 t} \qquad \tau = \frac{M \sin\theta}{2\pi r^2 t} \tag{3}$$

or $\sigma_{MAX} = \frac{M}{\pi r^2 t}$ and $\tau_{MAX} = \frac{M}{2\pi r^2 t}$ (4)

See Fig. 1.

This is a very simple result, but it gives the maximum shear stress which a tube must resist in order to carry

a certain bending moment. The dotted curve in Fig. 6 shows the curve obtained by applying the above equation to data found in N.A.C.A. Tech. Note 479. (1)

TORSION

Next we will deal with pure torsion. If it is assumed that, before buckling occurs, Batho's expression holds, then, as long as the sheet thickness is constant, the shear stress due to torsion is approximately equal to

$$\tau = \frac{M_t}{2At} \qquad (5)$$

where M_t = torque, in.-lbs.,

A = area enclosed, sq.in.,

t = thickness, in.

Considerable work has been done on pure torsion of thin-walled cylindrical members, proving the correctness of the above equation, so that no further consideration of this case is necessary. (Ref. 4.)

DIRECT SHEAR AND BENDING

The next case to consider is that of direct shear plus bending moment. This case was treated in N.A.C.A. Tech. Note 523, (2) However, the author would like to make some additions to the work of Lundquist in this Tech. Note.

The standard equations for combined plane stresses are,

$$\sigma_{MAX} = \frac{\sigma_x + \sigma_y}{2} + \sqrt{\frac{(\sigma_x - \sigma_y)^2}{4} + \tau_{xy}^2} \qquad (6)$$

$$\tau_{MAX} = \pm \sqrt{\frac{(\sigma_x - \sigma_y)^2}{4} + \tau_{xy}^2} \qquad (7)$$

$$TAN\ 2\psi = \frac{2\tau_{xy}}{(\sigma_x - \sigma_y)} \qquad (8)$$

If it is again assumed that the ordinary beam theory applies,

then

$$\sigma_x = \frac{My}{I} \qquad \sigma_y = 0 \qquad (9)$$

and

$$\tau_{xy} = \frac{F\bar{y}A'}{I\,b} = \frac{1}{I}\int \frac{dM}{dX}\,\frac{y}{b}\,dA \qquad (10)$$

where τ_{xy} = horizontal shear,

F = shear force, lbs.,

$\bar{y}$ = distance from neutral axis to center of gravity of area A', in.,

A' = area above y, sq.in.,

b = total thickness under horizontal shear at a particular section y.

Thus,

$$\sigma_{MAX} = \frac{My}{2I} + \sqrt{\frac{M^2y^2}{4I^2} + \frac{F^2\bar{y}^2A'^2}{I^2b^2}} \qquad (11)$$

$$\tau_{MAX} = \pm \sqrt{\frac{M^2y^2}{4I^2} + \frac{F^2\bar{y}^2A'^2}{I^2b^2}} \qquad (12)$$

$$TAN\ 2\psi = \frac{2F\bar{y}A'}{Mby} \qquad (13)$$

For a thin-walled circular cylinder (see Fig. 2), we get,

$$\sigma = \frac{M \sin\theta}{\pi r^2 t} \qquad y = r \sin\theta \qquad I = \pi r^3 t \tag{14}$$

$$\tau = \frac{F \cos\theta}{\pi r t} \qquad A' = (\pi - 2\theta) r t \qquad \bar{y} = \frac{r \cos\theta}{\left(\frac{\pi}{2} - \theta\right)} \tag{15}$$

$$\tan 2\psi = \frac{2 F r \cos\theta}{M \sin\theta} \qquad b = 2t \tag{16}$$

Let us use the parameter M/Fr found by Lundquist. By letting $\lambda = \frac{M}{Fr}$ we obtain;

$$\sigma_{MAX} = \frac{M}{2\pi r^2 t}\left[\sin\theta + \frac{1}{\lambda}\sqrt{4\cos^2\theta + \lambda^2 \sin^2\theta}\right] \tag{17}$$

But the extreme fiber stress at $\theta = 90^\circ$ is equal to $\frac{M}{\pi r^2 t}$. Therefore, we have,

$$\frac{\sigma_{MAX}}{\sigma_{\theta=90^\circ}} = \frac{\sin\theta}{2} + \frac{1}{2\lambda}\sqrt{4\cos^2\theta + \lambda^2 \sin^2\theta} \tag{18}$$

The plot of this ratio against θ for different values of λ is seen in Fig. 3.

From these curves it is seen that the maximum compressive stress occurs at $\theta = 90^\circ$ for values of λ greater than 1.0, and near to $\theta = 0^\circ$ for λ less than 1.0. It is interesting to note that for λ greater than 1.0 the maximum compressive stress is always at the top, (that is

at $\theta = 90°$, where the ratio $\sigma_{max}/\sigma_{\theta = 90°} = 1.0$) for one would naively think it would approach the top as λ become larger and larger. It is readily seen from this Fig. that for large values of shear the tube is critical near the neutral axis and not at the top.

SOLUTION FOR MAXIMUM SHEAR

From Eq. (12) we obtain,

$$\tau_{MAX} = \sqrt{\frac{M^2 \sin^2\theta}{4\pi^2 r^4 t^2} + \frac{F^2 \cos^2\theta}{\pi^2 r^2 t^2}} \qquad (19)$$

$$= \frac{F}{2\pi r t}\sqrt{\lambda^2 \sin^2\theta + 4\cos^2\theta}$$

Here we see that

$$\tau_{AVERAGE} = \frac{F}{2\pi r t} \qquad (20)$$

$$\frac{\tau_{MAX}}{\tau_{AVERAGE}} = \sqrt{\lambda^2 \sin^2\theta + 4\cos^2\theta} \qquad (21)$$

Fig. 4 shows a plot of $\tau_{max}/\tau_{average}$ as a function of θ for various values of λ. Here we obtain the result that for a value of λ less than 2 the maximum ratio of $\tau_{max}/\tau_{average}$ occurs at $\theta = 0°$ and has a value of 2, but for values of λ greater than 2 the ratio of $\tau_{max}/\tau_{average}$ is equal to λ or M/Fr

and occurs at $\theta^{\circ} = 90^{\circ}$. Fig. 5 shows a plot of the angle of maximum shear stress to the axis of the tube. Equation 16 was used in order to obtain these curves. This Fig. shows, as one would expect, that the angle of maximum shear is 0° at $\theta = 0^{\circ}$ and 45° at $\theta = 90^{\circ}$ for all values of λ. In order to obtain the angle of maximum compressive stress add 135° to ψ'.

To investigate how τ max. varied with different types of loading, all of the test specimens in N.A.C.A. Tech. Note 523 (2) were computed. (See Table 1.) Fig. 7 shows a very interesting result obtained from this data, namely that the maximum shear stress which the cylinders will resist is independant of the ratio of the moment to the vertical shear. In this Fig. it is seen that the ratio of $\frac{M}{Fr}$ changes by a factor of eight and the maximum variation of the shear stress from an average is less than 17% even with a considerable variation in R/t. Fig. 6 shows a plot of τ max against R/t obtained from the above mentioned data. The material used in these tests was duralumin (17ST). The three solid curves were faired through the points in order to obtain an approximation of variation. There seems to be a definite variation with L/R and the reason for this can be, at least in part, explained by the support effect of the ends. The points plotted represent the failing stress. On circular tubes, however, the buckling stress

and failing stress are almost exactly the same. The maximum allowable shear stress in combined bending and shear agrees very satisfactorily with that of bending alone, (the dotted curve in Fig. 6). This curve was obtained from material found in N.A.C.A. Tech. Note. 479 (1.)

If we calculate the theoretical curves for the torsion buckling stress of duralumin tubes as a function of the radius to thickness ratio by Donnell's equations 3), we obtain the curves seen in Fig. 8. The experimental points are the same as those in Fig. 6 and show a remarkable agreement with Donnell's theoretical equation. However, one must realize that the stress patterns in the test specimens were entirely different from those assumed in deriving Donnell's theory. We can say that the experimental points represent the maximum shearing stress at any point in the specimen at failure, and the theoretical curves are for the case where every point on the specimen is at that stress. It is very unfortunate that at L/r's equal to 0.5 and 2.0, not enough variation of r/t was taken to check the curves, but it appears, as one would expect, that Donnell's torsion equation gives a larger variation with length than would be expected in this type of loading.

TORSION PLUS BENDING AND SHEAR

If a particular member is subjected to a given bending moment and sheer, then it has a definite maximum combined shearing stress. Now, if we also apply torsion to the member, the circumferential shear increases (assume that there were no waves before applying the torsion).

Thus we get,

$$\sigma_x = \frac{My}{I} \qquad \tau_{xy} = \frac{F\bar{y}A'}{Ib} + \frac{M_t}{2At} \tag{22}$$

and

$$\sigma_{MAX} = \frac{My}{I} + \sqrt{\frac{M^2y^2}{4I^2} + \left(\frac{F\bar{y}A'}{Ib} + \frac{M_t}{2At}\right)^2} \tag{23}$$

$$\tau_{MAX} = \pm\sqrt{\frac{M^2y^2}{4I^2} + \left(\frac{F\bar{y}A'}{Ib} + \frac{M_t}{2At}\right)^2} \tag{24}$$

The author has been unable to find experimental results with which to substitute in the above equations, however, if we assume in the above equations that we have no shear force, that is the case of pure bending plus torsion, then we get from Eq. (24)

$$\tau_{MAX}^2 = \left(\frac{My}{2I}\right)^2 + \left(\frac{M_t}{2At}\right)^2 \tag{25}$$

This equation actually checks, within an average variation of ±4.8% and a maximum variation of 11.7%, the experimental results of Air Corps Information Circular No. 669, on circular steel tubes. See table II.

A slight modification of the above equation can be developed in the following manner,

$$1 = \left(\frac{\frac{My}{2I}}{\tau_{MAX}}\right)^2 + \left(\frac{\frac{Mt}{2At}}{\tau_{MAX}}\right)^2 \qquad (26)$$

but $$\frac{My}{2I} = \tau_{BENDING} \quad \text{AND} \quad \frac{Mt}{2At} = \tau_{TORSION}$$

therefore, $$1 = \left(\frac{\tau_B}{\tau_{MAX}}\right)^2 + \left(\frac{\tau_T}{\tau_{MAX}}\right)^2 \qquad (27)$$

By first setting $\tau_T = 0$, and then $\tau_B = 0$, we find that

$$1 = \left(\frac{\tau_B}{\tau_{MAX\,(BENDING)}}\right)^2 + \left(\frac{\tau_T}{\tau_{MAX\,(TORSION)}}\right)^2 \qquad (28)$$

Discussion on Maximum Allowable Shear Stress

From this investigation so far it is seen that, at least for two different combined loading conditions, bending plus vertical shear and bending plus torsion, the critical shearing stress of a curved sheet is primarily a function of the total maximum shearing stress and the r/t ratio. A secondary parameter is the length divided by the radius.

The curves shown in Fig. (6) represent the maximum

allowable shear stress for dural sheets at various ratios of r/t. It also shows agreement between pure bending and bending plus shear. For a given r/t these curves give probably the maximum obtainable values, because actually the shear value holds only for a point on the curved sheet. If these curves do give the maximum allowable shear stress then there should be some correlation between these curves and the results of pure compression tests, since compression stresses create a shear stress at 45° to its direction.
It is not to be understood that the shear stresses are the ones which create failure, for undoubtedly the direct stresses play the more important part. The reason for dealing principably with the maximum shearing stresses instead of the maximum direct stresses is that this research was primarily interested in determining the maximum allowable shearing stress for airplane design purposes. It is really immaterial whether one deals with maximum shear stress or maximum direct stress as long as one is consistent. ($\sigma_{max} = 2\tau_{max} + \sigma_{min}$ sometimes σ_{min} equals zero which makes the transformation from one to the other very simple)

From a general result standpoint, Fig. 6 tends to show that the instability failure of curved sheet is nearly independent of the type of loading (that is, stress

distribution), and only a function of the maximum stress, radius-thickness ratio and modulus of elasticity. This result at first sight appears to be in contradiction with the findings of Lundquist and Donnell. Lundquist suggests from his experimental points (see Fig. 9) that the maximum compression stress on the extreme fiber at failure σ_B in a thin-walled cylinder subjected to pure bending is from 1.3 to 1.8 times the maximum compressive stress at failure if the cylinder is subjected to pure compression, and Donnell recommends a ratio of 1.4. In Figs. 9 and 10 are plotted Lundquist's and Donnell's results, and there appears to be a definite difference between σ_B and σ_c. However, a large amount of this difference can be accounted for by other reasons than a definite difference in the maximum stress that the curved sheet will resist.

First, on an average the compression points will be lower than the bending because pure compression is a much more severe type of loading from the standpoint of effect of initial irregularities or eccentricities. In a somewhat mathematical form, we can say that the pure compression values are affected by the summation of all initial irregularities such as variation in radius, thickness, eccentricity of loading and any

initial stresses. The author's experience with failure of curved sheet definitely bears out the above statement. In the case of pure bending, the maximum stress only acts on a comparatively small portion of the total area, thus the number of irregularities affecting the stress pattern must physically be less. In addition, the specimens must have a joint in them if they are made of very thin material, in which case the joint can be placed in the bending test such that it does not affect the strength of the specimen, however, in the case of pure compression, it must be at as high a stress as the rest of the specimen. This may or may not lower the maximum failing stress, but it is much more apt to lower it than to raise it.

A second reason, of more theoretical significance, for the compression points to be lower than those for bending is that the bending stress is calculated on the basis of the original cross-section. Since several men (Brazier [5] Chwalla [6], and Heck [7]), have pointed out that the strain of the cross-section of thin walled tubes under pure bending is not negligible, the calculation of the maximum bending stress based on the original section is in error. The strain or deflection (flattening of the section) forces a circular cylinder into approximately a ellipse. (Chwalla [6]). If we make the assumption that the cylinder is always of elliptical

form with a circumference equal to that of the original circle, (that is inextensional deformation) then the change in section — modulus is given in Fig. 11. This figure shows that the section-modulus decreases if the cross-section flattens, therefore the actual fiber stress would be less then the calculated stress based on the original dimensions of the cylinder.

The only remaining unknown is how much flattening takes place under pure bending. N.J. Hoff(8.) by the use of the energy method found an expression for the amount of flattening which gives the minimum energy. This expression is

$$\left(\frac{w}{r}\right)_{MAX} = \left(\frac{r}{t}\right)^2 \left(\frac{\sigma_{MAX}}{E}\right)^2 \qquad (29)$$

where w = radial deflection

r = original radius of cylinder

σ_{max} = maximum fiber stress.

If the cylinder is very short the above expression does not hold valid, since the length effect is not present. For lack of a better equation or experimental data, equation (29) was used in order to secure the approximate size of the correction which must be applied to pure bending tests of circular cylinders. The results of calculating $\frac{w}{r}$ from eq. (29) and picking off the value of Z/Z_o from Fig. 11. for Lundquist's bending tests

are seen in table III and plotted in Fig. 12.

Fig. 12 shows that this correction brings the results of bending and compression tests closer together and it also makes the curve from combined stress data ($\frac{L}{r} = 1.0$) more nearly the upper limit of the experimental points. If the first reason for the bending values tending to be higher than the compression is now taken into consideration, it seems logical to make the statement that the instabilility failure of curved sheet is nearly independent of the type of loading (that is, stress distribution), and only a function of the maximum stress, radius-thickness ratio and modulus of elasticity. In some cases in which the author has been unable to carefully study, it may be necessary to take into account the angle between the maximum compressive stress and the axis of principal curvature in order to obtain the "effective radius-thickness ratio."

III THE STABILITY OF UNSTIFFENED CURVED NOSE SECTIONS UNDER PURE BENDING

The theoretical critical stress of cylindrical shells has been investigated by several men. Prandtl[9] showed that the general application of Navier's simple bending theory to thin-walled beams is no longer permissible because of the possibly large strain of the section under load. The bending of curved thin-walled pipes was investigated by von Karman [10] but his results do not apply to straight pipes. The first to study the pure bending of infinitely long isotropic circular cylindrical shells was Brazier [5]. He showed that the bending moment does not increase linearly with the curvature of the shell axis and that it assumes a maximum (critical) value for a certain curvature of the shell axis, for greater curvature the system is no longer stable. His value of the critical stress is,

$$\sigma_{(critical)} = .329\, E\, \frac{t}{r} \qquad (30)$$

where E = Young's modulus lbs/sq.in.
t = thickness ins.
r = radius ins.

Brazier arrives at this result by neglecting the higher powers of the displacement components v and w relative to the first power of these quantities, and by solving exactly the resulting differential equation.
(where w is the normal displacement and v the tangential)

Chwalla [6] obtains a solution of the same problem by

using an energy method and assuming an arbitrary elliptical deformation, such that the circumference of the cross section remains constant and equal to the circumference of the undeformed shell, regardless of the magnitude of the strain. His value of the critical stress is,

$$\sigma_{(critical)} = .379\, E\, \frac{t}{r} \qquad (31)$$

It is interesting to note here that Chwalla has attempted to develop a large deflection theory and it is only 15% different from Brazier's equation.

Heck [7] made an extension of the Brazier and Chwalla results to the case of elliptical cylinders in pure bending. He arrives at a solution by an energy method after neglecting higher powers of the deflection components v and w and their derivatives relative to the first powers of these quantities. As a result of these simplifications the validity of his formula is confined to relatively small values of v and w. Heck's equation checks Brazier's when the two axes of the ellipse are equal. A few experimental tests on elliptical cylinders bent about either the major or minor axis check his results quite closely.

None of the previous investigators of cylindrical shells have considered a case which approximates a nose section of an airplane wing. In the rest of this thesis thin-walled elliptical cylinders supported at the minor axis will be refered to as nose-sections. It is the object of the present investigation to make a preliminary analysis of this type of section.

One of the simplest cases which could first be considered is that of a cylindrical half circular shell supported at the top and bottom and under the action of pure bending. See Fig. (A)

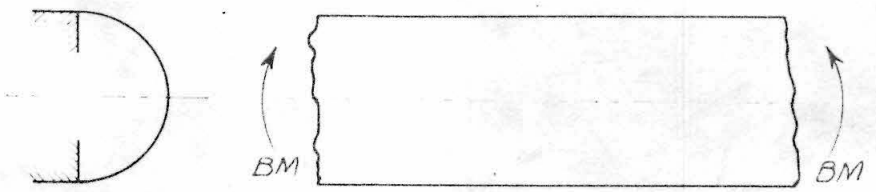

Fig. A.

The supports at the top and bottom simulate beam caps in an actual wing. It is at once apparent that this problem is quite different from that of Brazier's or Heck's for the support to the tube is greatest where the stress is largest.

The most difficult part of any stability problem is the determination of the form of the deflection and the present problem is no exception. Several methods of obtaining the form of the deflection of such a section were tried but all failed. Finally the idea of external pressure was conceived from Brazier's paper.

If a curved sheet is strained in bending by end-moments (BM) (no shear forces) and we consider an element cut out of the state of equilibrium occuring after bending, we see that the resultant forces Fc, F_T of the bending moment have a resultant pressure P which tends

to compress the element perpendicular to its axis.

See Fig. B.

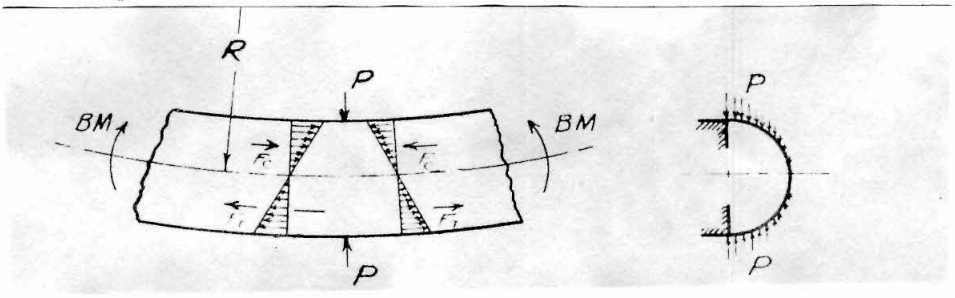

Fig. B.

In a solid cross section this transversal pressure is absorbed without noticeable deformations of the cross section and therefore is an unimportant factor in bending strength. However with thin walled hollow profiles there results a decrease in bending stiffness which produces an increase of the curvature of the axis--consquently a further increase of the transversal pressure.

If a fiber in the axial direction is considered as a part of a hoop with a radius of R and an internal pressure P_i , the following equation is obtained,

$$\sigma = \frac{P_i R}{t} \tag{32}$$

From the usual approximation for the curvature of the deflection curve.

$$\frac{d^2y}{dx^2} = \frac{1}{R} = \frac{M}{EI} \tag{33}$$

But

$$\sigma = \frac{My}{I} = \frac{Mr\sin\theta}{I} \tag{34}$$

Substituting eq. (32) in. eq. (34) and using the relationship of eq. (33),

$$\frac{P_i R}{t} = \frac{Mr}{I} \sin\theta \tag{35}$$

or

$$P_i = \frac{E}{R^2} rt \sin\theta \tag{36}$$

This is the equation of the loading on the cross-section as a function of θ and r. It represents a vertical force down on the top side and up on the bottom. In order to convert this to a pressure normal to the shell surface we must multiply it by $\sin\theta$.

Thus,

$$P = \frac{E}{R^2} rt \sin^2\theta \tag{37}$$

The problem of deflection can now be approached from the standpoint of a infinite tube under an external pressure of the form of equation (37). See Fig. 13. Dividing the tube in half, and applying the neccessary forces we have Fig. C.

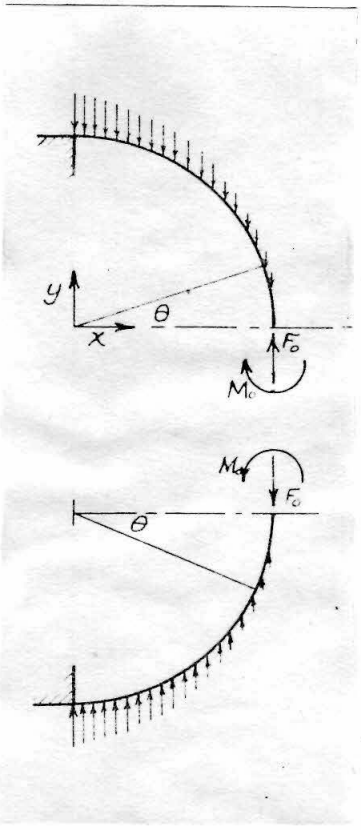

FIG. C.

If P_i is positive when acting down and bending moment is positive when the compression side is inside of the shell, then the moment at any point c is equal to

$$M_c = M_o + \int_{X_c}^{r} P_i\,(X - X_c)\,dX - F_o\,(r - X_c) \qquad (38)$$

Since $X = r\cos\theta$, then

$dX = -r\sin\theta\,d\theta + \cos\theta\,dr$

if dr is assumed to be very small

then $dX = -r\sin\theta\,d\theta$.

Substituting in eq. (38), integrating and collecting, the moment at any point is equal to

$$M_\theta = M_o - F_o\,r(1-\cos\theta) + \frac{E\,r^3 t}{12R^2}\left[4\sin^3\theta - 6\theta\cos\theta + 6\sin\theta\cos^2\theta\right] \qquad (39)$$

For a long circular shell the differential equation for the deflection normal to the surface (w) in terms of bending moment per unit length of the shell is,

$$\frac{d^2w}{d\theta^2} + w = -\frac{12(1-\mu^2)M r_o^2}{E t^3} \qquad (40)$$

Substituting in the above expression for the bending moment [eq. (39)], the differential equation of the deflection curve becomes,

$$\frac{d^2w}{d\theta^2} + w = -\frac{12(1-\mu^2)r^2}{E t^3}\left[M_o - F_o\,r\,(1-\cos\theta) + \frac{E r^3 t}{12R^2}\left(4\sin^3\theta - 6\theta\cos\theta + 6\sin\theta\cos^2\theta\right)\right] \qquad (41)$$

To be consistent with the assumption that dr is very small, then w, must be small in comparison with r. The above differential equation holds exactly if this condition is satisfied.

Equation (41) can be solved by the method of variation of parameters. After collecting and simplifying, the solution becomes,

$$w = C_1 \sin\theta + C_2 \cos\theta - \frac{12(1-\mu^2)r^2 M_o}{E t^3} + \frac{12(1-\mu^2)r^3}{E t^3} F_o \left(1 - \frac{\theta}{2}\sin\theta\right) - \frac{(1-\mu^2)r^5}{4t^2R^2}\left[(9-6\theta^2)\sin\theta - (16+15\theta)\cos\theta + 7\sin\theta\cos^2\theta + 48\cos^3\theta - 4\sin\theta\cos^4\theta - 32\cos^5\theta\right] \quad (42)$$

This is the general solution of equation (41), and it is seen that there are four unknowns C_1, C_2, Mo, and Fo. So far nothing has been said about the tangential deflection v. Since it has been noticed that in the case of bending thin rings the displacements due to extension of the center line of a ring are very small in comparison with the displacement due to bending, the former usually can be neglected. Thus the condition of inextensional deformation of a unit length tube can be assumed to hold. The equation for this condition according to Timoshenko [11] is,

$$\frac{dv}{d\theta} - w = 0 \quad (43)$$

Substituting in the value of w from eq. (42) integrating, collecting and simplifying, the general

equation for v becomes,

$$V = C_3 - C_1 \cos\theta + C_2 \sin\theta - \frac{12(1-\mu^2)r^2 M_o \theta}{E t^3} + \frac{12(1-\mu^2)r^3 F_o}{E t^3}\left(\theta - \frac{1}{2}\sin\theta + \frac{\theta}{2}\cos\theta\right) - \frac{(1-\mu^2)r^5}{4t^2R^2}\left[\left(-\frac{16}{15} - 27\theta\right)\sin\theta + \left(-36 + 6\theta^2\right)\cos\theta + \frac{112}{15}\sin\theta\cos^2\theta - \frac{7}{3}\cos^3\theta - \frac{32}{5}\sin\theta\cos^4\theta + \frac{4}{5}\cos^5\theta\right] \quad (44)$$

It is now apparent that there are five unknowns C_1 , C_2 , C_3 , Mo, and Fo, which must be evaluated by boundary conditions.

Upon examination of Fig. 13 the following boundary conditions are discovered,

(a) $w = 0$ at $\theta = \frac{\pi}{2}$ due to supporting action of beam cap,

(b) $\frac{dw}{d\theta} = 0$ at $\theta = \frac{\pi}{2}$ due to fixed end condition,

(c) $\frac{dw}{d\theta} = 0$ at $\theta = 0°$ due to symmetry, (45)

(d) $v = 0$ at $\theta = 0°$ due to symmetry,

(e) $v = 0$ at $\theta = \frac{\pi}{2}$ due to supporting action of beam cap.

Substituting these conditions in eq's. (42), and (44), five equations are obtained which when solved simultaneously give the following values for C_1 , C_2 , C_3 , Mo, and Fo,

$$C_1 = -\frac{3}{4}\frac{(1-\mu^2)r^5}{t^2R^2} \quad (46)$$

$$C_2 = -17.037\frac{(1-\mu^2)r^5}{t^2R^2} \quad (47)$$

$$C_3 = -10.1333 \frac{(1-\mu^2)\, r^5}{t^2 R^2} \tag{48}$$

$$M_o = .4825 \frac{E t r^3}{R^2} \tag{49}$$

$$F_o = 1.9765 \frac{E t r^2}{R^2} \tag{50}$$

Substituting these values in equation (39) and equation (42), the bending moment becomes,

$$M_\theta = \frac{E r^3 t}{R^2}\left[-\frac{3}{2} + 2\cos\theta + \frac{1}{3}\sin^3\theta - \frac{1}{2}\theta\cos\theta + \frac{1}{4}\sin 2\theta\cos\theta\right] \tag{51}$$

and the normal deflection becomes,

$$w = -\frac{(1-\mu^2)\, r^5}{4 t^2 R^2}\left[\begin{array}{l}(12 - 6\theta^2 + 47.4400)\sin\theta \\ + (52.1524 - 15\theta)\cos\theta \\ + 7\sin\theta\cos^2\theta + 48\cos^3\theta \\ - 4\sin\theta\cos^4\theta - 32\cos^5\theta \\ - 71.7139\end{array}\right] \tag{52}$$

A plot of w is seen in Fig. 13.

CALCULATION OF ENERGY

In order to determine the critical stress of the section in question the principle of minimum potential energy was tried. The assumption of infinite length eliminates any end effects. Since all sections of the shell are strained equal amounts, the analysis can be restricted to a piece of shell of unit length.

The potential energy in the shell is comprised of three parts,

(a) The energy of axial bending stored up in the length-wise elements of the shell. V_B

(b) The energy of deformation of the cross section corresponding to the strain of the shell section. V_c

(c) The energy of deformation of the overall length of the circumference of the cross-section. V_D

In general V_D will be very small and due to the assumption of inextensional deformation it will be zero in this case. Thus the total energy in the shell is equal to,

$$V_T = V_B + V_c \tag{53}$$

The general expression for the strain energy of bending is given by the equation,

$$V_B = \frac{E I}{2} \int_0^{\ell} \left(\frac{d^2y}{dx^2}\right)^2 dx \tag{54}$$

from the usual approximation for the curvature of the deflection curve,

$$\frac{d^2y}{dx^2} = \frac{1}{R} \tag{55}$$

Therefore

$$V_B = \frac{E I}{2 R^2} \tag{56}$$

This assumes that the value of I does not change much which is a consistant assumption with those made previously.

The energy of deformation of the cross section V_c is equal to

$$V_c = \int \frac{M^2 r}{2E'I}\, d\theta \tag{57}$$

Substituting in the values of E', I and the limits for the case at hand.

$$V_c = \frac{12(1-\mu^2)}{E t^3} \int_0^{\frac{\pi}{2}} M^2 r\, d\theta \tag{58}$$

Substituting in the value of the bending moment (equation (51)) integrating, collecting and simplifying, the energy becomes,

$$V_c = 5.82\, \frac{(1-\mu^2) E r^7}{t R^4} \tag{59}$$

Thus the total energy is equal to,

$$V_T = \frac{E I}{2R^2} + 5.82\, \frac{(1-\mu^2) E r^7}{t R^4} \tag{60}$$

The condition that V_T equal a minimum with respect to the radius of the axis of the section determines the magnitude of the critical bending moment. However, an inspection of the above equation shows that it has no minimum or maximum except at R equal to infinity, which corresponds to zero bending moment.

Since it was found from experiments (Table III) that a specimen built to satisfy the conditions for the above theory (accept not of infinite length) had a definite critical bending moment, then something must be wrong with the above theory. It was noticed in the experiments (which will be described in detail later) that the failure was of a very local nature.

Local Instability

In the case of local instability of thin curved sheet under compression Dr. J. E. Lipp in his Doctor's thesis[12] says, the generally accepted relation for the critical stress of thin curved sheet under compression is,

$$\sigma_{cr.} = .3\, E\, \frac{t}{r} \qquad (61)$$

The above equation is of correct theoretical form but has an empirical constant. Table III shows reasonably good agreement between this equation and experiments.

It is believed that the conclusion to be drawn from this is that semicircular nose sections fail by local instability rather than any flattening phenomenon. It is interesting that even in the case of long unsupported tubes under pure bending as those Brazier-tested[5] that local instability of the

curved sheet takes place before general flattening. This was noticed by Brazier in some tests in which he tried to verify his theory on the critical bending moment of long thin tubes under pure bending. In his paper he states that he made the tubes especially long so that end effect would not enter in. However, he went on to state that even in spite of the long length of his specimens, the cylinders failed locally before reaching a critical bending moment caused by flattening. His agreement between theory and experiments was not bad since his theory gave (see equation (30)) $\sigma_{cr} = .327 E \, t/r$ which is less than ten percent greater than the value given by the equation for local instability. (Eq. (61)) The theoretical assumption of an infinite length tube appears to give erroneous theoretical results for tubes of a reasonable finite length. The general conclusion is that the failure of semi-circular nose sections under pure bending is a result of instability in a localized area rather than a general failure involving the whole cross-section and it must be dealt with as such.

IV EXPERIMENTAL INVESTIGATION

Since no experimental results were available on the strength of wing nose sections at the beginning of this research, it was thought adviseable to spend a large part of the investigation on experimental work, for a certain amount of experimental work is necessary or desirable before satisfactory theoretical work can be done. In such an investigation it is difficult to decide just where to begin, for an airplane nose section has four main variables besides the material used. These four variables are, the thickness of the material, (t), the amount of ellipticity, (i.e. the ratio of a/b, see Fig. 14), the length or rib spacing, and the ratio of radius to thickness (R/t or b/t). In addition to these variables of dimension of the section, the load imposed on airplane nose sections may have almost any ratio of bending moment, vertical shear and torsion. The prediction at the onset of the most important factors was practically impossible so the work had to adopt an exploratory attitude.

Description of Apparatus

The requirement of any ratio of bending moment, vertical shear and torsion necessitated a special testing machine. As a result a testing machine was designed and built in which specimens could be tested

under any combination of these three types of loading. See Figs. 31, 32, and 33. The machine is comprised of a fixed face plate which is seen at the right side of Fig. 31, and a movable face plate which is fastened to a loading arm. (Center of Fig. 31.) One end of the specimen to be tested is fastened to the fixed face plate and the other to the movable one. The movable face plate and loading arm are supported by wires which hang from a knife-edged lever system causing the wires to exert a constant force independant of deflection. (i.e. vertical motion) The loading head is thereby made"floating" and cannot by itself produce loads on the specimen. The knife-edged lever system is supported by a carriage which rolls on wheels enabling the whole loading head to be moved back and forth to accommodate different length specimens. Torsion is applied by fastening a second loading arm at right angles to the one seen in Figs. 31, 32, and 33. This second arm can be fastened at different points on the first arm and it also is supported by a constant force wire. Various types of loading are obtained by placing a screw-jack at different points on the loading arm. The screw-jack acts on a dynamometer which measures the applied force. The dynamometer rests on the base of the machine to which the fixed face plate is fastened. Between the top of the screw-jack and the loading arm there is a ball joint similar to that described by Donnell[3] which eliminates the possibility of any moment being applied or resisted by the loading device.

The machine has been designed to withstand 1,000,000 in.-lbs. in bending, 1,000,000 in.-lbs. in torsion, and 50,000 lb. in direct shear, with a factor of safety of four. It is built up of large I-beams securely fastened together with three-quarter inch bolts or welds.

The pure bending tests and some of the pure torsion tests were made in a machine described by Donnell in ref. 3. This machine was also built at the California Institute of Technology and it has a capacity of 500,000 in.-lbs. in bending and torsion. The short torsion specimens were tested in a 50,000 in.-lbs. Olsen torsion testing machine. The strain measurements on some of the specimens were made with Huggenberger extensometers which have a magnification of approximately 300 times.

Description of Specimens

The specimens were elliptical in form with a beam along the minor axis. This simulates two airplane nose sections on a common beam spar and testing it as a unit. The effect of the spar was subtracted in order to obtain the load carried by the curved sheet itself. (see Fig. 14) The beam was designed so that it would not carry an appreciable shear load, however, in order to be able to go to the required stress to fail the sheet, gusset plates were necessary in the corners. These gusset plates obviously made the end portions of the test section much stiffer in shear. (see Fig. 15) After eight tests and considerable work,

it was decided that the spar would have to be eliminated, for even after a great deal of study of its effect, the influence of the spar on the behavior of the specimen was doubtful. A sample of the type of results obtained in this manner is seen in Fig. 34. The difference in deflection was measured by two dial gauges mounted as shown in Figs. 16, and 29. The method found to be the most successful after trying several different extensometer methods, was to calibrate the load in the beam alone as a function of the difference in deflection. The calibration was nearly independent of the length of the moment arm and it was assumed that the beam took the same amount of load for a given amount of deflection with or without the sheet. The chief difficulty with this method was that the moment taken by the skin was small in comparison with that taken by the beam (approximately one-third).

Because of the difficulties mentioned above in evaluating the effect of the beam, it was decided to simulate the beam caps by vertical spacers which could move up and down and rotate about the center or neutral axis of the beam (see Fig. 17). Each spacer could move vertically relative to the ones next to it, thus the specimen could take any amount of shear deflection and not be effected by the beam support system. In order to prevent the skin from

buckling between the spacers, strips were placed above and below the junction of the two semi-elliptical sections. The thickness of these strips was chosen such that they would have a slightly higher buckling load than that of the sheets. It can readily be seen that these strips (.037" thick) would contribute a negligible amount to the shear strength and take a definate calculable amount of bending moment. This method was used on all of the tests except the first eight.

At each end of the specimen there was a steel plate one inch thick (see Fig. 17) which had the cross-section of the specimen, plus a two inch strip in the middle in which to put in the above mentioned beam support. These plates served two purposes, first of all they held the ends of the specimen to the correct contour and second they provided a base which could be conveniently fastened to the face plates of the testing machine. The sheet was firmly held to the solid steel plates by 1/4" bolts which were screwed into tapped holes. These bolts were spaced one inch apart all around the circumference. On specimens where the failing stress was quite high cover plates were placed between the bolt heads and the specimen in order to distribute the force due to the bolt. Considerable care was taken to insure each specimen being as accurately formed as possible. The physical properties of the material used are given in Figs. 62, 63, and 64.

Experimental Results

a) Bending plus vertical shear tests.

The first type of tests to be run was bending plus vertical shear of semi-circular nose-sections. The data obtained from these first tests are shown in Table V and plotted in Figs. 35, and 36. Fig. 35 shows the average shear stress, which is obtained by dividing the vertical load by the total sheet area, plotted against $\frac{M}{Vr}$, where $\frac{M}{Vr}$ is a non-dimensional parameter equal to the moment taken by the sheet divided by the shear times the radius. The points for ultimate and buckling stress show little if any correlation. It is believed that if the specimens were perfect and loaded correctly, the ultimate and buckling loads would be identical in every case. Usually if both specimens on each side of the center line buckled at the same load, that load was also the ultimate. By ultimate is meant that load at which deflection increases with no increase in load.

The maximum compressive stress withstood by the specimen is shown in Fig. 36. These values were calculated on the basis of the standard beam equation $\sigma = \frac{My}{I}$. The agreement between the calculated maximum stress by the above method and that measured by Huggenberger extensometers is seen in Table VII and Fig. 40. These figures show that the correlation

is fairly good, thus permitting the acceptance of the calculated values. The curve in Fig. 36 tends to indicate that for any value of $\frac{M}{Vr}$ greater than 5 the maximum compressive stress is nearly independent of $\frac{M}{Vr}$. The slight decrease at larger values of $\frac{M}{Vr}$ is explained later. The shape of the curve for values of $\frac{M}{Vr}$ less than 4 is primarily governed by the shear strength of the specimen and above that by the bending strength. Observation of the tests indicate that for values of $\frac{M}{Vr}$ greater than 5 the failing and buckling loads are independent of length. The reason for this is that the wave which is formed upon buckling runs very nearly normal to the leading edge and is narrow in width. Such a wave pattern is independent of the length of the specimen unless the specimen becomes very short.

The second set of data is shown in Table VI and plotted in Figs. 37 and 38. Fig. 37 is similar to Fig. 35 except for the sheet thickness. Again there is no correlation between buckling and ultimate stress, for all practical purposes they are the same.

The third set of data is shown in Table VII, and is plotted in Fig's. 39 and 40. The specimens were semi-elliptical sections with a major to minor axis ratio of 2 to 1, and the same thickness as those in Figs. 35 and 36. Figure 39 gives the variation of the average shear stress as a function

of $\frac{M}{Vb}$ where b is the minor axis. The maximum bending stress is plotted in Fig. 40. This figure indicates that similar to the case of a/b = 1, Fig. 36, the maximum compressive stress is nearly independent of $\frac{M}{Vb}$ for values greater than 3 or 4. The reason for the slight decrease in maximum compressive stress will be dealt with later. Agreement between the calculated values of the maximum compressive stress and measured is interesting. It should be noted that usually the measured value is less than the calculated.

Test results for the case where the ratio of a/b was equal to 3.0 are shown in Table VIII. The data are plotted in Figs. 41 and 42. The shape of the curve in Fig. 41 is very similar to the previous ones, however, it is much lower. The absence of a serious length effect is apparent from the fact that for the two lengths plotted, there is no appreciable difference. Fig. 42 shows some difference in the maximum bending stress for pure bending of two specimens of different lengths. The reason for the apparent peak will be discussed later.

The results of all the tests for one thickness are shown in Figs. 43 and 44. Here one sees how marked the influence of the ratio a/b is on the strength of a section. Figure 44 definitely shows that for ratios of $\frac{M}{Vb}$ greater than 4 or 5 that the shear force has little to do with the failure.

b) Pure bending of nose sections.

Since the above results show that the bending strength dominates or governs the larger portion of the range of ratios between bending moment and vertical shear, it was believed adviseable to study pure bending. Table X and Fig. 45 give the experimental results obtained by making pure bending tests on several nose sections of different ellipticity. Fig. 45 shows the maximum bending stress calculated by the simple bending equation, plotted against the ratio a/b.

c) Torsion tests of nose sections.

As no test results were available on allowable torsional stress of elliptical cylinders supported at the minor axis, it was again thought advisable to study pure torsion on nose sections before adding torsion to the case of vertical shear plus bending. The type of specimen used was the same as that described under the section on specimens. The results obtained from the first set of tests are seen in Table XI. The shear stress at buckling and at failure were calculated from Batho's equation $\tau = \frac{Mt}{2At}$ in which the original enclosed area (A) was used in both cases. The results in Table XI are plotted in Fig. 46. Here we see that the stress at buckling falls off as the ratio a/b increases but the failure stress decreases at a slower rate than the buckling.

The reason the buckling stress falls off is because, as the a/b ratio increases, the effective flat area becomes larger, the failure stress then acts in a different manner because for a large a/b a diagonal tension field is set up after buckling. The nose is very strong for large a/b ratios so instead of the waves going around the nose, it acts as a stiffener which can resist tension forces, which of course results in a tension field.

Fig. 47 shows the effect of a/b ratio on angular deflection of the sections under torsion. Again the torsional stress was obtained by using $\tau = \frac{Mt}{2At}$ where A was held constant at the original enclosed area. It is obvious from these curves where buckling takes place, and the effect of the diagonal tension field can also be seen.

One important question is the magnitude of the effect of changing the material on the torsional strength. This was answered by useing two different materials 24ST and 24SO, see Table XII. This table shows that the torsional strength is not very critical to change in material. In this case the ratio of the two defined yield points of the material was 4.3 and the ratio of the change in strength was only 1.23. (Yield point for 24SO is 10,000 lbs/sq.in.) Thus, small variations in the properties of the material used in testing are not important.

Since most airplane manufactures form the nose sections by pulling the sheet around the ribs and riveting it down under bending stress, it was believed desirable to determine the magnitude of the effect of preforming the curved sheet instead of having the sheet under initial bending stresses. Change due to this bending stress and for the particular section whose dimensions are given in Table XIII is 8.7%. This effect of bending stresses on torsional strength is undoubtedly a function of R/t and a/b and the tests given in Table XIII only show that it does have an effect.

One of the most important variables effecting the strength of thin-sheet cylinders under torsion, is its length. In order to be able to measure the magnitude of this effect on nose-sections, several torsion tests on specimens of different length and of two different thicknesses were made. The results of these tests are tabulated in Table XIV, and are plotted in Figs. 48 and 49. Here again the same equation $\tau = \frac{Mt}{2At}$ was used to obtain the critical stress. The theoretical curves plotted in the two figures were calculated by the equation given by L.H. Donnell. (Ref.3)

$$(1-\mu^2)\frac{\tau_{cr}\,L^2}{E\,t^2} = 4.6 + \sqrt{7.8 + 1.67\left(\sqrt{1-\mu^2}\,\frac{L^2}{2tR}\right)^{3/2}} \qquad (62)$$

The above equation is for short and moderately long

circular tubes clamped at the ends. It must be kept in mind that the above equation is for a cylinder with 360 degrees of unsupported arc, where as the experimental points seen in Fig. 48 and 49 are for only 180 degrees of unsupported arc. The experimental curves show that the length-effect is very nearly the same as that for a cylinder. Undoubtedly by changing the boundary conditions used by L. H. Donnell a solution could be arrived at which would correspond to the case at hand. The reason for the experimental curves falling below the theoretical ones for length/radius ratios less than 2, is that the shorter the length the larger the number of waves in the circumferential direction, and as the number of waves increases the effect of the amount of unsupported arc decreases. This naturally causes the experimental results for a semi-circular nose-section to approach those of circular tubes whose average experimental value is about 75 percent of theoretical.

d) Deflection in bending plus shear tests.

In the design of a modern wing it is necessary to determine or estimate the amount of load carried by the various elements of the wing. The nose-section has always caused trouble in this respect. In the present study a deflection curve was obtained for each specimen. This deflection was taken as the

difference in deflection of two points on the specimen. (see Fig. 30). As long as the fixed end plate was fastened securely to the testing machine, this means of measuring the deflection eliminated the effect of end reinforcement on the bending deflection. It is believed that if the designer of a wing knew the rate of deflection with load for the nose-section and the main beam or beams, by a method of equal deformations he could proportion the load carried by each.

A plot of the experimental data is shown in Figs. 50 and 51. These curves have considerable scatter, but they definitely show a trend, and Fig. 52 puts this trend in a form which can be used by a designer. In this figure is seen the deformation per inch per unit average shear stress, as a function of M/Vr. It must be understood that this is an approximate curve and only gives the order of magnitude and trend. The curve was drawn such that it gives the circle points greater weight, for it was felt that these points were more reliable. More data regarding this effect should be obtained in the future.

It is interesting to note the magnitude of the rate of deflection. It actually appears to be between 50 and 100 times that of a solid beam of equivalent moment of inertia,. Comparatively little work has been done on the subject of deflection of monocoque structures,

but several men have mentioned that the deflections will be considerably larger, however, little published data on the exact magnitude are available. The tests shown were run quite carefully and all screws and bolts were tightened as tightly as possible before every test. It is known that the sheet may slip some, but the holes in the sheet were drilled exactly the size of the screws, which screwed into a 1" thick steel block, keeping the amount of slip small.

The present work on deflection of shells indicates that much more work is necessary. The curves in Fig. 51 definitely show that the deflection is not linear with load (even before buckling), as with a solid beam. Knowledge of the deflection of shells is important from the standpoint of overall flexural rigidity which affects flutter and vibration calculations.

CONCLUSIONS FROM EXPERIMENTAL WORK

The experimental results are not adequate to give many definite conclusions, but a few are possible. First, it can be said that for ratios of $\frac{M}{Vr}$ greater than 3 or 4 the buckling stress of a nose section is nearly independent of its length, i.e. rib spacing, unless the length becomes very small. Second, that for ratios of $\frac{M}{Vr}$ less than 4 or 5 the buckling stress of a nose section is governed by the shear strength and for greater values of $\frac{M}{Vr}$ it is controlled by the bending strength. Within reasonable limits the value of the average shear stress at failure for various values of $\frac{M}{Vr}$ can be extrapolated to other ratios of $\frac{r}{t}$ by assuming it to be directly proportional to $\frac{t}{r}$.

It can be said that there is fair agreement between calculated maximum bending-stress based on the standard equation $\sigma = \frac{My}{I}$ and measured values. The effect of increasing the amount of ellipticity greatly reduces the bending and shear strength of nose sections. Under torsional loads the stress at buckling falls off as the ratio a/b increases but the failure stress decreases at a slower rate than the buckling. The sharp nose on an elliptical section has very strong resistance to buckling and can withstand large diagonal tension forces. The torsional strength of elliptical nose sections is not sensitive

to slight changes in physical properties of the material. Initial bending stresses in a curved sheet tends to decrease its strength but not in a vital way. The length effect of semi-circular sections under torsion is similar to that of a circular tube, and can be obtained by L.H. Donnell's theoretical equation. (Ref. 3)

V DISCUSSION AND APPLICATION TO DESIGN CALCULATIONS

It has been advocated by some men that more than one type of loading always reduces the maximum load which the structure will take. E.E. Lundquist states in Ref. 2. that when an elastic body is subjected to one type of loading such as torsion, pure bending, compression or any other loading, it has in general a definite resistance to that loading at which elastic failure occurs and this resistance is ordinarily different for each type of loading. If such a body should be subjected to two or more different types of loading simultaneously, it cannot offer as great a resistance to either type of loading as if that type of loading were acting alone. In such a case the following approximation may be used,

$$\frac{f_1}{S_1} + \frac{f_2}{S_2} + \cdots\cdots \frac{f_n}{S_n} = 1 \qquad (63)$$

where S_1, S_2.....Sn are the allowable stress values for different types of loading acting alone on the body, and f_1, f_2 .....fn are the allowable stress values for those same type of loading when acting simultaneously. An obvious modification to the above equation and a generalization is,

$$\left(\frac{f_1}{S_1}\right)^a + \left(\frac{f_2}{S_2}\right)^b + \cdots\cdots + \left(\frac{f_n}{S_n}\right)^d = 1 \qquad (64)$$

where a, b.....d are greater than zero. It can easily be seen that the above equation covers the special case given by equation (28), Part II.

Two examples in the present investigation are interesting exceptions to the above idea or notion. It is possible for a thin-walled structure to take more bending moment when accompanied by a certain amount of shear, than it can with just a pure bending moment (see Table IV and Fig. 42). A plot of some experimental data which shows this effect is shown in Fig. 53. Considerable scatter is seen in this figure, however some points are noted which definitely have both more shear and more bending moment at failure than others. Because of the rather large amount of scatter in Fig. 53, the author decided to investigate other experimental data before drawing the conclusion that the above mentioned phenomenon really existed.

In N.A.C.A. Technical Note 527 (Ref. 13) on elliptical cylinders under combined bending and shear, the author discovered the same effect. Fig. 54 shows a plot of the experimental results as tabulated in the report. Here is seen not only an effect on the failure load but also on the

buckling load. After reducing the data into a form of stresses which takes into account variation of skin thickness, Fig. 55 is obtained. In this figure the ordinates are directly proportional to the bending moment. These data definitely prove the statement made above. Upon further search a most interesting example was found in a paper by H. Ebner (Ref. 14). In this particular case the tests were made on stiffened circular cylinders. The experimental results are given in Table XV. This table shows that in every case the ultimate bending moment was higher when some vertical shear was present. This effect has never been mentioned before as far as the author knows.

The results of the first part of this research are very useful in design calculations. For example, suppose one wishes to know the curve of average allowable shear stress against $\frac{M}{Vr}$ for a semi-circular nose section of different thickness than those investigated in this research. In Fig. 8 the value of the critical shearing stress is given as a function of R/t and L/R, from this figure a value of the maximum critical stress can be picked off and then by the use of Fig. 4 the allowable stress for various values of $\frac{M}{Vr}$ can be calculated.

Of course the results given in Figs. 4 and 8 are for cylinders and not nose sections but they should give a fair approximation.

As a check the above method was used on the two cases shown in Figs. 35 and 37. Here the ratios of R/t and L/R are known, and from Fig. 6 it is seen that τ_{max} = 10,000 lbs/sq.in. for the first case and 8,000 lbs/sq.in. for the second. In Fig. 4 one sees that $\tau_{average} = \tau_{max}/2$ for values of $\frac{M}{Vr}$ less than 2 and $\tau_{average} = \tau_{max}/\frac{M}{Vr}$ for values greater than 2. The results of these calculations are seen in Figs. 56 and 57. The agreement as far as variation with $\frac{M}{Vr}$ is very good but the magnitude of the calculated values are a little high. It is interesting that the calculated curves are higher than the experimental, for one would naturally think that the nose section had more support and would therefore be stronger.

Another method which can be used on elliptical nose sections as well as circular for extrapolating from the experimental results given by this research to different ratios of radius over thickness, is to assume the critical stress is directly proportional to t/r. This is a good assumption if the amount of extrapolation in not too large, which is not likely in most modern airplanes.

In an actual design of an airplane nose section the structural designer or engineer has little or no control over the shape of the wing nose, which is determined by the aerodynamicist. However, he does have some control over the position of the front spar but even this helps but little for its position is governed by factors other than the strength of the nose section. Nearly all airplanes of reasonable size which are efficiently designed have some kind of span-wise stiffeners ahead of the front spar. (see Fig. 58) This figure shows typical modern day wing construction. From this figure it is seen that the three factors which the structural engineer can change in order to alter the strength of the nose section are the position of the first stiffener, the skin thickness, and the rib spacing.

The method of calculating the strength of the nose section is to, first, determine the ellipse which best fits the leading edge back to the position of first stiffener. The major axis (x-x) of the ellipse should be nearly parallel to a tangent to the skin at the first stiffener. (point p in Fig. 58) The axes and ratio of a/b for the ellipse are obtained as shown in Fig. 58. Since under normal loads the bottom of the wing is under tension, the position of the first stiffener on the bottom side of the wing is of little importance. Except for the case where the vertical

shear is quite large, (i.e. small values of $\frac{M}{Vr}$) it is also of secondary importance whether or not the ellipse fits the skin of the wing below the axis, as this side is under tensile stresses and therefore not critical. In the case of small ratios of $\frac{M}{Vr}$ (less than 4) it is important to fit the ellipse equally well above and below the axis, because at small values of $\frac{M}{Vr}$ the sheet is critical at the axis. The first stiffener aft of the leading edge will nearly always be rigid enough so that for all practical purposes it will act as the support or what was called the beam in the experimental work. Behind the first stiffener the radius of curvature of the sheet will usually be so large that the strength of the structure can be analyzed by the same methods used for stiffened flat or slightly curved sheets. To calculate the strength of the leading edge under inverted flight conditions the method described above will apply in exactly the same way only the ellipse should be fitted to the first stiffener on the bottom side of the wing.

The percentage of the total vertical shear taken by the leading edge of a wing can be estimated by the results given under the section on deflection of bending plus shear tests. By knowing the rate of deflection per inch with load for each beam or shear web in a particular wing, and by useing Fig. 52, the designer

can, by assuming sufficient torsional rigidity to cause equal bending deflection chord-wise (i.e. no torsional deflection, or differential bending), calculate the percentage of shear taken by the nose-section. Until further experimental work is done this method is believed to be the most satisfactory. Additional curves to aid in the design of wing nose sections are given in Figs. 59, 60, and 61.

REFERENCES AND BIBLIOGRAPHY

1. E. E. Lundquist — "Strength Tests of Thin-Walled Duralumin Cylinders in Pure Bending" N.A.C.A Tech. Note 479, 1933

2. E. E. Lundquist — "Strength Tests of Thin-Walled Duralumin Cylinders in Combined Transverse Shear and Bending" N.A.C.A Tech. Note 523, 1935

3. L. H. Donnell — "Stability of Thin-Walled Tubes Under Torsion" N.A.C.A. Tech. Report 479

4. D. Williams, A. M. I. Mech, J. Taylor — "Variation of Shear Stress in Thin-Walled Tubes Under Torque" R.M. 1812

5. L. G. Brazier — "The Flexure of Thin Cylindrical Shells and Other 'Thin Sections' " R and M 1081. British A.R.C. 1927, and Proc. Roy. Soc. London, Ser. A, Vol. 116, 1937, pp. 104-114

6. E. Chwalla — "Reine Biegung Schlanker, Dünnwandiger Rohre mit Gerader Achse", Z.A.M.M. Vol. 13, 1933. pp. 48-53

7. O. S. Heck — "The Stability of Orthotropic Elliptic Cylinders in Pure Bending" N.A.C.A. Technical Memorandum 834.

8. N. J. Hoff — "Instability of Monocoque Structures in Pure Bending" Journal of Royal Aeronautical Society. Vol XLII No 328 April 1938 pp.291

9. L. Prandtl — "Kipperscheinungen" Nuremberg 1899.

10. Th. von Karman — "Uber die Formanderung dunnwandiger Rohre, insbesondere federn der Ausgleichsrohre" Z.d.V.D.I., Bd. 55, Heft 45, 1911, S. 1889-1895

11. S. Timoshenko — "Theory of Elastic Stability" Mc Graw-Hill Book Company, Inc. 1936 pp. 208.

12. James E. Lipp — "Strength of Thin Walled Cylinders Subjected to Combined compression and Torsion" Ph.d Thesis of California Institute of Technology 1935

13. Eugene. E. Lundquist — "Strength Tests of Thin-Walled Duralumin Cylinders of Elliptic Section" N.A.C.A. Tech. Note 527.

14. H. Ebner — "The Strength of Shell Bodies--Theory and Practice" N.A.C.A. Tech. Memorandum No.838

15. "Allowable Shear from Combined and Torsion in Round, Elliptical and Streamlined Tubes and Allowable Normal Stress from Bending in Thin-Walled Tubes" Washington D. C. 1932. ACIC. 669

16. W. J. Duncan "Torsion and Flexure of Cylinders and Tubes" London, H. M. Stat. Off., 1932. R. M. 1444.

17. Sutton A. J. Pippard "Distortion of Thin Tubes under Flexure" H. M. Stat. Off., London, 1932. R. M. 1465

18. Paul Kuhn "The Torsional Stiffness of Thin Duralumin Shells Subjected to large Torques" Washington D. C. , 1934 N.A.C.A. Tech. Note 500.

19. C. Williams "Behavior in Bending of Thin-Walled Tubes and Channels" H. M. Stat. Off., London. 1935 R.M. 1609

20. G. M. Smith — "Strength in Shear of Thin Curved Sheets of Alclad" N.A.C.A. Tech. Note 343.

21. E. E. Lundquist — "Strength Tests on Thin-Walled Duralumin Cylinders in Torsion" N.A.C.A. Tech. Note. No. 427.

22. L. H. Donnell — "Stability of Thin-walled Tubes under Torsion" Tran. A.S.M.E. Vol. 56, No. 3 1934

23. E. Treffty — "The Equations for the Bending of Thin Shells Deduced from Castigliano's Principle. ZAMM. Vol. 15. No. 1/2 1935

24. C. Mazzoni — "Torsion in Hollow Thin-Walled Cylinders" L'Aerotecnica Vol. XV No. 2 1935

25. — "The Allowable Stress in Tubes Subjected to Torsion" A.C.I.C. No. 641

26. E. Scheverin — "Stabilitat Des Dunnwandigen Rohes" ZFAMM. Vol. V. No. 3. pp. 235-243.

27. E. H. Atkin — "Stresses in Metal-Covered Planes." Aircraft Engineering Vol 5, no. 53. 1933. pp. 162-164

28. R. W. Mossman, R. G. Robinson — "Bending Tests of Metal Monocoque Fuselage Construction" N.A.C.A. Tech. Note 357.

29. Maximillian T. Huber — "Bending of Beams of Thin Sections" Washington D. C. N.A.C.A. Tech. Memorandum No. 793.

30. Andrew Robertson — "The Strength of Tubular Struts" Proceedings of the Royal Society of London. Series A. Vol. 121, 1928 pp. 558.

31. J. E. Younger — "Principle of Similitude as Applied to Research on Thin-Sheet Structures" A.S.M.E. Aero. Eng. Oct.--Dec. 1933. pp.163--169

TABLE I

Results of Combined Transverse Shear and Bending Tests

Data taken from NACA T.N. 523

Specimen	V. lbs.	t. in.	λ	$\tau_{max.}$	From TM τ_{max}	$\frac{r}{t}$
177	3593	.0232	1.02	6565	6580	323
183	2686	.0209	2.01	5480	5460	359
188	2413	.0210	2.57	6260	4880	357
184	1753	.0209	3.09	5500	3560	359
187	2488	.0208	3.14	8650	5080	361
189	1978	.0210	3.43	6850	4000	357
185	1268	.0205	4.21	5520	2630	366
186	1508	.0208	4.87	7490	3080	361
190	1138	.0207	4.94	5750	2330	362
191	992	.0207	7.76	7900	2030	362
176	1723	.0166	1.00	4400	4410	452
175	1593	.0156	1.00	4330	4330	481
181	1398	.0164	2.02	3950	3620	457
178	1103	.0157	2.09	3115	2980	478
182	1148	.0159	2.57	3955	3060	472
180	1128	.0157	2.94	4480	3050	478
179	708	.0153	4.38	4300	1960	490
173	381	.0155	8.78	4575	1045	484
174	273	.0157	9.40	3465	737	478

From page 13. $r = 7.5"$ $l/r = 1.0$

TABLE I CONTINUED

Specimen	V lbs.	t. in.	λ	τ_{max}	From TM τ_{max}	$\frac{r}{t}$
111	1143	.0121	.85	4010	4010	620
78	928	.0115	1.45	3425	3425	652
1	905	.0112	1.53	3430	3430	670
114	653	.0117	2.05	2424	2365	641
110	753	.0120	2.04	2713	2660	625
108	688	.0119	2.04	2510	2460	630
76	753	.0113	2.04	2887	2830	663
113	658	.0116	2.05	2470	2410	646
107	738	.0118	2.58	3426	2655	635
104	628	.0114	2.61	3048	2535	658
77	678	.0114	2.64	3327	2520	658
106	563	.0116	3.20	3295	2060	646
94	513	.0128	4.80	4080	1700	586
97	413	.0121	4.96	3596	1450	620
105	358	.0116	5.09	3335	1310	646
95	413	.0119	5.81	4285	1475	630
101	358	.0116	6.18	3822	1257	646
96	318	.0120	6.31	3550	1125	625
103	308	.0120	6.38	3477	1090	625

From page 14. $r = 7.5"$ $1/r = 0.5$

TABLE I CONTINUED

Specimen	V. lbs.	t. in.	λ	τ_{max}	From TM τ_{max}	$\frac{r}{t}$
15	696	.0110	1.07	2690	2690	682
85	722	.0114	1.07	2680	2680	658
11	666	.0111	1.62	2540	2540	675
87	599	.0110	1.64	2310	2310	682
83	609	.0115	1.64	2245	2245	652
81	581	.0115	2.28	2444	2145	652
12	575	.0112	2.32	2530	2180	669
75	504	.0113	2.54	2407	1895	663
31	472	.0111	2.61	2360	1810	675
74	458	.0114	2.98	2533	1700	658
73	453	.0112	2.98	2555	1715	669
13	400	.0108	3.13	2457	1517	649
92	433	.0114	3.68	2962	1610	658
91	393	.0112	3.72	2770	1490	669
72	378	.0116	4.70	3255	1385	646
89	329	.0112	3.81	2372	1245	669
71	378	.0117	4.70	3220	1370	641
16	375	.0110	4.75	3444	1450	682
69	308	.0119	6.83	3740	1095	630
70	2.98	.0119	6.90	3657	1060	630
14	186	.0108	8.48	3095	730	694
112	157	.0120	12.83	3560	555	625
93	152	.0115	1300	3640	560	652
37	126	.0118	14.28	3235	453	635

From page 15. $r = 7.5"$ $1/r = 1.0$

TABLE I CONTINUED

Specimen	V. lbs.	t. in.	λ	τ_{max}	From TM τ_{max}	$\frac{r}{t}$
65	506	.0114	1.47	1880	1880	658
17	510	.0111	1.54	1950	1950	676
100	503	.0115	1.96	1860	1860	652
18	510	.0111	1.96	1950	1950	675
29	537	.0113	2.87	2900	2020	664
67	491	.0120	2.88	2505	1740	625
19	410	.0110	2.90	2290	1580	682
99	469	.0120	3.46	2870	1660	625
98	464	.0120	3.47	2845	1640	625
64	361	.0116	4.39	2900	1320	646
20	385	.0116	4.40	3090	1405	647
66	509	.0129	4.44	3720	1675	581
65	289	.0114	4.49	2423	1080	658
63	249	.0111	6.64	3170	954	675
21	260	.0109	6.66	3362	1010	688
62	220	.0117	8.70	3468	797	641
61	210	.0117	8.86	3370	760	641
22	205	.0104	9.02	3450	765	658

From page 16. $r = 7.5"$ $1/r = 2.0$

TABLE I CONTINUED

Specimen	V. lbs.	t. in.	λ	τ_{max}	From TM τ_{max}	$\frac{r}{t}$
224	2315	.0306	1.05	2385	2386	728
223	2375	.0221	1.49	2280	2280	679
228	2145	.0224	2.08	2120	2030	670
226	1885	.0213	2.09	1962	1880	704
225	1185	.0201	3.22	2015	1250	746
227	1485	.0231	3.28	2240	1365	649
218	1165	.0155	1.04	1597	1597	968
222	1010	.0153	1.52	1400	1400	980
219	985	.0161	2.16	1402	1300	932
220	765	.0161	2.69	1357	1008	932
217	585	.0161	3.51	1353	770	932
221	525	.0158	5.92	1382	705	949
209	405	.0103	1.12	835	834	1455
214	425	.0111	2.07	841	812	1352
210	485	.0116	2.32	1030	887	1293
213	335	.0106	2.90	972	672	1415
212	305	.0110	3.30	971	588	1364
211	275	.0110	4.10	1090	530	1364
216	125	.0103	7.06	910	257	1455
215	105	.0105	7.83	831	212	1428

From page 17. $r = 15"$ $1/r = 1.00$

TABLE II

Results on Combined Bending and Torsion of Steel Tubes

Data Taken from A.C.I.C. 669

Test No.	Specimen 12 R/t = 15.3		Specimen 13 R/t = 12.9		Specimen 14 R/t = 9.0		Specimen 15 R/t = 7.3	
	% Bending	$\tau_{max.}$	% Bending	$\tau_{max.}$	% Bending	$\tau_{max.}$	% Bending	$\tau_{max.}$
1	0	30,550	0	32,900	0	32,600	0	40,500
2	6.3	30,500	12.6	32,730	0	32,600	16.5	41,750
3	12.8	26,100	25.2	34,750	12.8	32,500	33.4	44,500
4	24.6	28,350	33.4	33,800	25.0	33,500	50.3	42,700
5	25.0	30,050	50.8	36,650	50.5	39,050	60.5	43,000
6	27.7	31,200	61.0	36,250	67.5	37,850	75.8	42,880
7	33.5	27,000	87.5	34,100	100.0	37,450	100.0	41,650
8	50.5	28,680	88.0	34,370	100.0	37,450		
9	60.5	27,950	100.0	32,650				
10	76.0	27,500						
11	87.2	27,450						
12	100.0	32,350						
Average		28,970		34,240		35,380		42,425
Maximum Difference		11.7%		7.0%		10.4%		4.9%

$$\% \text{ Bending} = \frac{\sigma_{Bending}}{\sigma_{Bending} + \sigma_{Torsion}}$$

TABLE III

Bending Strength of Dural Cylinders Including Correction due to Flattening

Data from N.A.C.A. Technical Note 479

r/t	$\frac{\sigma_o}{\sigma_{theory}}$	$\frac{\sigma_o r}{Et}$	z/z_o	$\frac{\sigma_c}{\sigma_{theory}}$	r/t	$\frac{\sigma_o}{\sigma_{theory}}$	$\frac{\sigma_o r}{Et}$	z/z_o	$\frac{\sigma_c}{\sigma_{theory}}$
320	.925	.560	.790	.730	640	.597	.362	.925	.553
330	.971	.528	.821	.717	640	.601	.365	.924	.557
340	.869	.527	.821	.715	670	.619	.375	.919	.570
345	.882	.535	.815	.720	680	.628	.381	.916	.577
345	.865	.535	.815	.720	650	.579	.351	.930	.539
360	.874	.529	.820	.717	650	.557	.338	.936	.522
335	.774	.469	.864	.669	670	.575	.348	.931	.535
345	.803	.486	.853	.684	680	.589	.357	.928	.547
325	.697	.423	.893	.624	680	.566	.343	.933	.529
340	.757	.459	.871	.661	640	.528	.320	.943	.499
460	.760	.460	.870	.661	640	.517	.314	.944	.489
460	.728	.442	.882	.644	690	.546	.331	.938	.512
462	.709	.430	.889	.631	685	.531	.322	.942	.502
450	.661	.401	.906	.601	680	.521	.316	.944	.492
440	.595	.361	.926	.552	690	.512	.311	.946	.486
457	.615	.372	.921	.567	620	.455	.276	.958	.436
465	.595	.360	.926	.552	710	.421	.256	.964	.408
450	.556	.338	.936	.522	915	.642	.389	.913	.586
610	.785	.476	.859	.676	940	.659	.400	.906	.600
655	.778	.472	.862	.672	920	.637	.386	.914	.583
600	.604	.366	.923	.558	980	.525	.319	.943	.497
615	.624	.378	.918	.573	990	.392	.238	.969	.380
660	.659	.399	.907	.598	1420	.539	.327	.940	.507
650	.633	.384	.915	.582	1430	.543	.329	.939	.510
620	.593	.360	.926	.552	1380	.478	.290	.954	.458
670	.635	.385	.914	.582	1350	.407	.247	.967	.395
670	.630	.382	.916	.578	1400	.358	.217	.975	.350

σ_o = Experimental failing stress calculated by original dimensions.

σ_c = Experimental failing stress corrected for effect of flattening.

$$\sigma_{theory} = \frac{Et}{R\sqrt{3(1-u^2)}} = .6\,E\,\frac{t}{R} \text{ for } u = .3$$

TABLE IV

Experimental and Theoretical Values of Maximum Bending Stress for Semi-Circular Nose Sections

Specimen	Material	E	Thickness	Radius	R/t	M/Vr	$\sigma_{experimental}$	Theory $\sigma = .3E(t/R)$
1	Dural	10×10^6 #/in.^{2}	.0165 in.	3.01 in.	182	8.01	15,405 #/in.^{2}	16,500 #/in.^{2}
2	"	"	.020	"	151	7.08	18,500	19,850
3	Steel	30×10^6	.008	3.00	375	9.79	22,580	24,000
4	"	"	.0085	"	353	∞ (Pure Bending)	22,521	25,500
5a	Dural	10×10^6	.020	3.01	151	∞ (Pure Bending)	15,900	
b							18,920	
c							18,250	
d							18,400	
						Average	17,870 #/in.^{2}	19,850 #/in.^{2}

TABLE V

Test Data of Semi-Circular Specimens under Combined Bending and Shear

Material: 24ST Dural Total length = 6.5"

Specimen No.	Radius r	Thickness t	Mom. of Inertia of Sheet I_s	Total Mom. of Inertia of Spec. I_T	$\frac{I_s}{I_T}$	Area of Sheet	Load Moment Arm (in.) L	$\frac{M}{Vr} = \frac{L}{r} \times \frac{I_s}{I_T}$	Buck. Load (lbs)	Ult. Load (lbs)	Buck. Aver. Shear Stress τ_B	Ult. Aver. Shear Stress τ_u	Buck. Max. Bending Stress σ_B	Ult. Max. Bending Stress σ_u
BS-16	3.01	.0215	1.824	5.704	.320	.407	3.88	.412	2345	2345	5762	5762	4,800	4,800
BS-20	"	.022	1.866	5.506	.339	.416	9.13	1.013	2621.5	2622	6302	6303	13,100	13,100
BS-10	"	.0215	1.824	5.224	.349	.407	13.63	1.58	1570	1700	3857	4177	12,350	13,370
BS-12B	"	"	"	5.704	.320	"	28.06	2.98	1170	1170	2875	2875	17,300	17,300
BS-12	"	"	"	5.464	.334	"	28.06	3.11	660	1040	1622	2555	10,200	16,050
BS-21B	"	"	"	5.464	.334	"	31.5	3.50	1046	1046	2569	2569	18,300	18,300
BS-13	"	"	"	5.704	.320	"	37.31	3.97	640	750	1572	1843	12,600	14,750
BS-13B	"	"	"	5.704	.320	"	37.31	3.97	825	885	2027	2174	16,230	17,386
BS-15B	"	"	"	5.704	.320	"	52.06	5.53	608	691	1494	1698	16,700	19,000
BS-21	"	"	"	5.464	.334	"	63.81	7.08	354	528.6	870	1299	12,400	18,500
BS-11	"	"	"	5.224	.349	"	79.0	9.16	310	317	762	779	14,100	14,400
BS-11B	"	"	"	5.224	.349	"	79.0	9.16	268	397	658	975	12,200	18,050

TABLE VI

Test Data of Semi-Circular Specimens under Combined Bending and Shear

Material: 24ST Dural Total length = 6.5"

Specimen No.	Radius r	Thickness t	Mom. of Inertia of Sheet I_s	Total Mom. of Inertia of Spec. I_T	$\frac{I_s}{I_T}$	Area of Sheet	Load Moment Arm (in.) L	$\frac{M}{Vr} = \frac{L}{r} \times \frac{I_s}{I_T}$	Buck. Load V_B (lbs)	Ult. Load V_u (lbs)	Buck. Aver. Shear Stress τ_B	Ult. Aver. Shear Stress τ_u	Buck. Max. Bending Stress σ_B	Ult. Max. Bending Stress σ_u
BS-17	3.01	.0165	1.415	5.107	.277	.312	3.88	.357	960	980	3077	3141	2194	2239
BS-18	"	"	"	5.107	.277	"	9.13	.840	1139	1176	3650	3769	6122	6321
BS-22	"	"	"	4.617	.306	"	9.13	.928	1326	1393	4250	4465	7890	8288
BS-19	"	"	"	"	"	"	13.63	1.386	1037	1213	3324	3888	9213	10776
BS-25	"	"	"	"	"	"	25.06	2.55	689	689	2208	2208	11258	11258
BS-24	"	"	"	"	"	"	37.38	3.80	378	567	1211	1817	9212	13818
BS-24B	"	"	"	"	"	"	37.38	3.80	397	519	1272	1663	9675	12648
BS-23B	"	"	"	"	"	"	58.25	5.92	260	425	833	1362	9875	16142
BS-23	"	"	"	"	"	"	78.75	8.01	300	300	962	962	15405	15405

TABLE VII

Test Data of Semi-Elliptical Specimens under Combined Bending and Shear

Material: 24ST Dural — a/b = 2.0

Total Length = 6 1/2" — b = 3.01"

Thickness = .020" — Area = .612 in.^{2}

Moment of Inertia of Sheet I_s = 3.14 in.^{4}

Total Moment of Inertia of Specimen I_T = 6.01 in.^{4}

Specimen No.	Load Moment Arm in.	M/Vb	Buckling Load lbs.	Average Shear Stress	Maximum Bending Stress Calculated	Maximum Measured Bending Stress
BS-37	78.75	13.69	152.3	249.0	6020	6240
BS-37B	"	"	233.2	381.0	9220	--
BS-38	9.13	1.59	1510.0	2469.0	6920	6500
BS-39	22.0	3.82	588.0	961.0	6490	5950
BS-39B	"	"	784.0	1281.0	8650	--
BS-40	34.63	6.02	398.0	640.0	6915	6790
BS-40B	"	"	471.0	770.0	8200	--
BS-41	49.38	8.58	338.0	553.0	8380	--
BS-41B	63.75	11.09	224.0	366.0	7170	5640
BS-41C	3.88	0.67	2064.0	3378.0	4010	--

TABLE VIII

Test Data of Elliptical Nose Sections under Combined Bending and Shear

Material: 24ST Dural — a/b = 3.0

Total Length = 16" — b = 3.01"

Thickness = .020" — Area = .802 in.^{2}

Moment of Inertia of Sheet I_s = 4.28 in.^{4}

Total Moment of Inertia of Specimen I_T = 7.11 in.^{4}

I_s/I_T = .601

Specimen No.	Load Moment Arm in.	M/Vb	Buckling Load Lbs.	Average Shear Stress	Maximum Bending Stress
BS-28	88.4	17.65	107.1	133.4	4020
BS-28B	"	"	95.2	118.7	3573
BS-29	18.6	3.72	670.1	834.9	5300
BS-29B	"	"	432.5	538.9	3421
BS-30	34.6	6.92	331.2	412.6	4870
BS-30B	"	"	327.3	407.8	4812
BS-31	46.9	9.37	233.2	290.6	4649
BS-32	67.9	13.56	145.2	180.9	4186
BS-33	52.8	10.54	161.8	201.6	3624
BS-33B	"	"	195.2	243.2	4373
PB-1a	∞	∞	--	0	5291
PB-1b	"	"	--	"	5096

TABLE IX

Test Data of Elliptical Nose Sections under Combined Bending and Shear

Material: 24ST Dural — a/b = 3.0

Total Length = 6 1/2" — b = 3.01"

Thickness = .020" — Area = .802 in.^{2}

Moment of Inertia of Sheet I_s = 4.28 in.^{4}

Total Moment of Inertia of Specimen I_T = 7.11 in.^{4}

I_s/I_T = .601

Specimen No.	Load Moment Arm in.	M/Vb	Buckling Load lbs.	Average Shear Stress	Maximum Bending Stress
BS-34	18.6	3.72	485	604	3838
BS-34B	"	"	916	1141	7244
BS-35	34.6	6.92	265	330	3896
BS-35B	67.9	13.56	174	216	5008
BS-36	9.1	1.82	1030	1283	3994
BS-36B	"	"	1169	1456	4533
PB-2	∞	∞	--	--	4035
PB-2B	"	"	--	--	3950

TABLE X

Test Data of Nose Sections under Pure Bending

Material: 24ST Dural b = 3.01"

Thickness = .020"

Specimen No.	Length L in.	a/b	Buckling Moment	Maximum Moment	Buckling Stress	Maximum Stress
PB-1a	16	3	12,500	12,500	5291	5291
PB-1b	"	"	12,000	12,000	5096	5096
PB-2a	6.5	"	8,600	12,000	3652	5096
PB-1b	"	"	8,700	--	3695	--
PB-3	"	2	17,700	17,700	8,885	8,885
PB-5	"	1	24,000	24,000	15,900	15,900
PB-5B	"	"	23,700	28,600	15,700	18,920
PB-6	"	"	23,800	27,600	15,730	18,250
PB-6B	"	"	24,700	27,900	16,300	18,400

TABLE XI

Pure Torsion of Elliptical Sections Similar to Wing Nose

Material: 24ST Dural

Specimen No.	b	a/b	Thickness t in.	Length L in.	Buckling Stress τ_B lbs./in.^{2}	Failure Stress τ_F lbs./in.^{2}
PT-9	3.01	1.0	.019	34	5775	5938
PT-11	"	"	"	"	5772	"
PT-16	"	2.0	.021	"	3217 3429	3605
PT-17	"	3.0	.020	"	1571 1977	3160

TABLE XII

Effect of Material on Torsional Strength

of Semi-Circular Nose Sections

Specimen No.	Material	Thickness t in.	a/b	Length L in.	Maximum Shear Stress τ_{max} lbs./in.^{2}
PT-9	24ST	.019	1.0	34	5938
PT-10	"	"	"	"	5782
PT-11	"	"	"	"	5938
PT-6	24SO	"	"	"	4529
PT-7	"	"	"	"	4973

Average for 24ST is 5866 lbs./sq.in.

Average for 24SO is 4751 lbs./sq.in.

TABLE XIII

Effect of Bending Stresses on Torsional Strength

Specimen No.	Material	Condition	Thickness t in.	a/b	Length L in.	Maximum Shear Stress τ_{max} lbs./in.^{2}
PT-9	24ST	Preformed	.019	1.0	34	5938
PT-10	"	"	"	"	"	5782
PT-11	"	"	"	"	"	5938
PT-12	"	Non-Preformed	"	"	"	5378
PT-13	"	"	"	"	"	5418

Average for preformed specimen is 5866 lbs./sq.in.

Average for non-preformed specimen is 5398 lbs./sq.in.

TABLE XIV

Effect of Length on Torsion Strength of Semi-Circular Nose Sections

Material: 24ST Dural Radius = 3.01"

Specimen No.	Thickness t in.	Length L in.	Length / Radius L/R in.	Number of Waves	Maximum Shear Stress τ_{max} lbs./in.^{2}
PT-32	.020	2.5	0.83	6	14,720
PT-33	"	"	"	5	15,300
PT-20	"	6.5	2.16	3	11,190
PT-21	"	"	"	"	12,065
PT-26	"	16	5.32	2	7,670
PT-27	"	"	"	"	8,200
PT-9	.019	34	11.3	1	5,938
PT-10	"	"	"	"	5,782
PT-11	"	"	"	"	5,938
PT-12	"	"	"	"	5,378
PT-13	"	"	"	"	5,418
PT-30	.016	2.5	0.83	6	13,290
PT-31	"	"	"	"	14,250
PT-23	"	6.5	2.16	3	9,956
PT-24	"	"	"	"	9,607
PT-28	"	16	5.32	2	6,130
PT-29	"	"	"	"	6,080
PT-14	"	34	11.3	1	4,706
PT-15	"	"	"	"	4,435

TABLE XV

Effect of Shear on Bending Tests of Stiffened Cylinders

Data Taken from N.A.C.A. T.M. 838, Ref. 14

Cylinder	Ultimate Bending Moment under Pure Bending	Similar cylinder tested under bending moment and shear force. Shear Force	Ultimate Bending Moment
1	347,000 kg. cm.	1450 kg.	380,000 kg. cm.
2	487,000 "	1870 "	497,000 "
3	397,000 "	1530 "	407,000 "

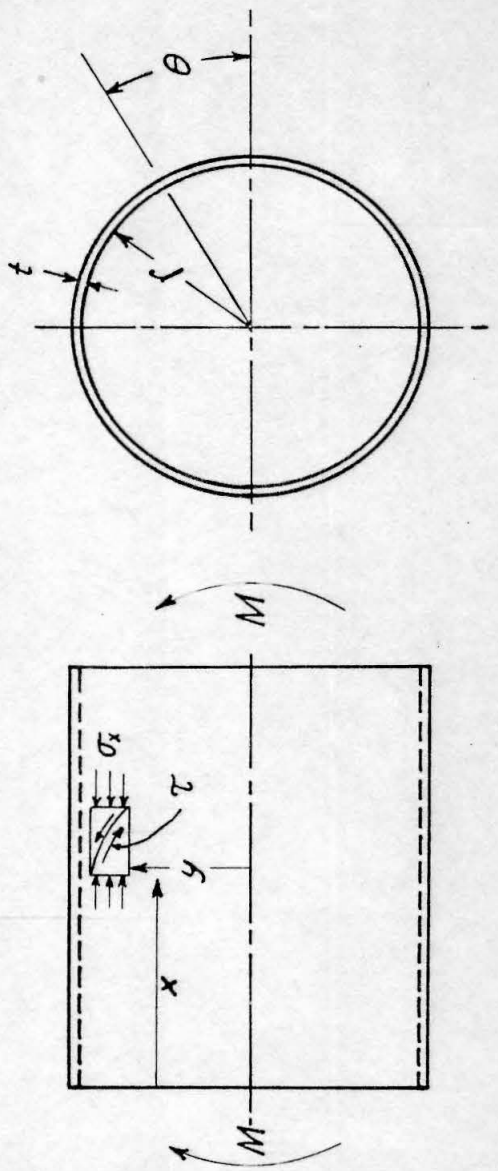

Fig. 1.

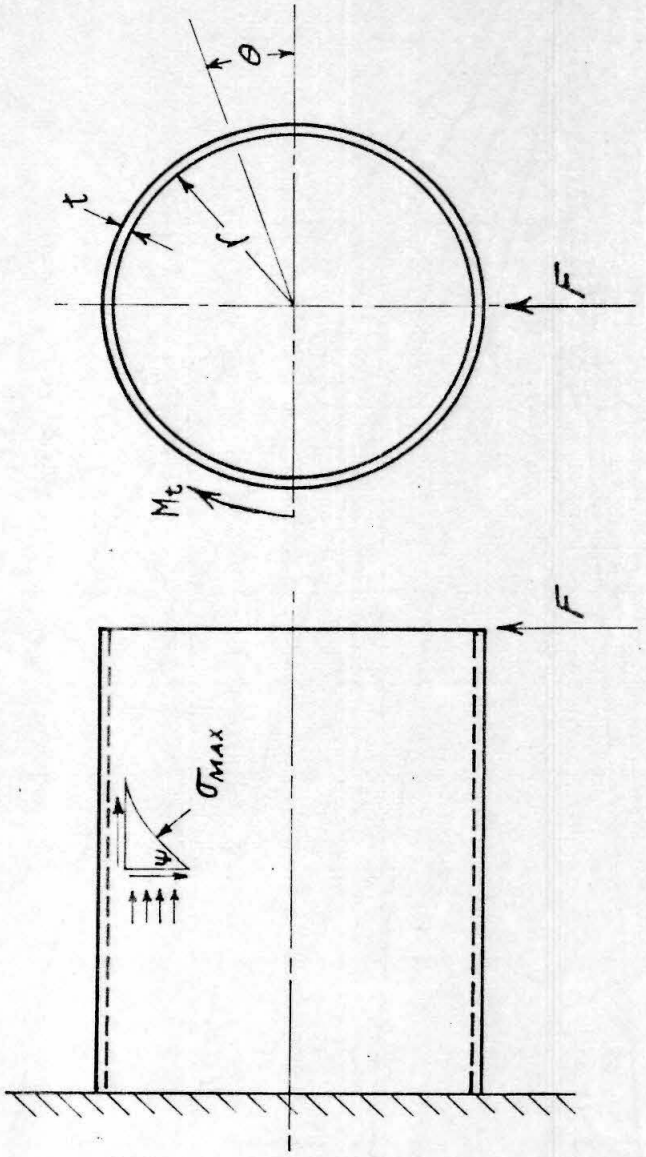

Fig. 2.

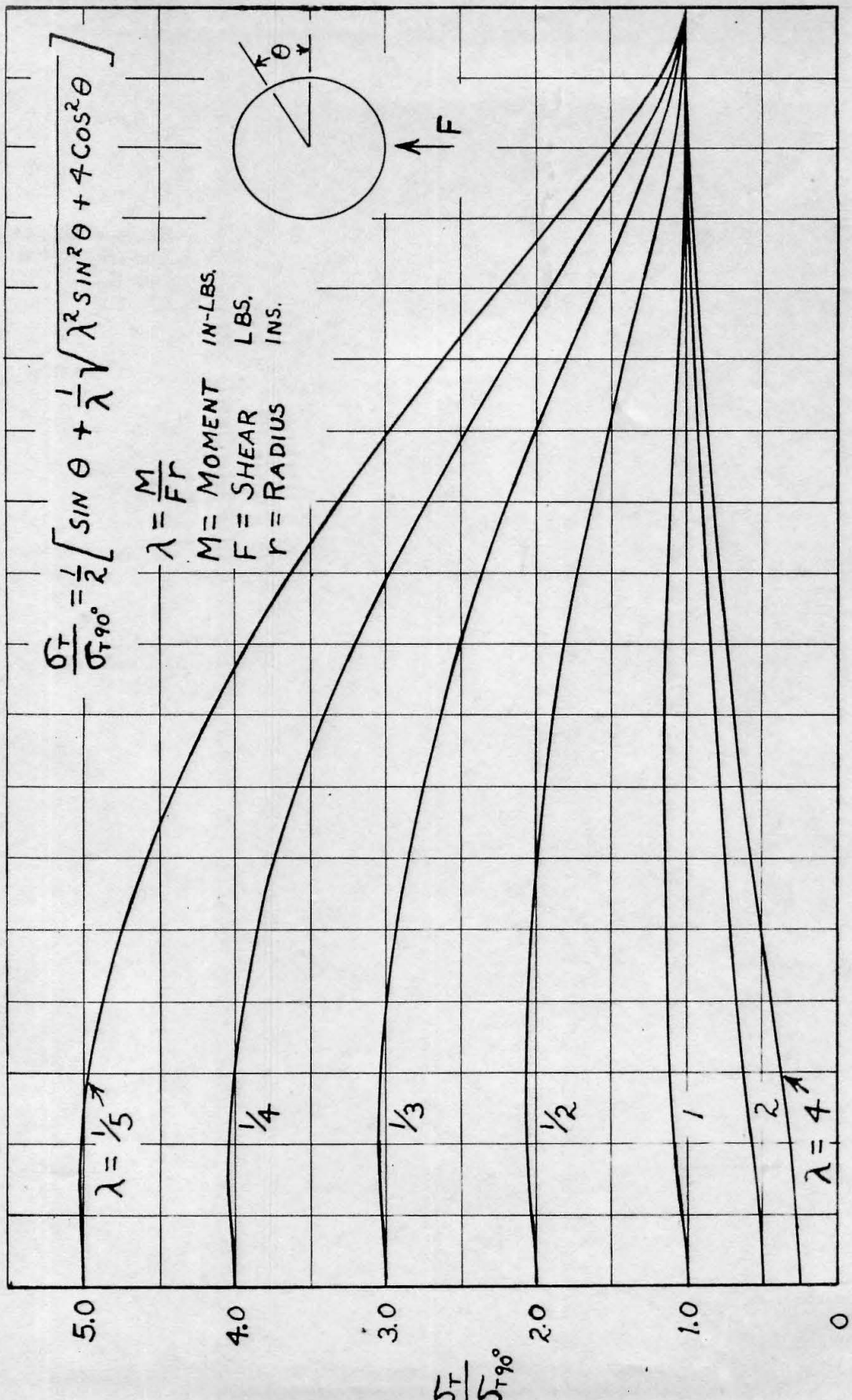

Fig. 3. Variation of $\frac{\sigma_{MAX.}}{\sigma_{\theta=90^\circ}}$ with θ for various values of λ.

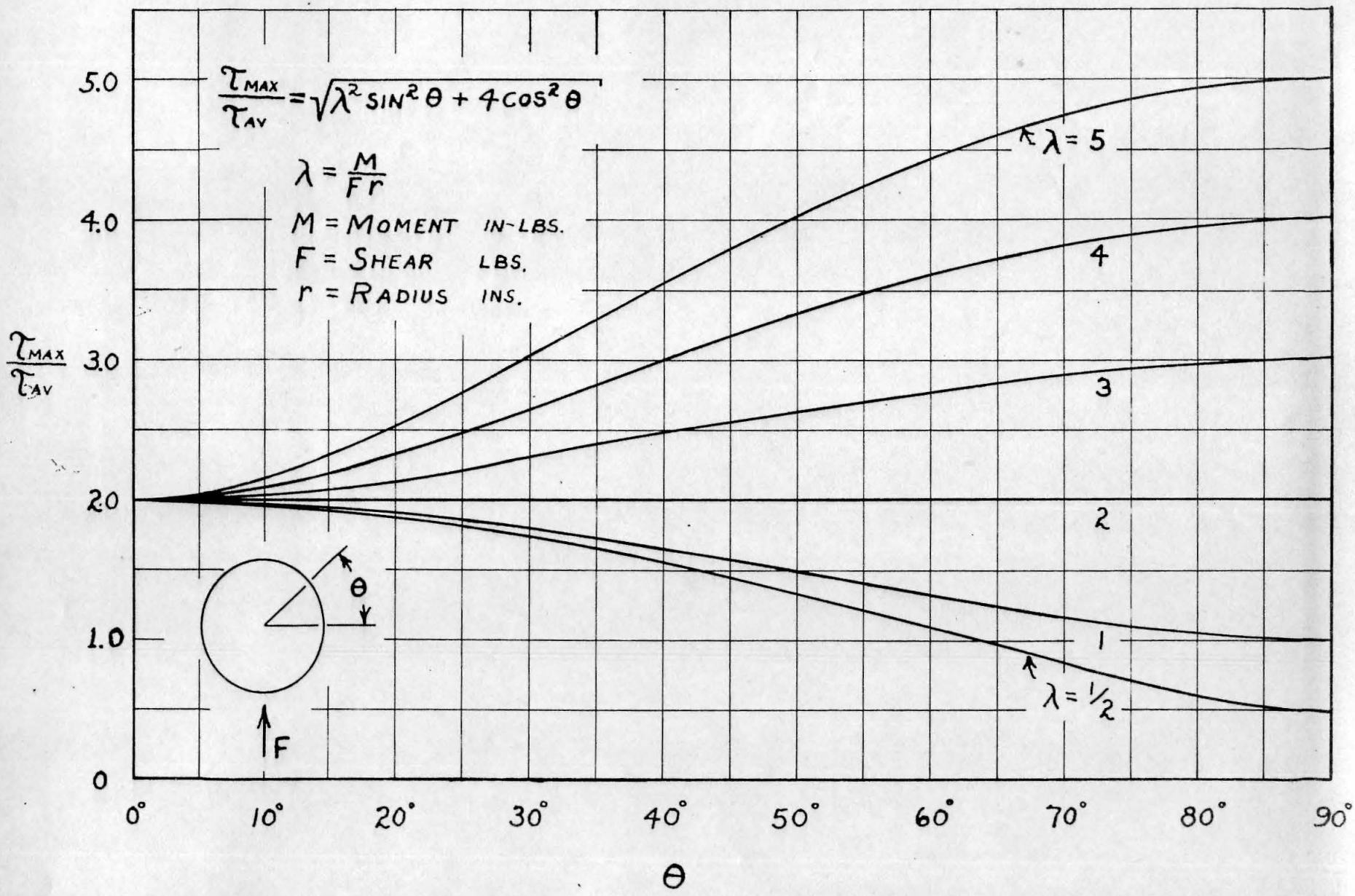

Fig. 4. Variation of $\frac{\tau_{MAX}}{\tau_{AVERAGE}}$ with θ for various values of λ .

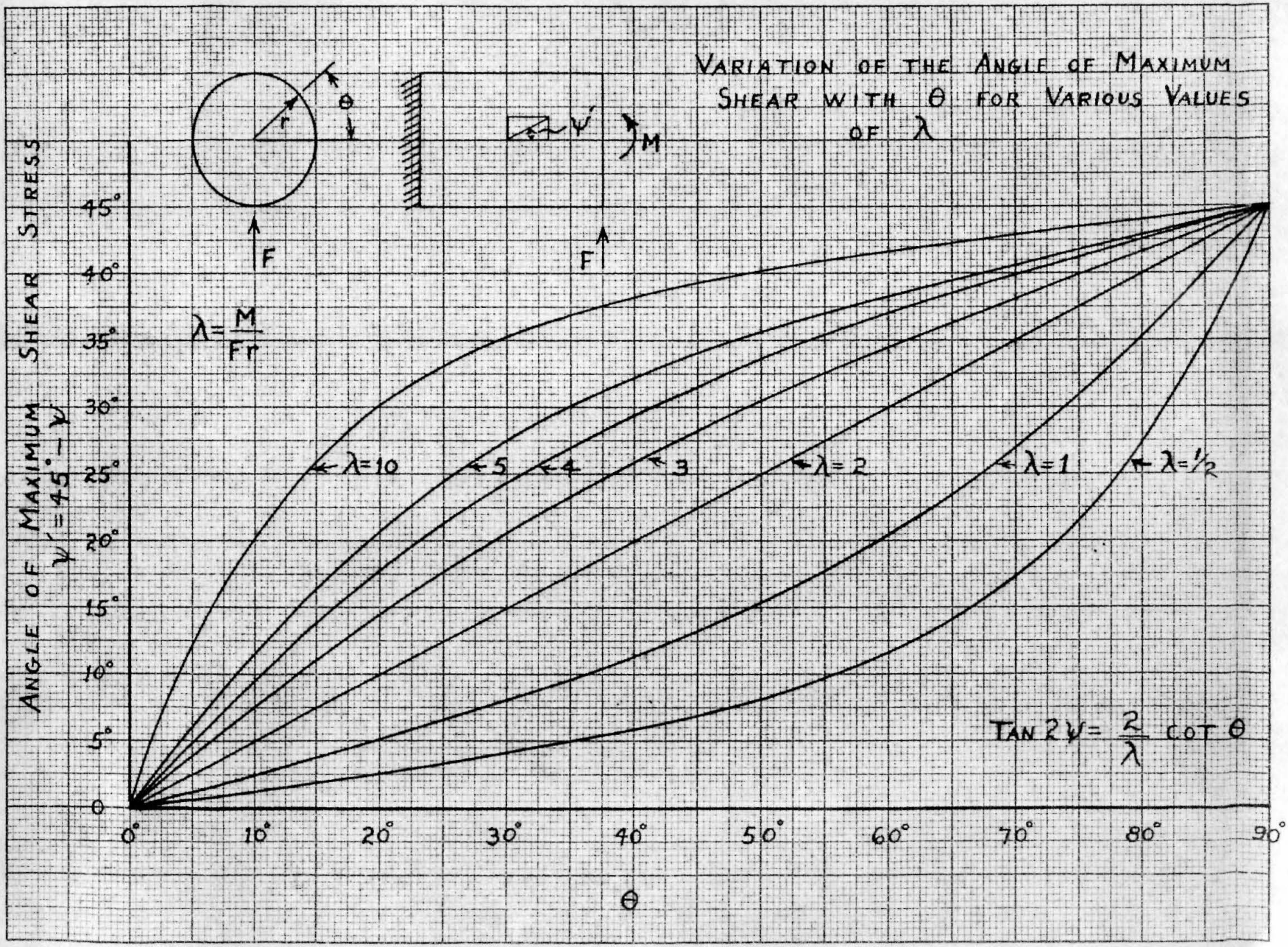
VARIATION OF THE ANGLE OF MAXIMUM SHEAR WITH θ FOR VARIOUS VALUES OF λ
ANGLE OF MAXIMUM SHEAR STRESS ψ' = 45° − ψ
θ
r
F
F
ψ'
M
λ = M/Fr
λ=10
5
4
3
λ=2
λ=1
λ=½
TAN 2ψ = 2/λ COT θ
45°
40°
35°
30°
25°
20°
15°
10°
5°
0
0°
10°
20°
30°
40°
50°
60°
70°
80°
90°
θ

FIG. 5.

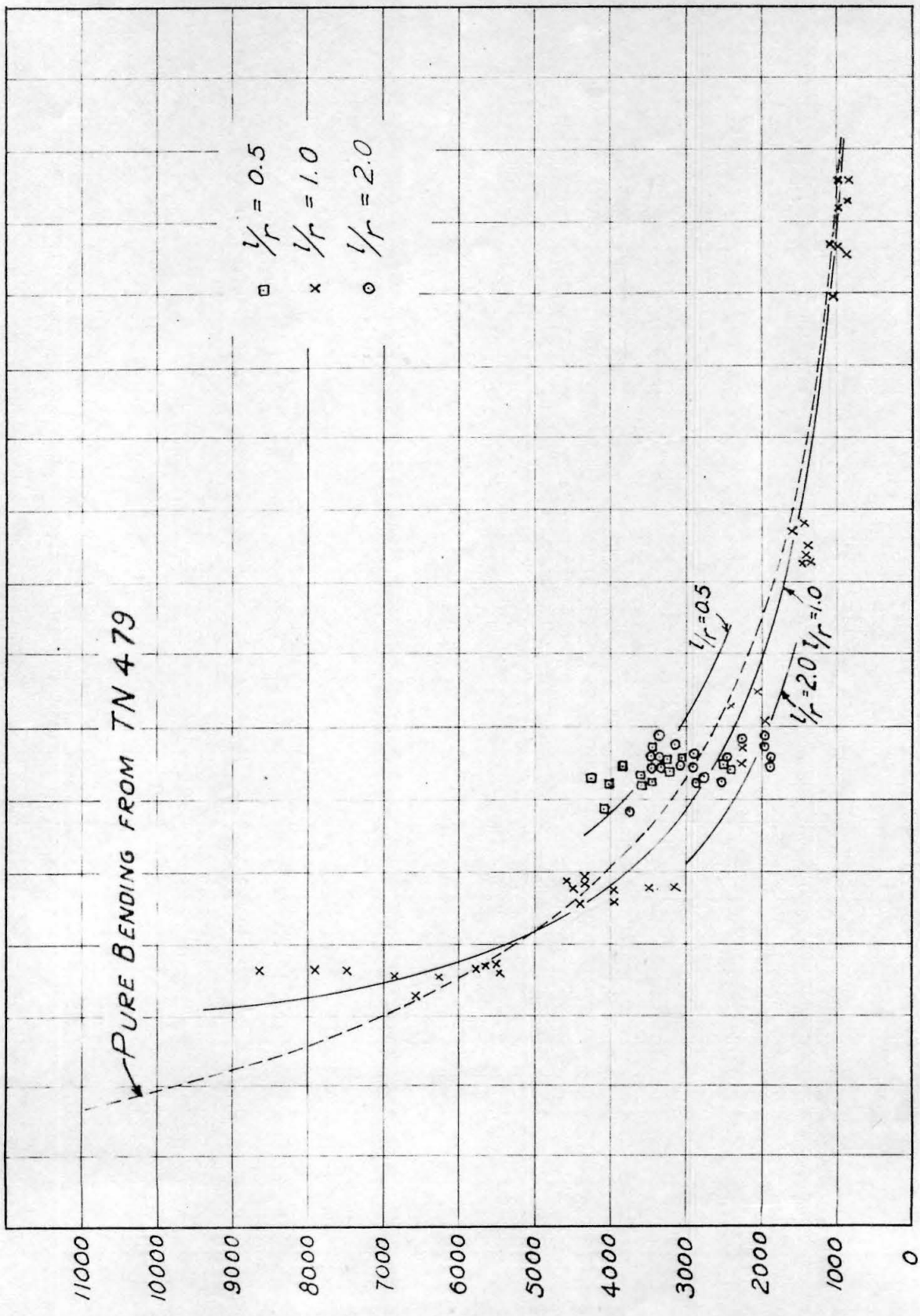

Fig. 6. Critical Shearing Stress of Curved 17ST Duralumin Sheet under Combined Bending plus Shear.

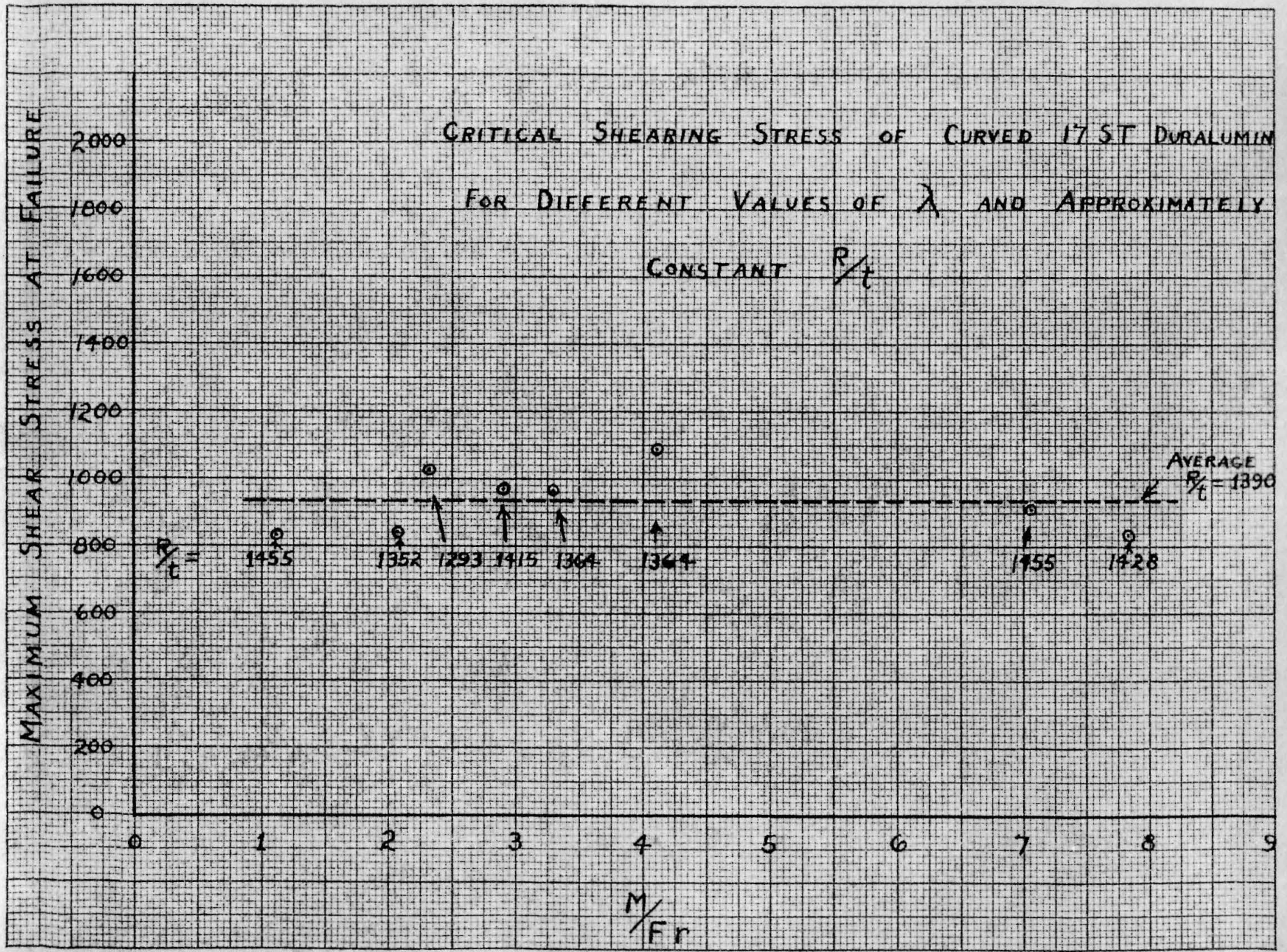
Critical Shearing Stress of Curved 17 ST Duralumin
For Different Values of λ and Approximately
Constant R/t
Maximum Shear Stress at Failure
2000
1800
1600
1400
1200
1000
800
600
400
200
0
R/t =
1455
1352
1293
1415
1364
1364
1455
1428
Average R/t = 1390
0
1
2
3
4
5
6
7
8
9
M/Fr

Fig. 7.

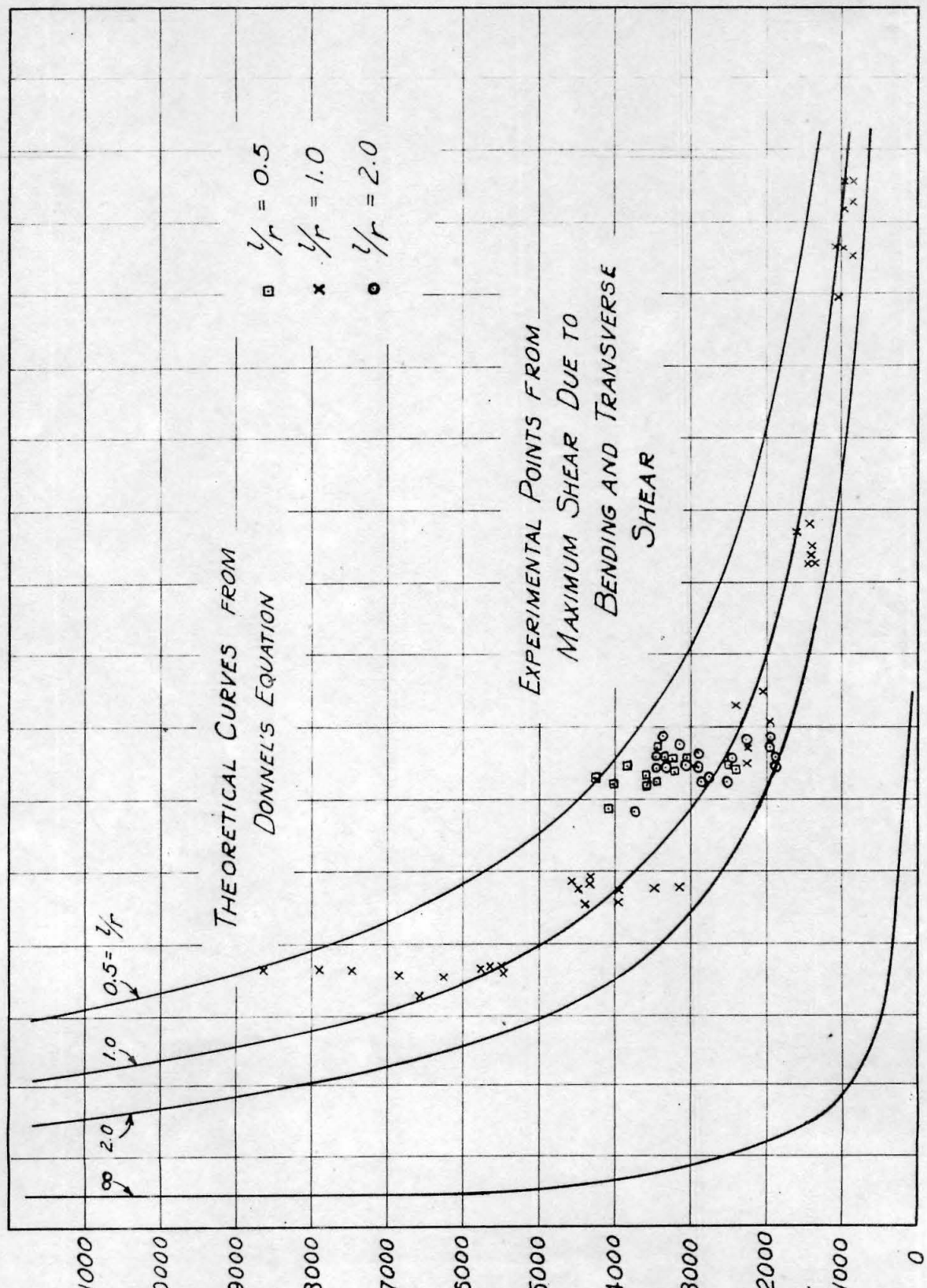

Fig. 8. Correlation Between Theoretical Critical Torsional Stress and Critical Shearing Stress due to Combined Bending plus Shear.

RATIO OF EXPERIMENTAL σ_c AND σ_b TO THEORETICAL VALUE PLOTTED AGAINST R/t
× LUNDQUIST'S TESTS COMPRESSION ON DURAL CYLINDERS
⊠ LUNDQUIST'S TESTS BENDING ON DURAL CYLINDERS
CURVE FROM HOWLAND'S COMBINED STRESS CURVE
$\sigma_{crit} \frac{R\sqrt{3(1-\nu^2)}}{Et}$
1.0
.9
.8
.7
.6
.5
.4
.3
.2
.1
0
0
500
1000
1500
R/t

FIG. 9.

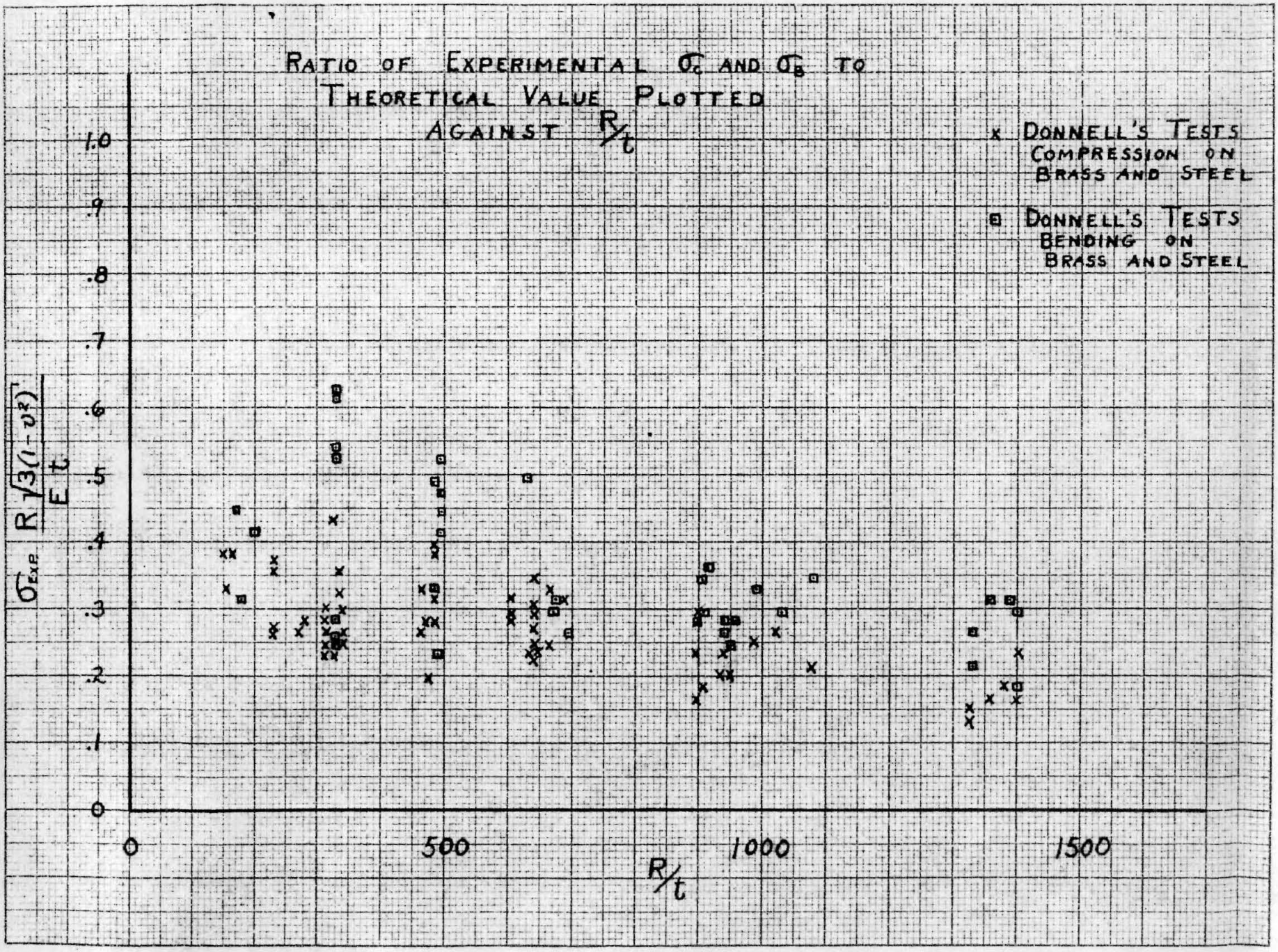
RATIO OF EXPERIMENTAL σ_c AND σ_b TO THEORETICAL VALUE PLOTTED AGAINST R/t
x DONNELL'S TESTS COMPRESSION ON BRASS AND STEEL
□ DONNELL'S TESTS BENDING ON BRASS AND STEEL
$\sigma_{exp} \frac{R\sqrt{3(1-\nu^2)}}{Et}$
1.0
.9
.8
.7
.6
.5
.4
.3
.2
.1
0
0
500
1000
1500
R/t

FIG. 10

VARIATION OF SECTION-MODULUS
AGAINST CROSS-SECTION DEFORMATION
FOR A CIRCULAR CYLINDER
RATIO OF SECTION-MODULUS
N/N°
1.00
.98
.96
.94
.92
.90
.88
.86
.84
.82
.80
0
.04
.08
.12
.16
.20
.24
.28
.32
w/R
DEGREE OF FLATTENING
w
R
t
σ Actual = Z/Z° x σ°
Z° = 1/π R² t
σ° = Z° M

FIG. 11.

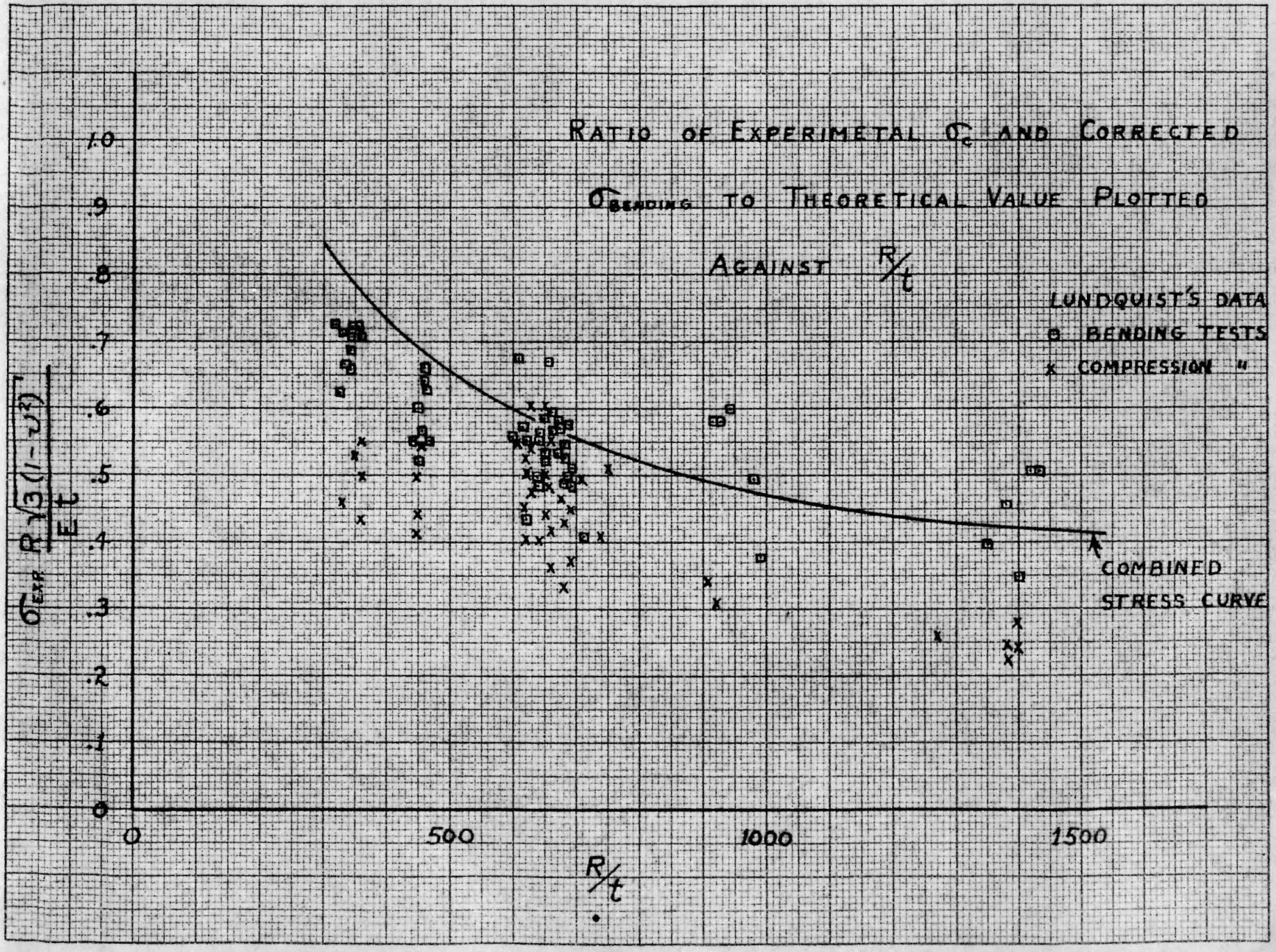
RATIO OF EXPERIMETAL σ_c AND CORRECTED
$\sigma_{BENDING}$ TO THEORETICAL VALUE PLOTTED
AGAINST R/t
LUNDQUIST'S DATA
□ BENDING TESTS
× COMPRESSION "
COMBINED
STRESS CURVE
$\sigma_{EXP} \frac{R}{E} \frac{\sqrt{3(1-\nu^2)}}{t}$
1.0
.9
.8
.7
.6
.5
.4
.3
.2
.1
0
0
500
1000
1500
R/t

FIG 13

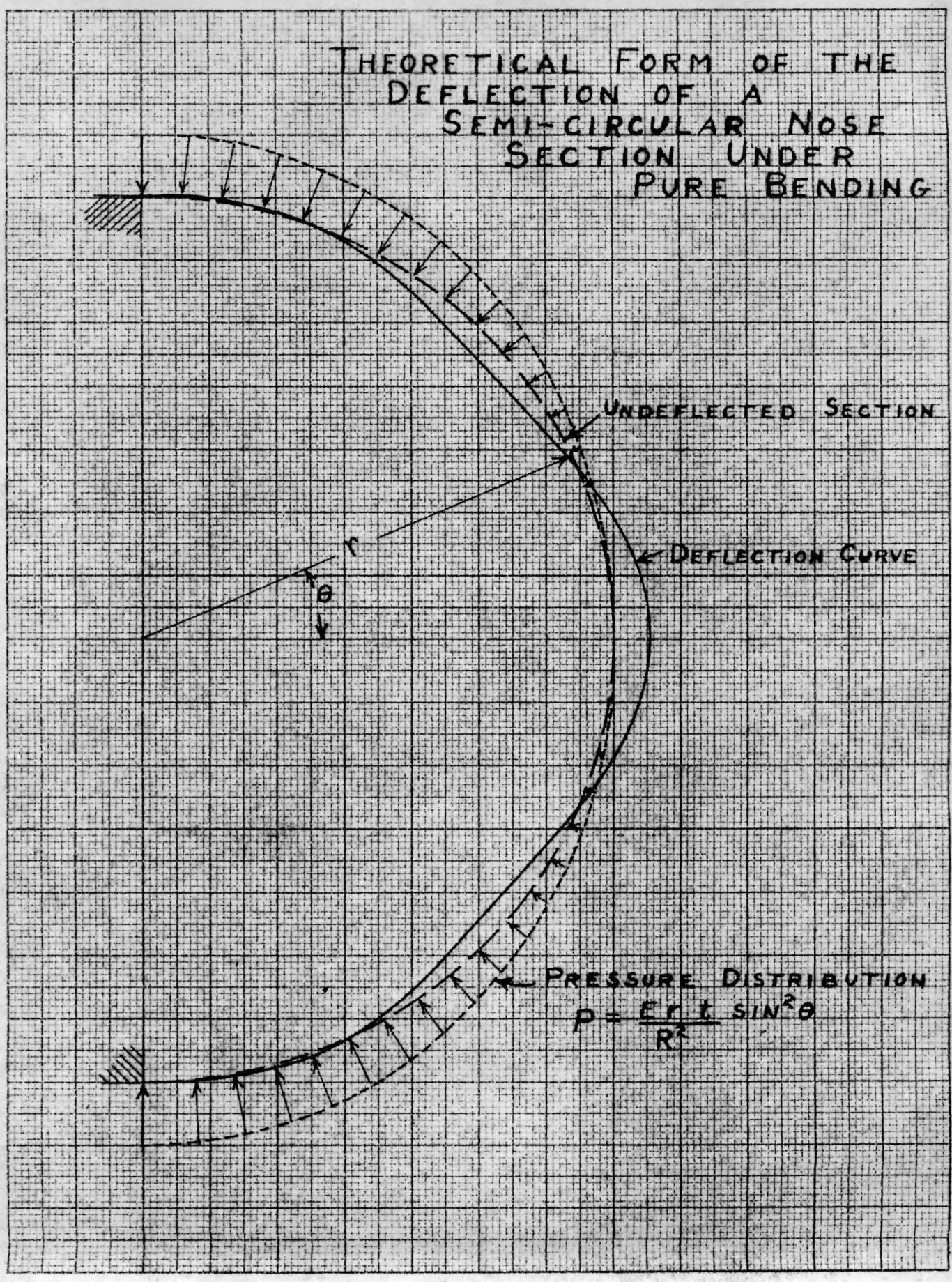
THEORETICAL FORM OF THE DEFLECTION OF A SEMI-CIRCULAR NOSE SECTION UNDER PURE BENDING
UNDEFLECTED SECTION
DEFLECTION CURVE
r
θ
PRESSURE DISTRIBUTION
$P = \frac{E r t}{R^2} \sin^2\theta$

FIG. 13

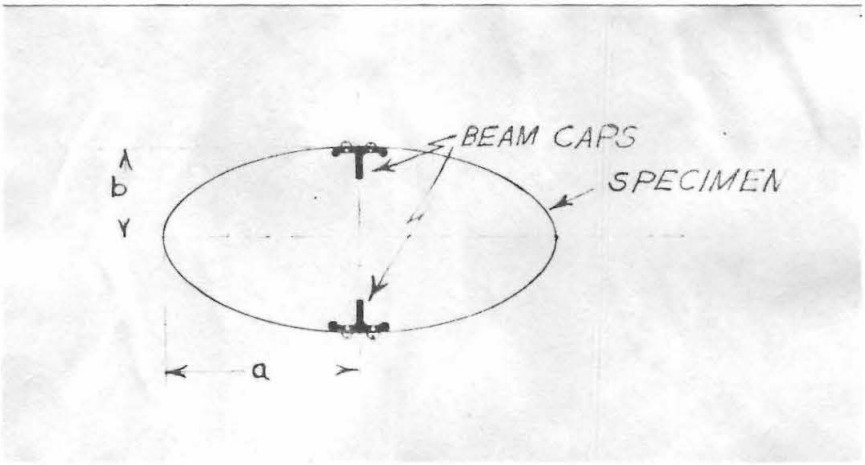

FIG. 14

Cross-section of specimen showing beam caps

FIG. 15

View of beam showing gusset plates in corners. Note no web, therefore large shear deflections

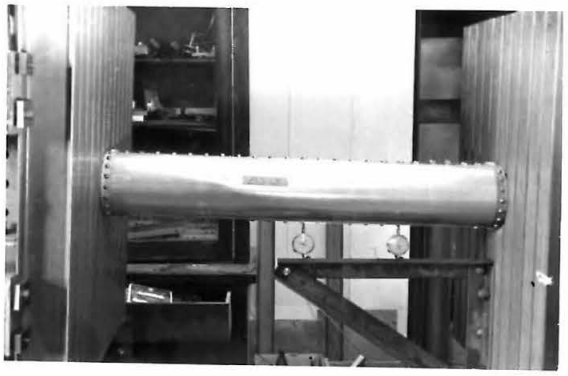

FIG. 16

Method of mounting dial gauges in order to get difference in deflection

FIG. 17

Artificial beam caps

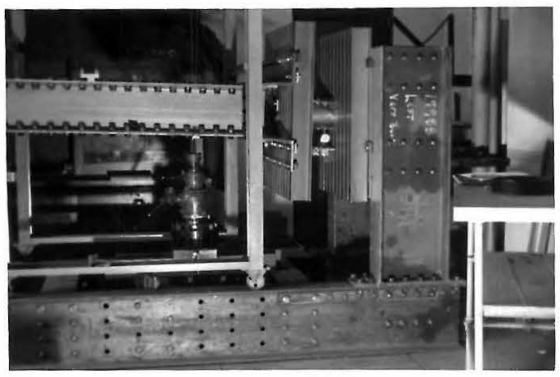

FIG. 18.

Side view of testing machine with short specimen in it.

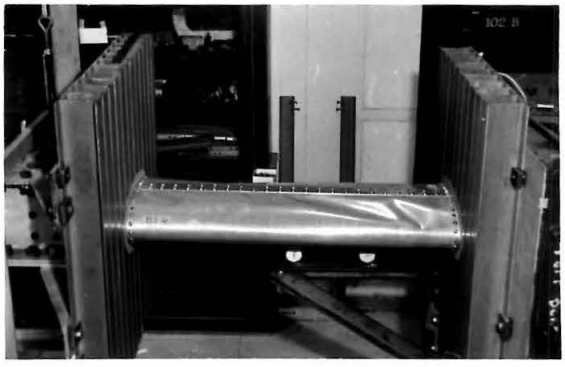

FIG. 19.

Combined bending and shear of semi-elliptical nose section. M/Vb = 4.72, a/b = 2, t = .020, length = 34" Note how nose stops wave.

FIG. 20

Combined bending and shear of semi-elliptical nose section. M/Vb = 6.05, a/b = 2, t = .020", length = 34", at buckling load.

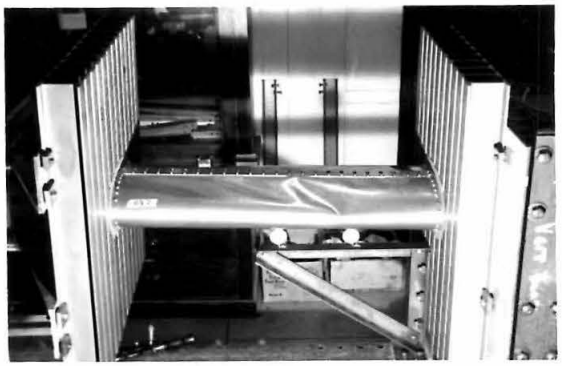

FIG. 21

Combined bending and shear of semi-elliptical nose section. M/Vb = 6.05, a/b = 2, t = .020", length = 34", at failure load.
Note diagonal nature of waves.

FIG. 22

Combined bending and shear of semi-elliptical nose section. M/Vb = 7.32, a/b = 2, t = .020", length = 34". Note compression buckle near fixed end where moment is largest and diagonal shear near loaded end.

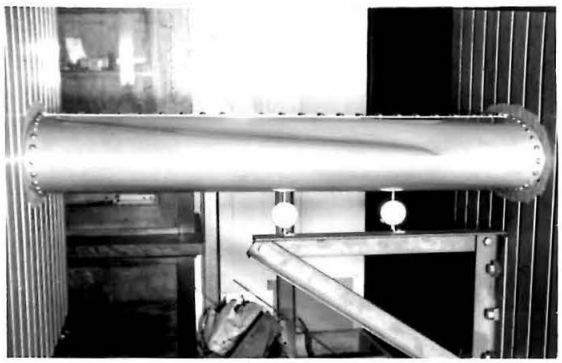

FIG. 23

Combined bending and shear of semi-elliptical nose section. M/Vb = 3.42, a/b = 2, t = .020", length = 34". Rather large vertical shear, note similarity with Fig. 24 which was loaded under pure shear (torsion).

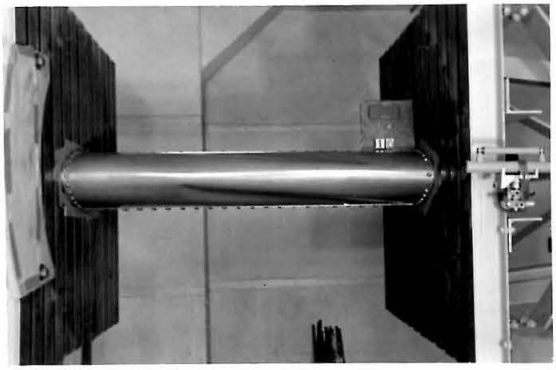

FIG. 24

Torsion of semi-elliptical nose section. a/b = 2, t = .020", length = 34".

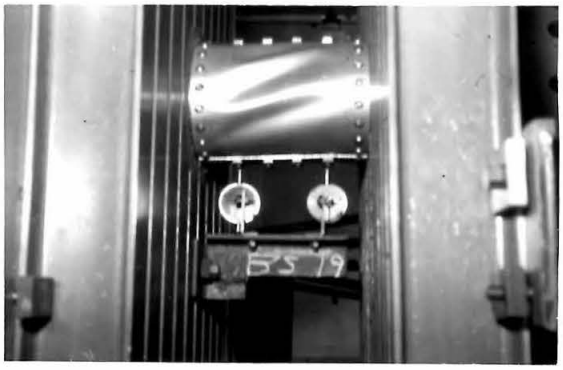

FIG. 25.

Combined bending and shear of semi-circular nose section. M/Vr = 1.39, t = .0165", length = 6.5". Force up on right side, note waves on bottom half of specimen as well as on top.

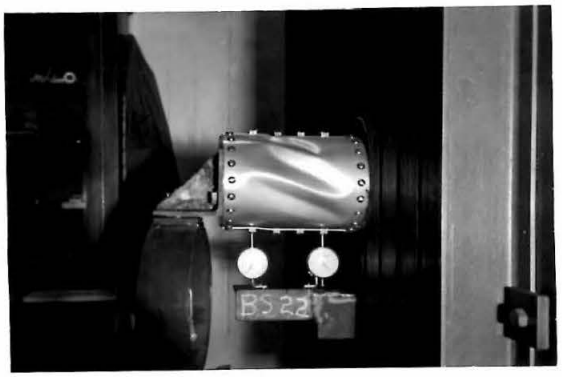

FIG. 26.

Combined bending and shear of semi-circular nose section. M/Vr = 0.93, t = .0165", length = 6.5". Force up on left side.

FIG. 27.

Combined bending and shear of semi-circular nose section. Large moment M/Vr = 8.01, t = .0165", length = 6.5". Note small compression buckle only on top side near fixed end.

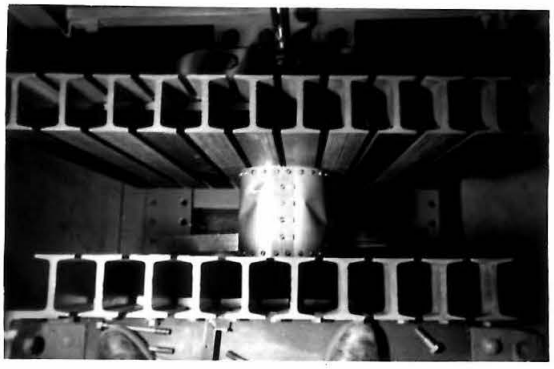

FIG. 28.

Top view of specimen similar to that seen in Fig. 27. Note symmetry.

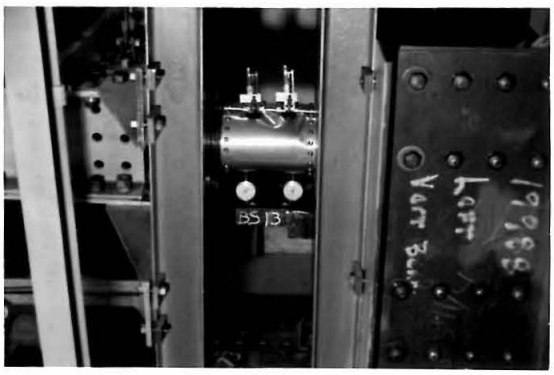

FIG. 29.

Specimen with extensometers on top, enabling a check of calculated maximun bending stresses.

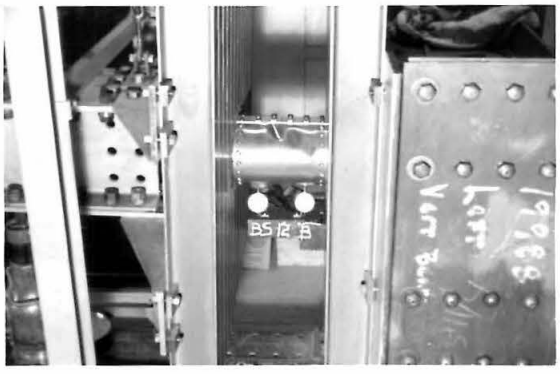

FIG. 30.

Combined bending and shear of a semi-circular nose section. M/Vr = 2.98, t = .0215", length = 6.5". Note three stair-step compression buckles.

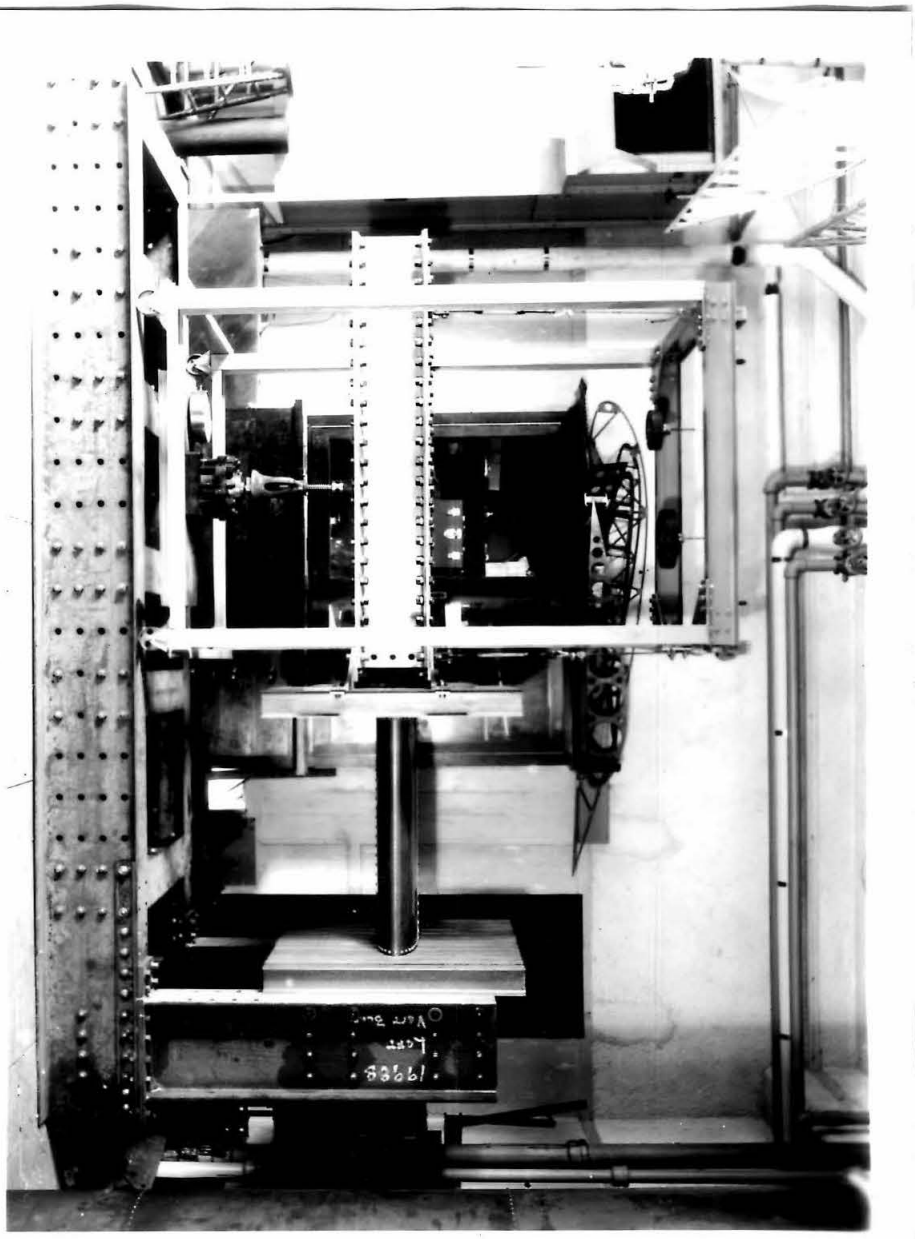

FIG. 31

Side view of testing machine. Notice constant force support cables for loading head.

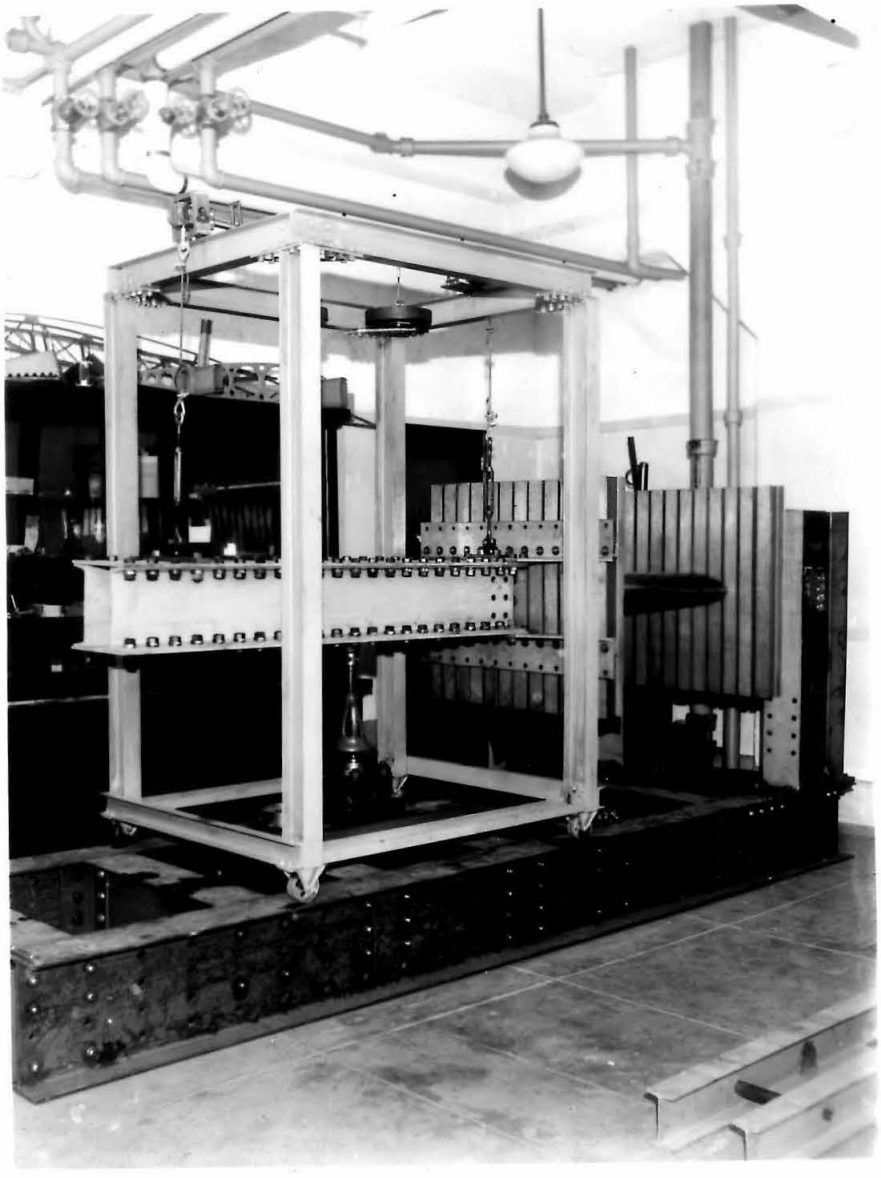

FIG. 32
3/4 side view of testing machine.

FIG. 33
Close up of loading head support system.

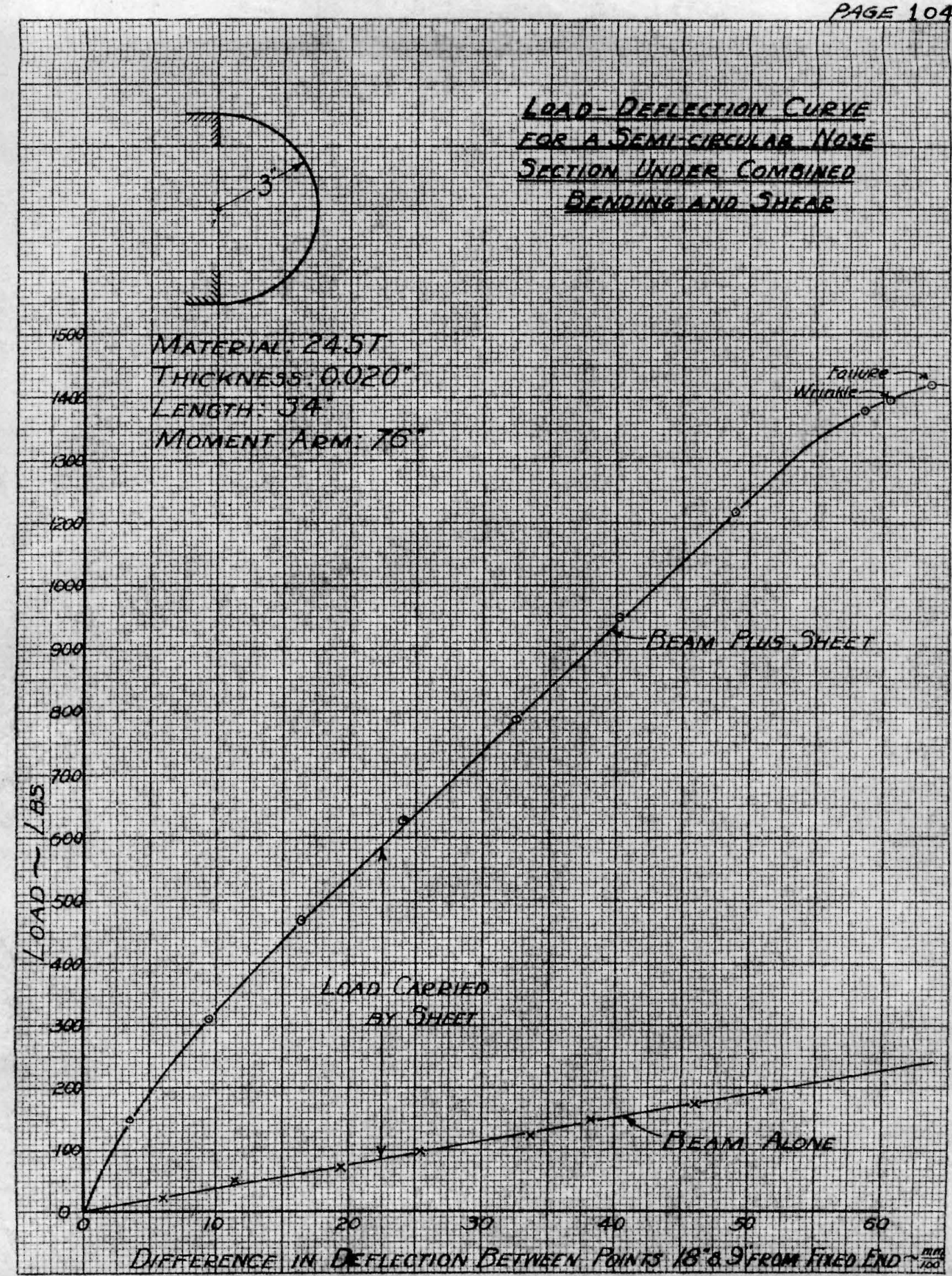
LOAD - DEFLECTION CURVE FOR A SEMI-CIRCULAR NOSE SECTION UNDER COMBINED BENDING AND SHEAR
3"
MATERIAL: 24ST
THICKNESS: 0.020"
LENGTH: 34"
MOMENT ARM: 76"
Failure
Wrinkle
BEAM PLUS SHEET
LOAD CARRIED BY SHEET
BEAM ALONE
LOAD — LBS
1500
1400
1300
1200
1000
900
800
700
600
500
400
300
200
100
0
0
10
20
30
40
50
60
DIFFERENCE IN DEFLECTION BETWEEN POINTS 18" & 9" FROM FIXED END — mm/100

FIG. 34.

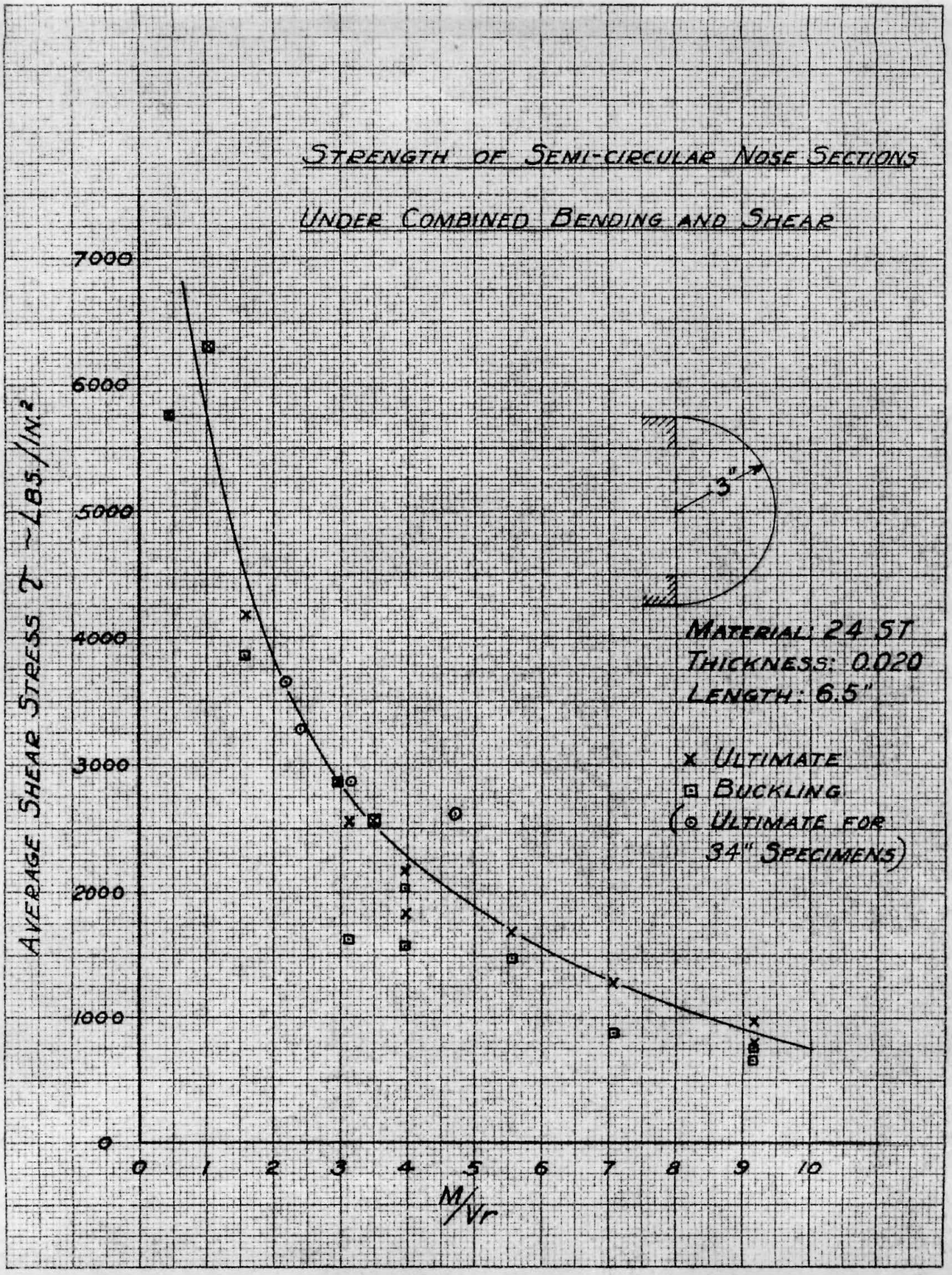
STRENGTH OF SEMI-CIRCULAR NOSE SECTIONS
UNDER COMBINED BENDING AND SHEAR
AVERAGE SHEAR STRESS τ ~ LBS./IN.²
7000
6000
5000
4000
3000
2000
1000
0
0 1 2 3 4 5 6 7 8 9 10
M/Vr
3"
MATERIAL: 24 ST
THICKNESS: 0.020
LENGTH: 6.5"
× ULTIMATE
□ BUCKLING
(⊙ ULTIMATE FOR 34" SPECIMENS)

FIG. 35.

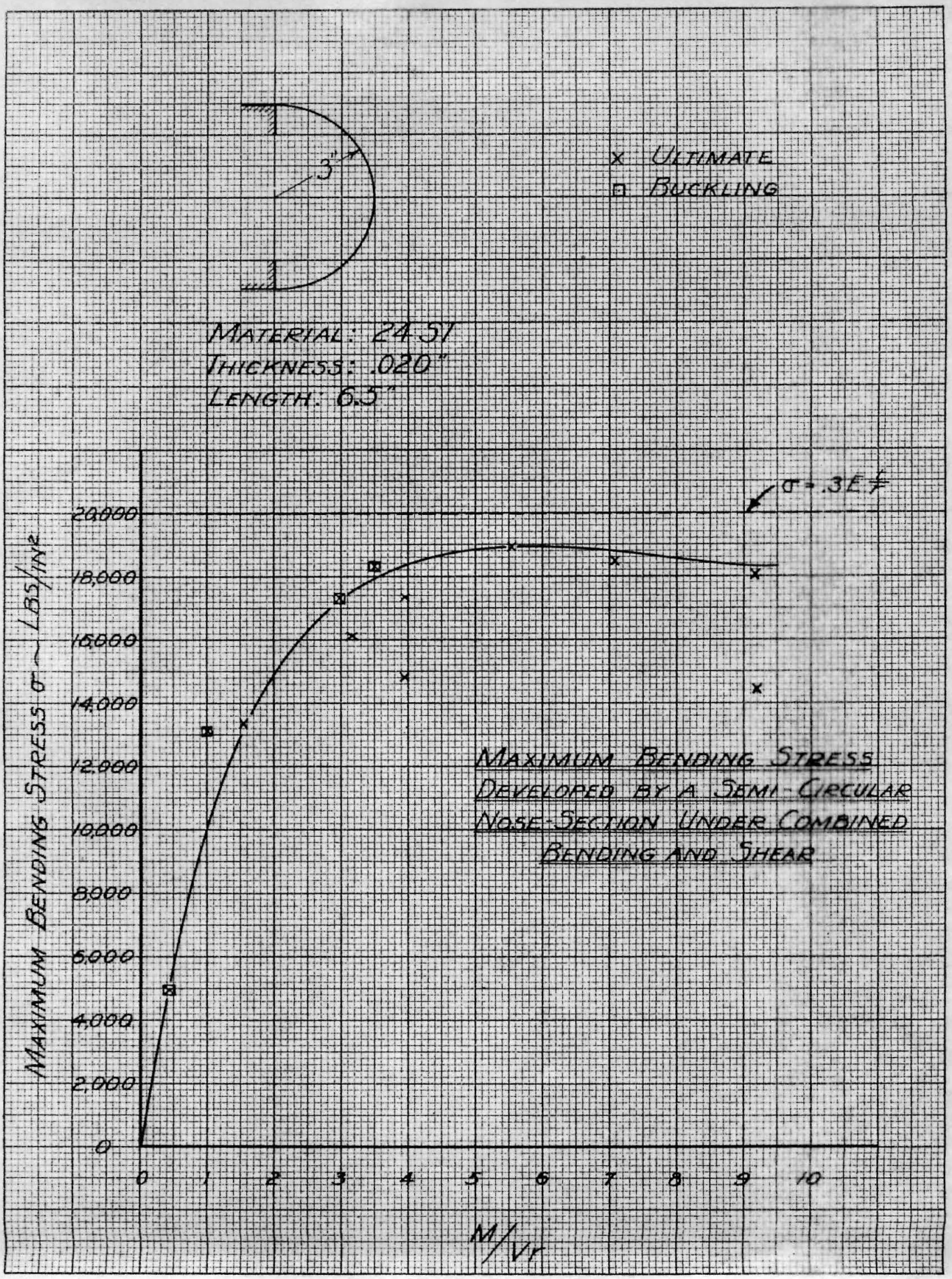
3"
× ULTIMATE
□ BUCKLING
MATERIAL: 24 ST
THICKNESS: .020"
LENGTH: 6.3"
σ = .3 E f
MAXIMUM BENDING STRESS DEVELOPED BY A SEMI-CIRCULAR NOSE-SECTION UNDER COMBINED BENDING AND SHEAR
MAXIMUM BENDING STRESS σ ~ LBS/IN²
20,000
18,000
16,000
14,000
12,000
10,000
8,000
6,000
4,000
2,000
0
0 1 2 3 4 5 6 7 8 9 10
M/Vr

FIG. 36.

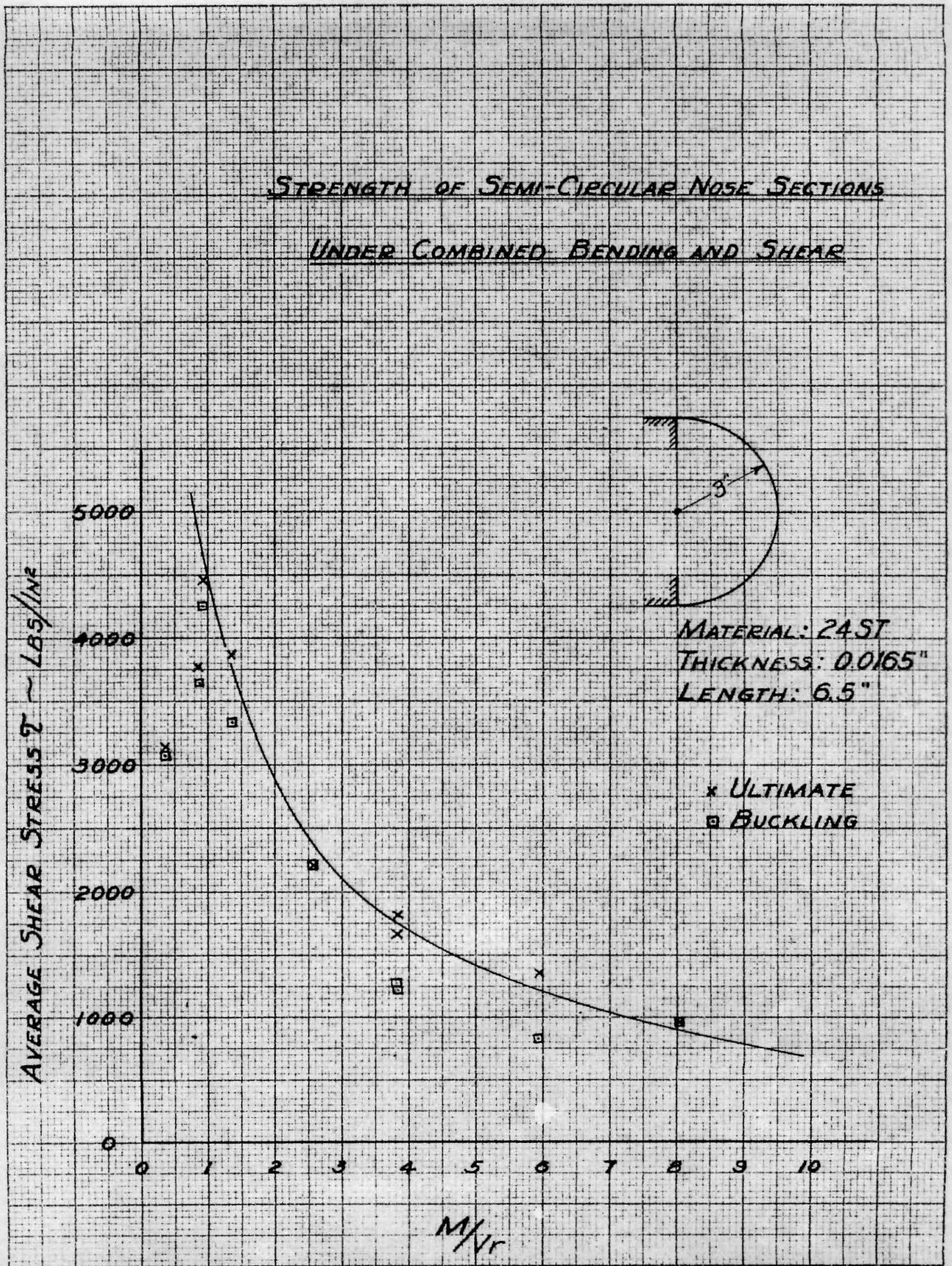
STRENGTH OF SEMI-CIRCULAR NOSE SECTIONS
UNDER COMBINED BENDING AND SHEAR
3"
MATERIAL: 24ST
THICKNESS: 0.0165"
LENGTH: 6.5"
x ULTIMATE
□ BUCKLING
AVERAGE SHEAR STRESS τ ~ LBS/IN²
5000
4000
3000
2000
1000
0
0
1
2
3
4
5
6
7
8
9
10
M/Mr

FIG. 37.

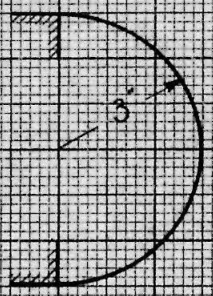

× ULTIMATE
□ BUCKLING

MATERIAL: 24S1
THICKNESS: .0165
LENGTH: 6.3"

MAXIMUM BENDING STRESS σ ~ LBS/IN²

20,000
18,000
16,000
14,000
12,000
10,000
8,000
6,000
4,000
2,000
0

σ = .3E t/r

0 1 2 3 4 5 6 7 8 9 10

M/Vr

MAXIMUM BENDING STRESS DEVELOPED BY A SEMI-CIRCULAR NOSE SECTION UNDER COMBINED BENDING AND SHEAR

FIG. 38.

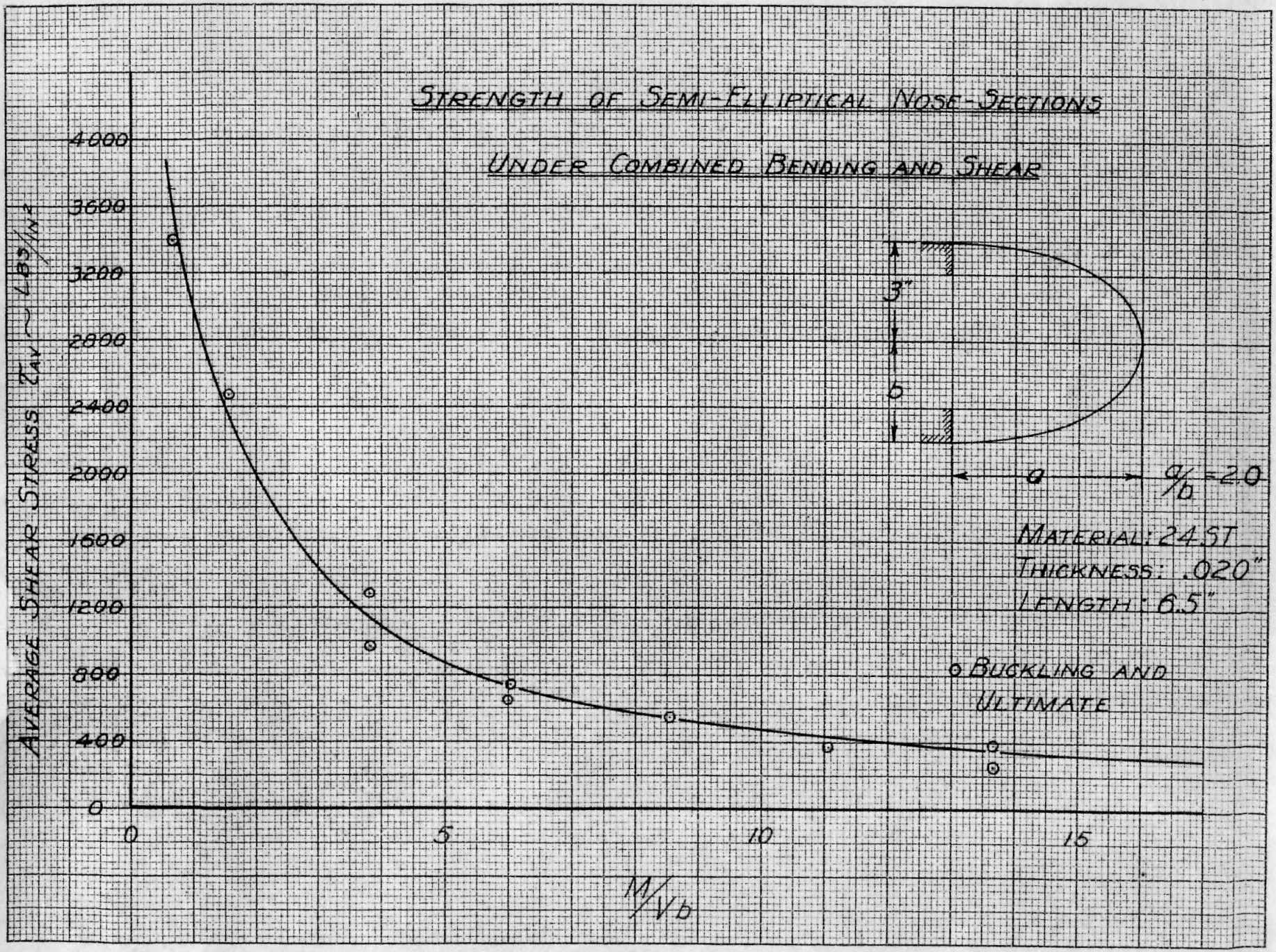
STRENGTH OF SEMI-ELLIPTICAL NOSE-SECTIONS
UNDER COMBINED BENDING AND SHEAR
AVERAGE SHEAR STRESS τ_{av} ~ LBS/IN²
4000
3600
3200
2800
2400
2000
1600
1200
800
400
0
0
5
10
15
M/Vb
3"
b
a
a/b = 2.0
MATERIAL: 24 ST
THICKNESS: .020"
LENGTH: 6.5"
BUCKLING AND ULTIMATE

FIG. 39.

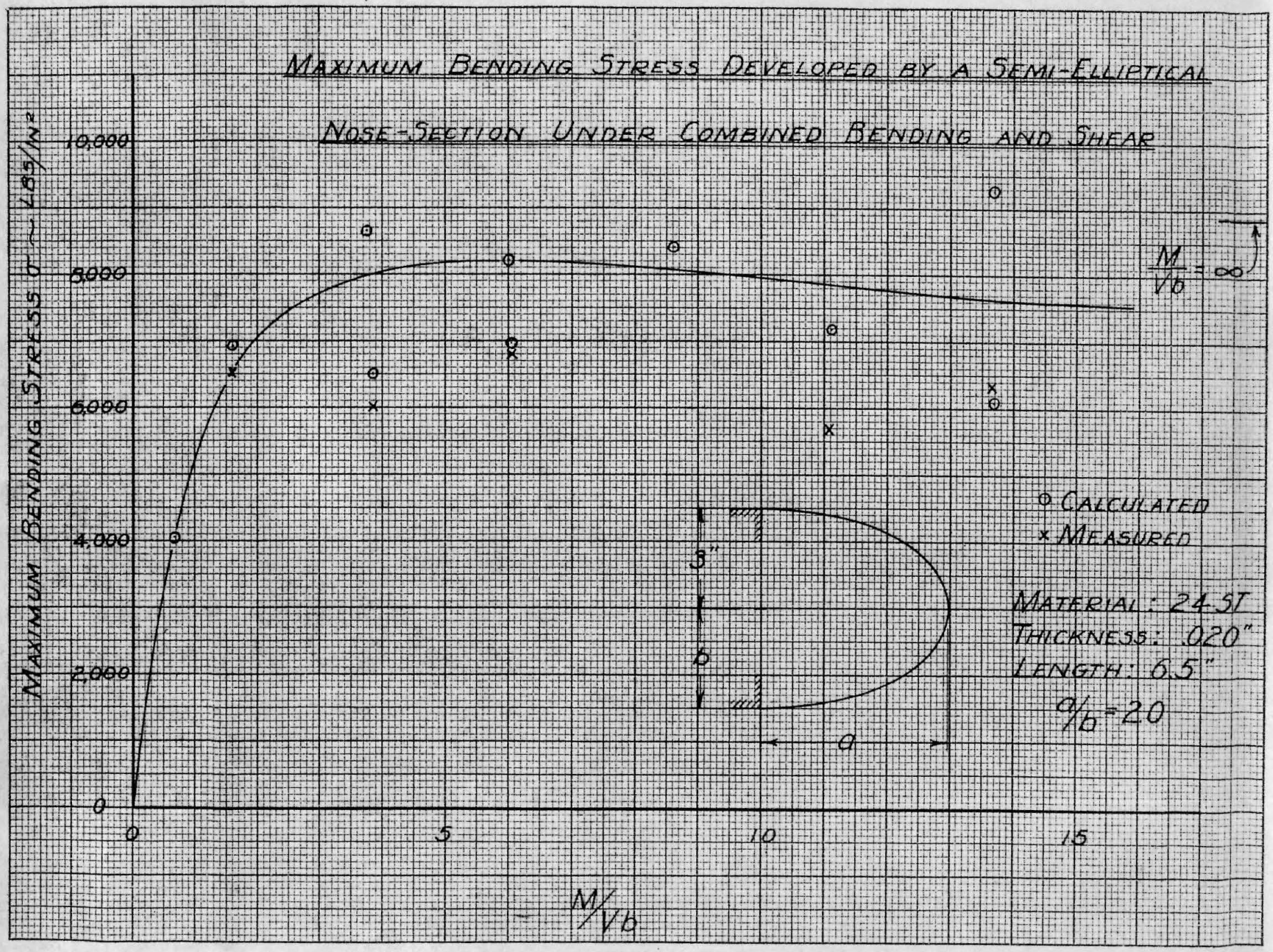
MAXIMUM BENDING STRESS DEVELOPED BY A SEMI-ELLIPTICAL NOSE-SECTION UNDER COMBINED BENDING AND SHEAR
MAXIMUM BENDING STRESS σ ~ LBS/IN²
10,000
8,000
6,000
4,000
2,000
0
0
5
10
15
M/Vb
M/Vb = ∞
CALCULATED
MEASURED
MATERIAL: 24 ST
THICKNESS: .020"
LENGTH: 6.5"
a/b = 20
3"
b
a

FIG. 40.

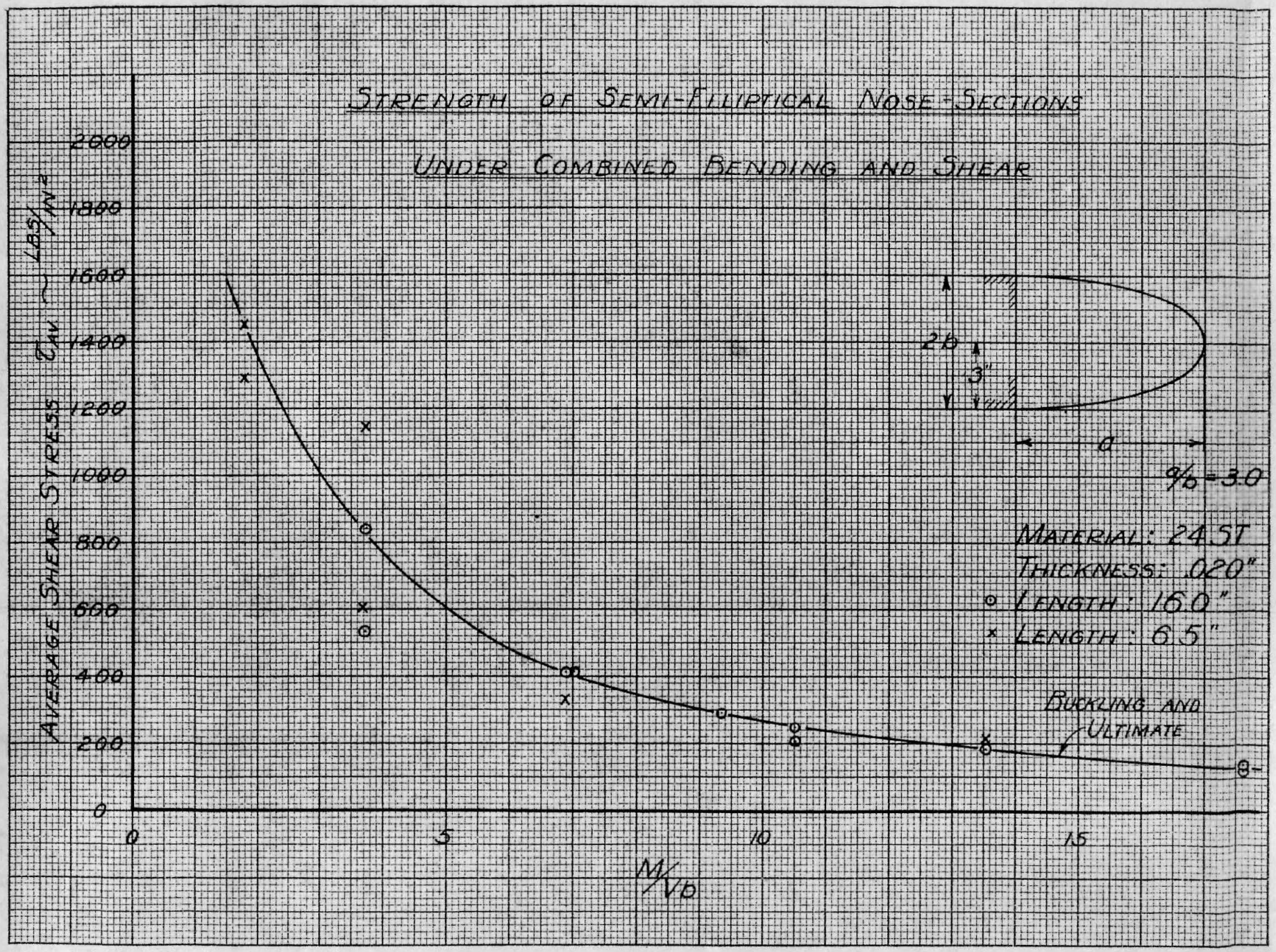
STRENGTH OF SEMI-ELLIPTICAL NOSE-SECTIONS
UNDER COMBINED BENDING AND SHEAR
AVERAGE SHEAR STRESS f_{sav} LBS/IN²
2000
1800
1600
1400
1200
1000
800
600
400
200
0
0
5
10
15
M/Vb
2b
3"
a
a/b = 3.0
MATERIAL: 24 ST
THICKNESS: .020"
LENGTH: 16.0"
LENGTH: 6.5"
BUCKLING AND ULTIMATE

FIG. 41.

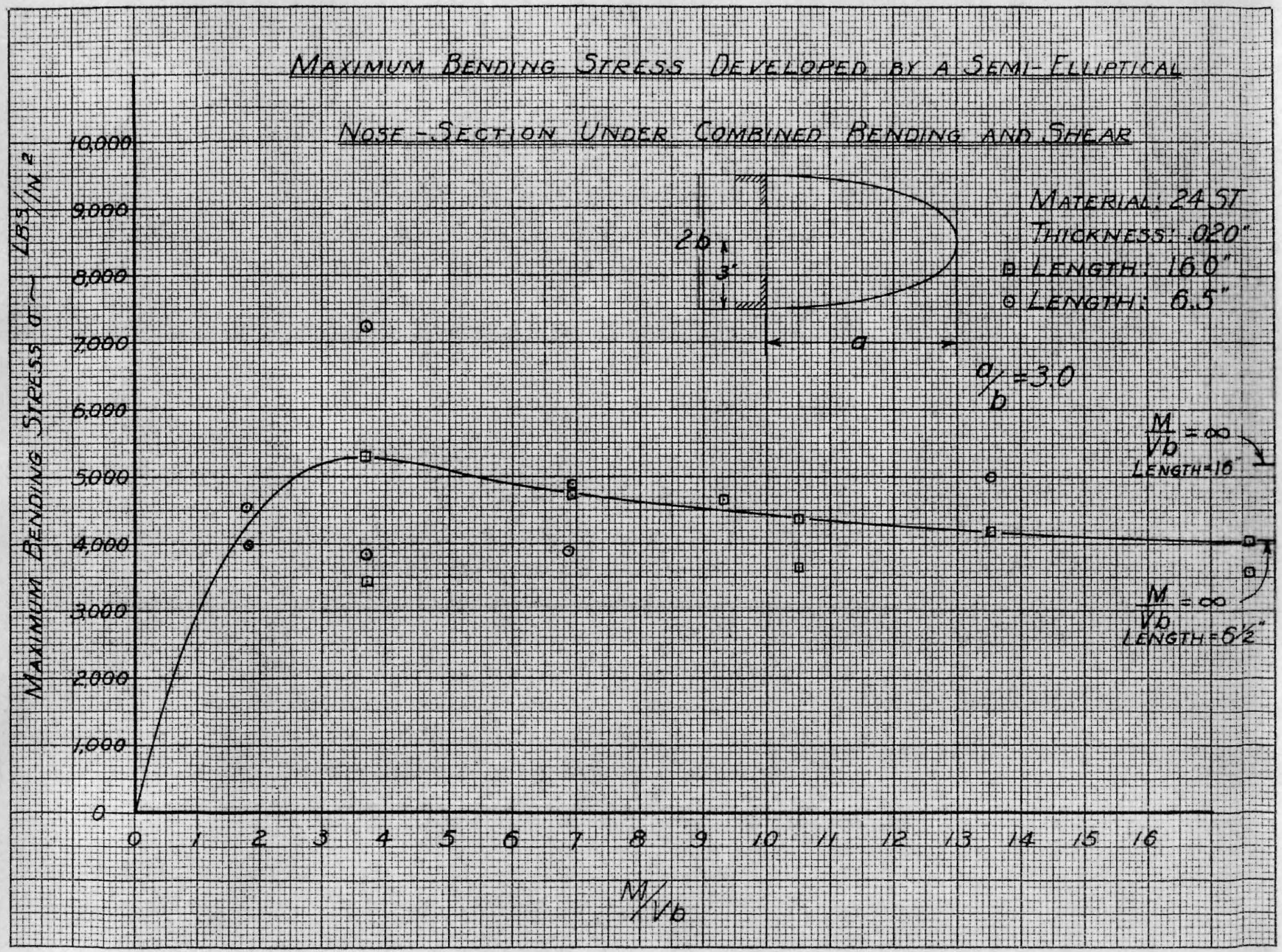
MAXIMUM BENDING STRESS DEVELOPED BY A SEMI-ELLIPTICAL
NOSE-SECTION UNDER COMBINED BENDING AND SHEAR
MATERIAL: 24 ST
THICKNESS: .020"
LENGTH: 16.0"
LENGTH: 6.5"
2b
3"
a
a/b = 3.0
M/Vb = ∞
LENGTH = 16"
M/Vb = ∞
LENGTH = 6½"
MAXIMUM BENDING STRESS σ — LBS/IN²
10,000
9,000
8,000
7,000
6,000
5,000
4,000
3,000
2,000
1,000
0
0 1 2 3 4 5 6 7 8 9 10 11 12 13 14 15 16
M/Vb

FIG. 42.

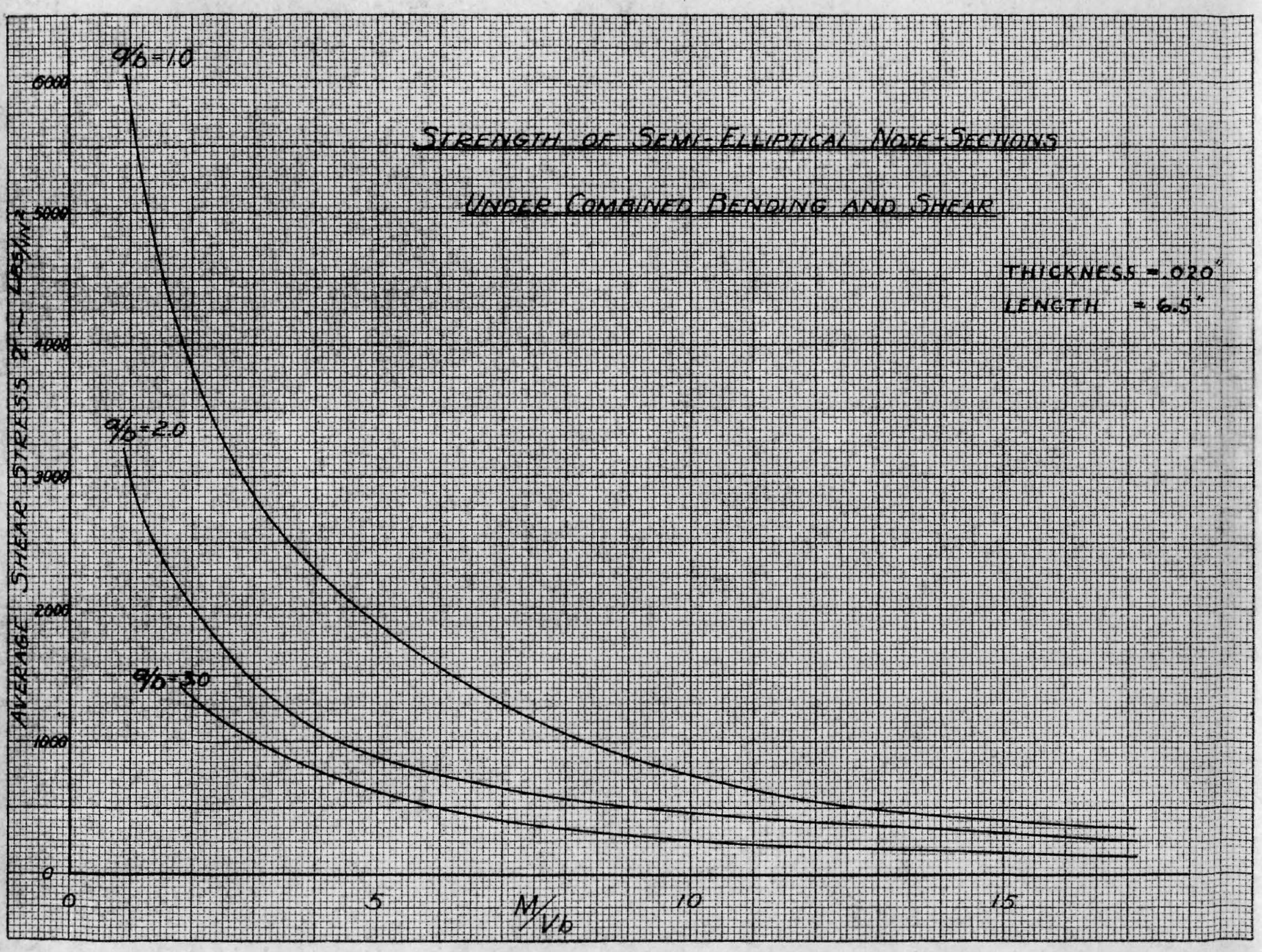
STRENGTH OF SEMI-ELLIPTICAL NOSE-SECTIONS
UNDER COMBINED BENDING AND SHEAR
THICKNESS = .020"
LENGTH = 6.5"
q/b = 1.0
q/b = 2.0
q/b = 3.0
AVERAGE SHEAR STRESS f = lbs/in²
6000
5000
4000
3000
2000
1000
0
0
5
10
15
M/Vb

FIG. 43.

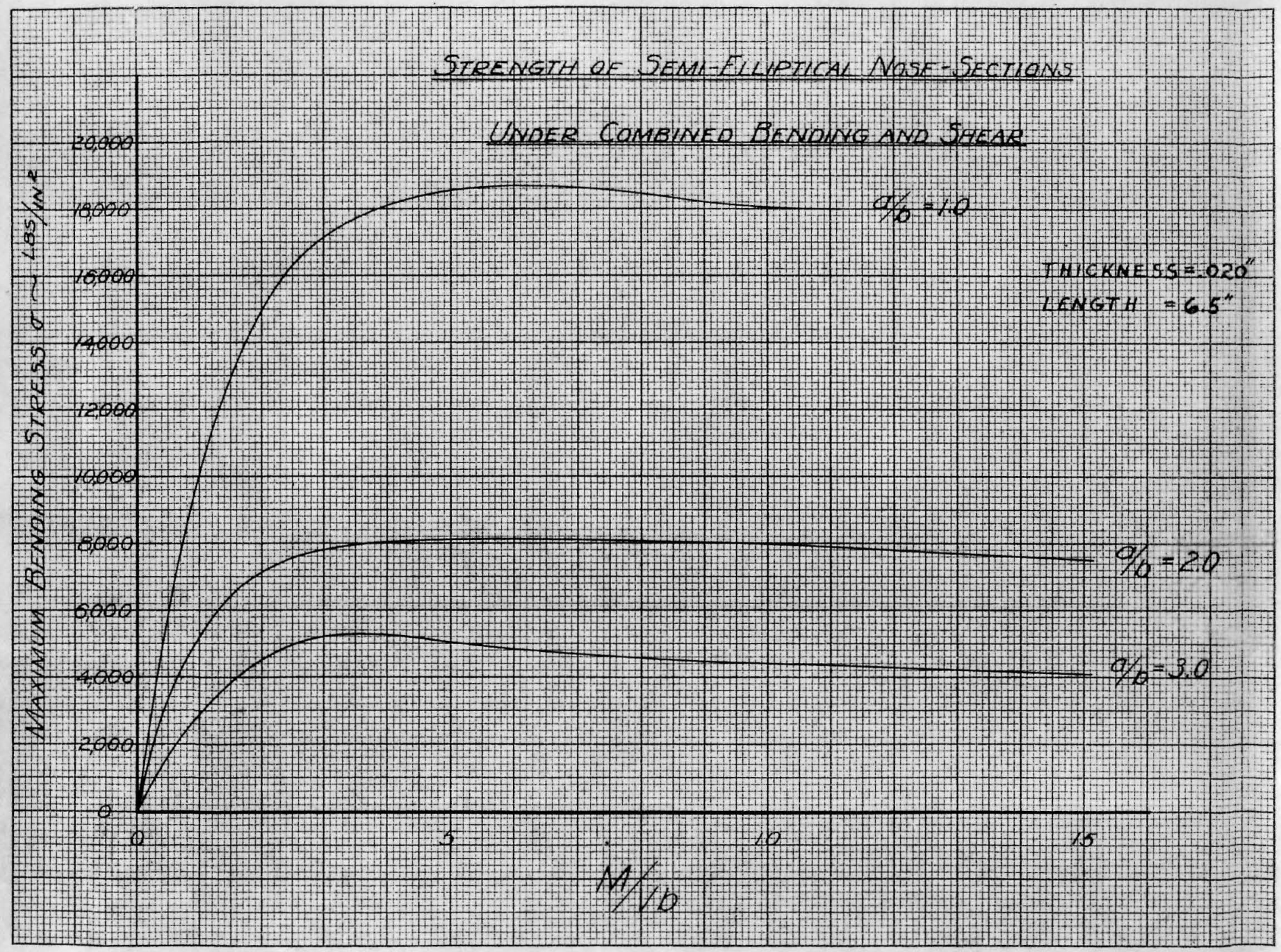
STRENGTH OF SEMI-ELLIPTICAL NOSE-SECTIONS
UNDER COMBINED BENDING AND SHEAR
MAXIMUM BENDING STRESS σ ~ LBS/IN²
20,000
18,000
16,000
14,000
12,000
10,000
8,000
6,000
4,000
2,000
0
0
5
10
15
M/Vb
a/b = 1.0
a/b = 2.0
a/b = 3.0
THICKNESS = .020"
LENGTH = 6.5"

FIG. 44.

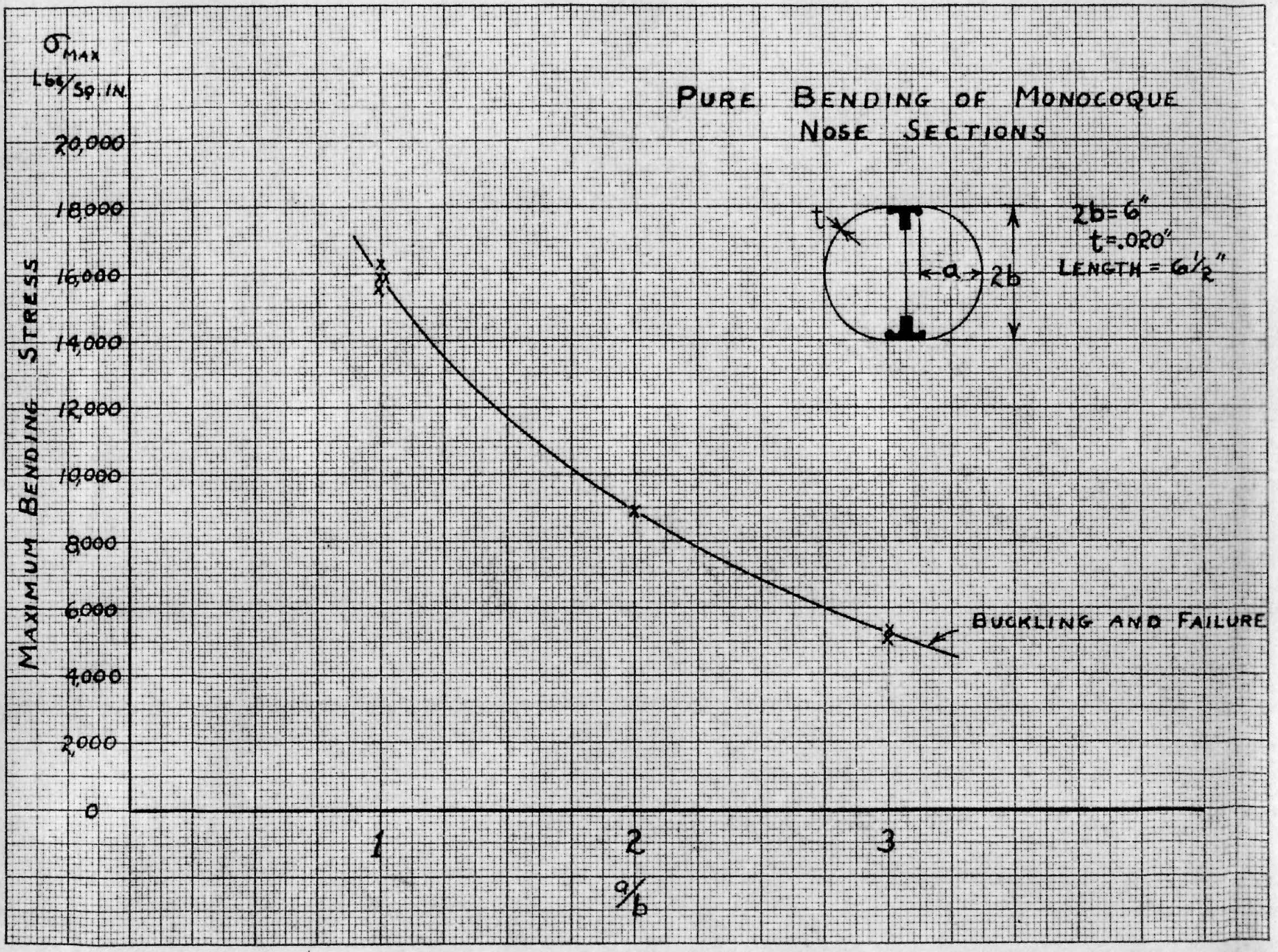
PURE BENDING OF MONOCOQUE NOSE SECTIONS
σ_{MAX} LBS/SQ. IN.
MAXIMUM BENDING STRESS
20,000
18,000
16,000
14,000
12,000
10,000
8000
6,000
4,000
2,000
0
1
2
3
a/b
t
a
2b
2b=6"
t=.020"
LENGTH = 6 1/2"
BUCKLING AND FAILURE

FIG. 45.

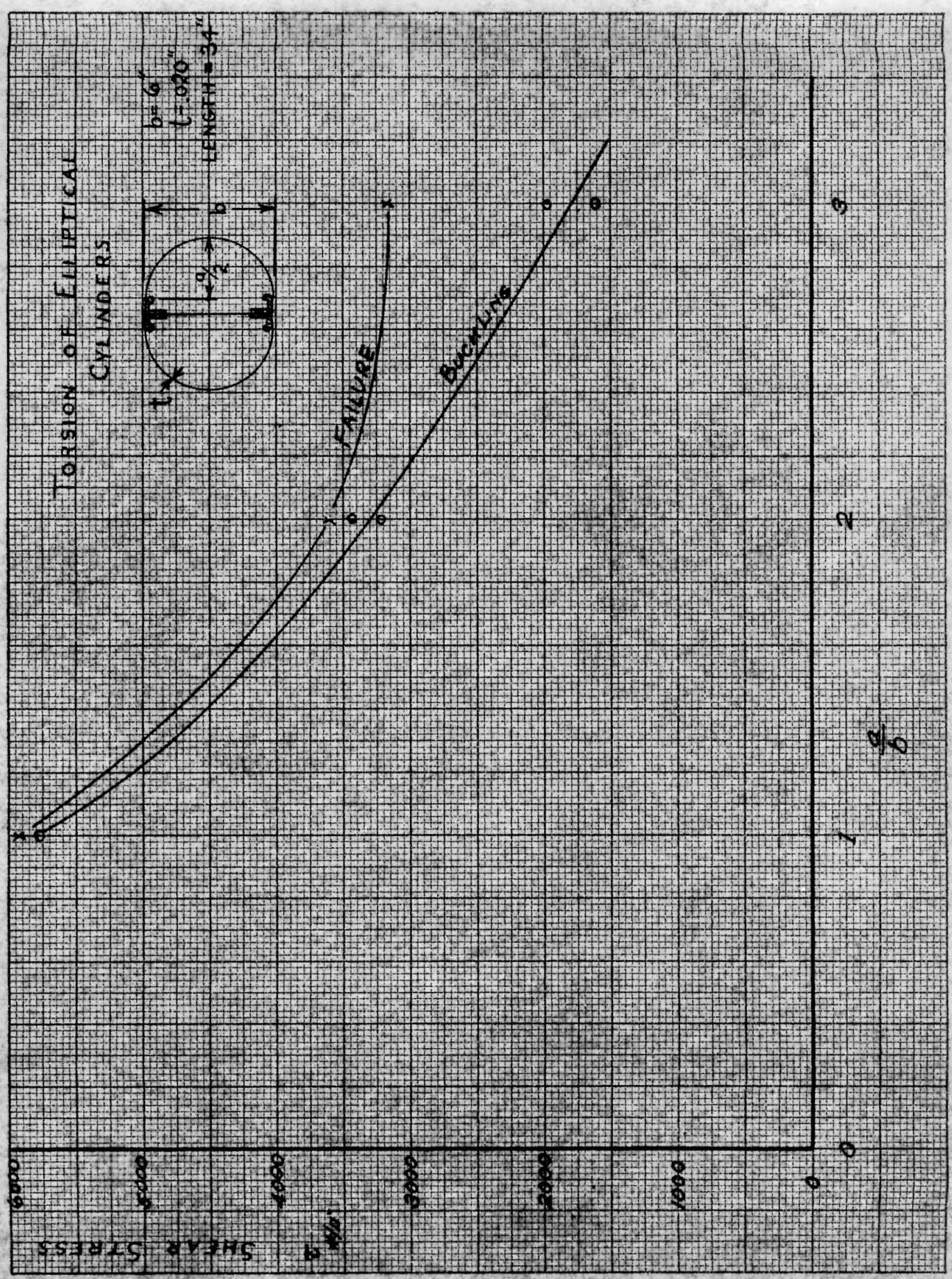
TORSION OF ELLIPTICAL CYLINDERS
b= 6"
t=.020"
LENGTH = 24"
a/2
b
t
FAILURE
BUCKLING
SHEAR STRESS
lbs/in²
6000
5000
4000
3000
2000
1000
0
0
1
2
3
a/b

FIG 46.

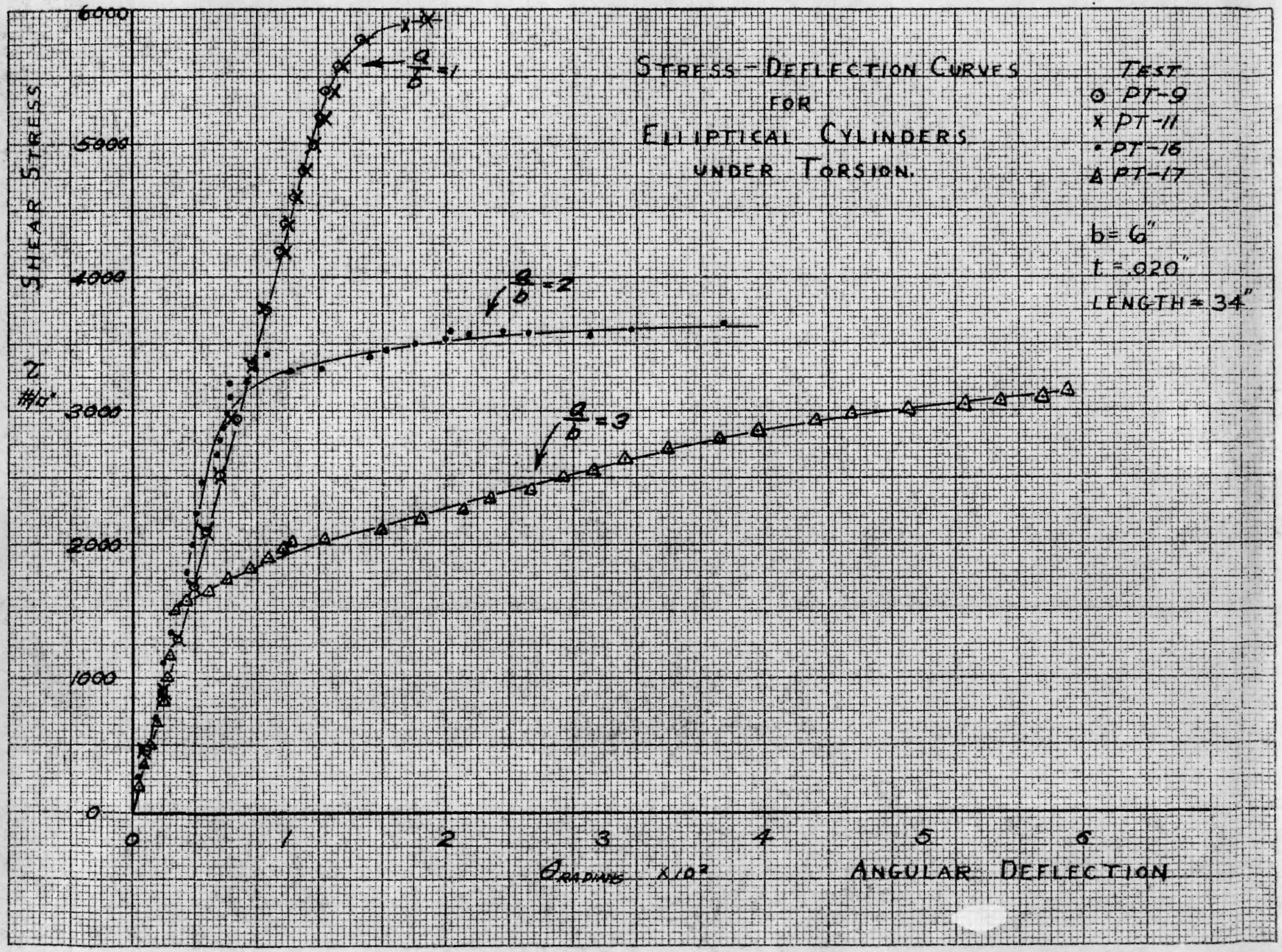
STRESS - DEFLECTION CURVES
FOR
ELLIPTICAL CYLINDERS
UNDER TORSION.
TEST
⊙ PT-9
X PT-11
• PT-16
Δ PT-17
b = 6"
t = .020"
LENGTH = 34"
a/b = 1
a/b = 2
a/b = 3
SHEAR STRESS
/ in²
6000
5000
4000
3000
2000
1000
0
0
1
2
3
4
5
6
θ RADIANS X 10²
ANGULAR DEFLECTION

FIG. 47.

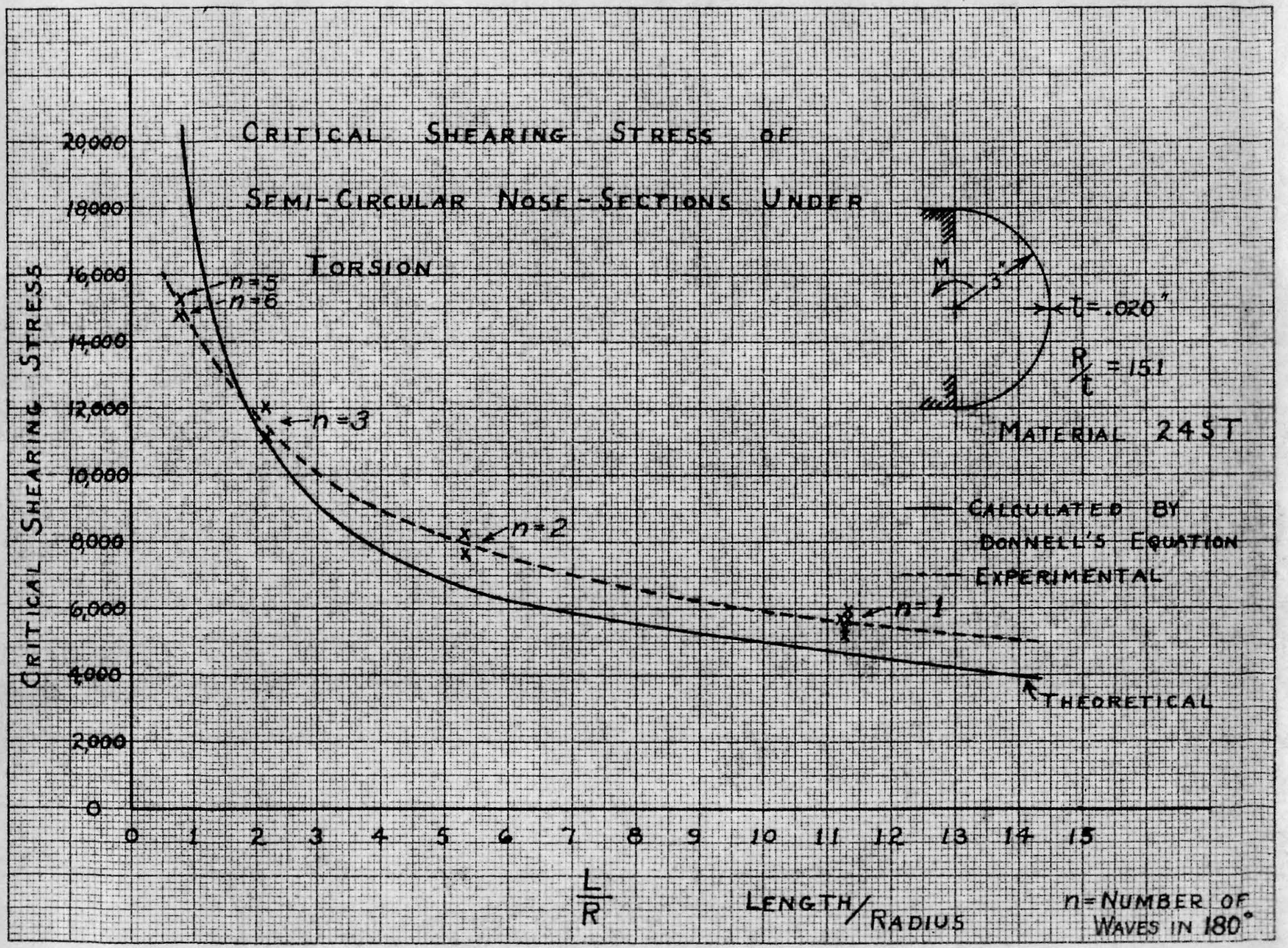
CRITICAL SHEARING STRESS OF
SEMI-CIRCULAR NOSE-SECTIONS UNDER
TORSION
CRITICAL SHEARING STRESS
20,000
18,000
16,000
14,000
12,000
10,000
8,000
6,000
4,000
2,000
0
n=5
n=6
n=3
n=2
n=1
M
3"
t=.020"
R/t = 151
MATERIAL 24ST
CALCULATED BY DONNELL'S EQUATION
EXPERIMENTAL
THEORETICAL
0 1 2 3 4 5 6 7 8 9 10 11 12 13 14 15
L/R
LENGTH/RADIUS
n=NUMBER OF WAVES IN 180°

FIG. 48.

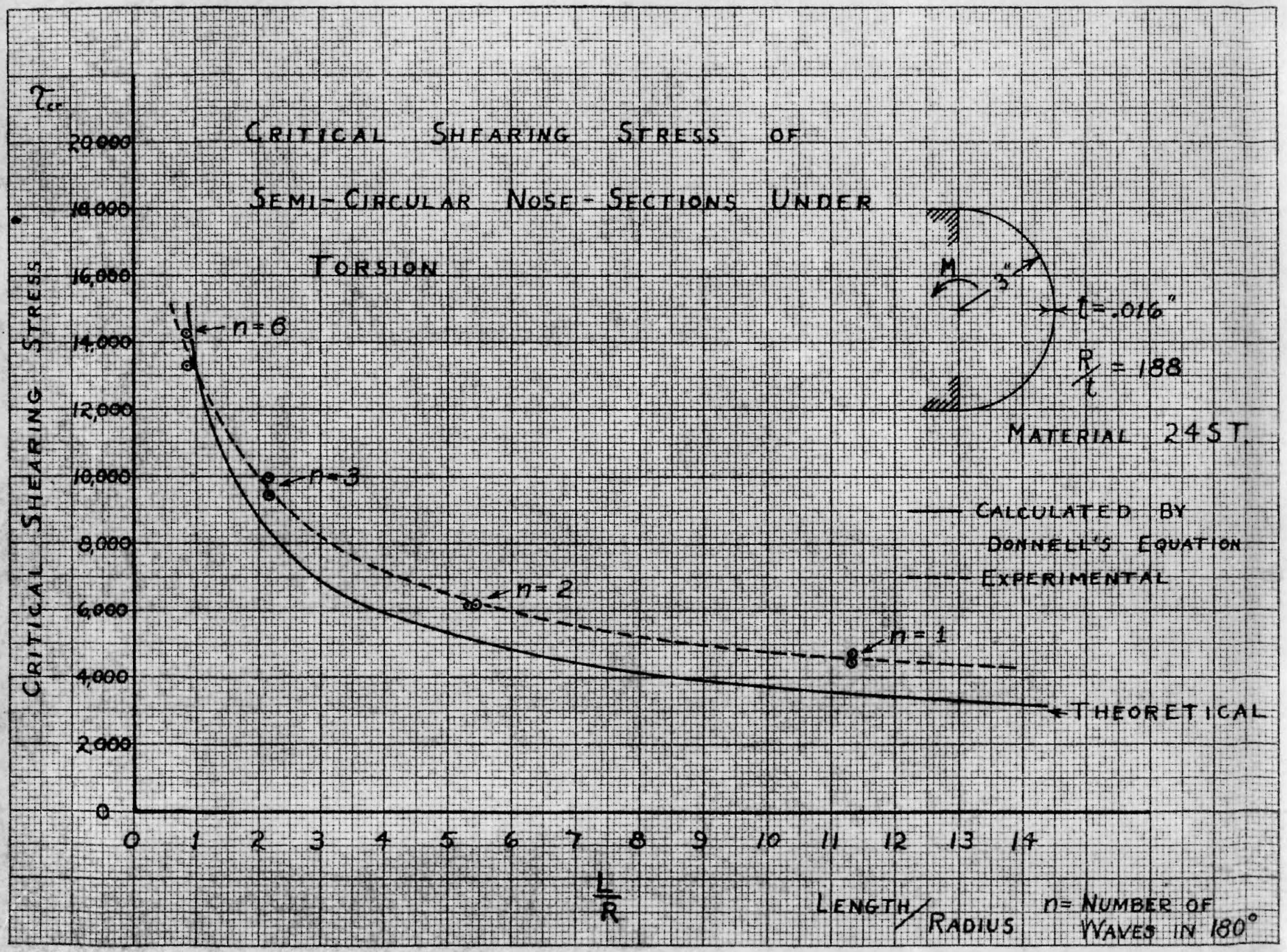
τ_{cr}
CRITICAL SHEARING STRESS OF
SEMI-CIRCULAR NOSE-SECTIONS UNDER
TORSION
CRITICAL SHEARING STRESS
20,000
18,000
16,000
14,000
12,000
10,000
8,000
6,000
4,000
2,000
0
n=6
n=3
n=2
n=1
M
3"
t=.016"
R/t = 188
MATERIAL 24 S.T.
CALCULATED BY DONNELL'S EQUATION
EXPERIMENTAL
THEORETICAL
0 1 2 3 4 5 6 7 8 9 10 11 12 13 14
L/R
LENGTH / RADIUS
n= NUMBER OF WAVES IN 180°

FIG. 49.

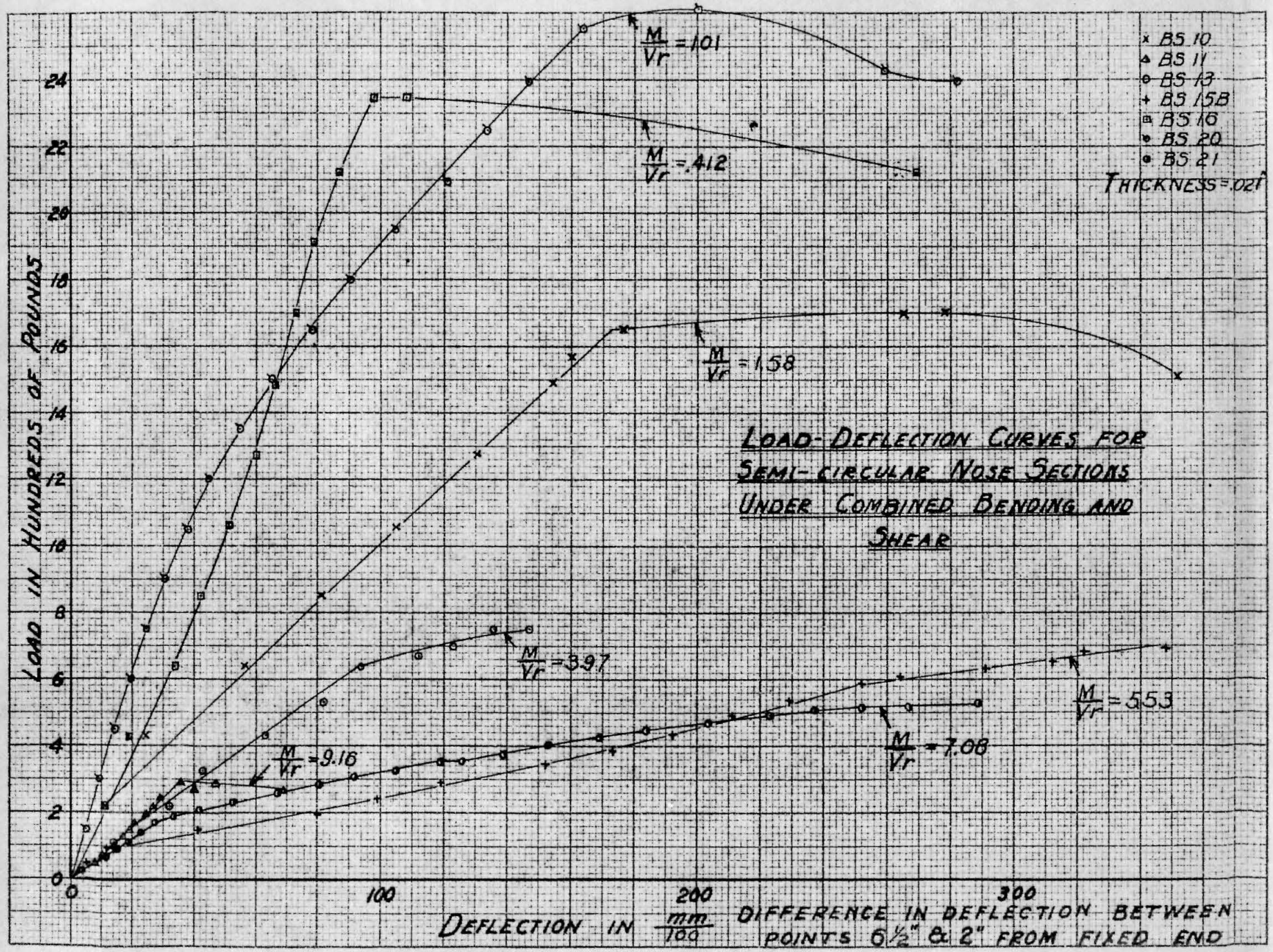
LOAD IN HUNDREDS OF POUNDS
0
2
4
6
8
10
12
14
16
18
20
22
24
0
100
200
300
DEFLECTION IN mm/100
DIFFERENCE IN DEFLECTION BETWEEN POINTS 6½" & 2" FROM FIXED END
M/Vr = 10.1
M/Vr = 4.12
M/Vr = 1.58
M/Vr = 3.97
M/Vr = 5.53
M/Vr = 9.16
M/Vr = 7.08
BS 10
BS 11
BS 13
BS 15B
BS 16
BS 20
BS 21
THICKNESS = .021"
LOAD-DEFLECTION CURVES FOR SEMI-CIRCULAR NOSE SECTIONS UNDER COMBINED BENDING AND SHEAR

Fig. 50.

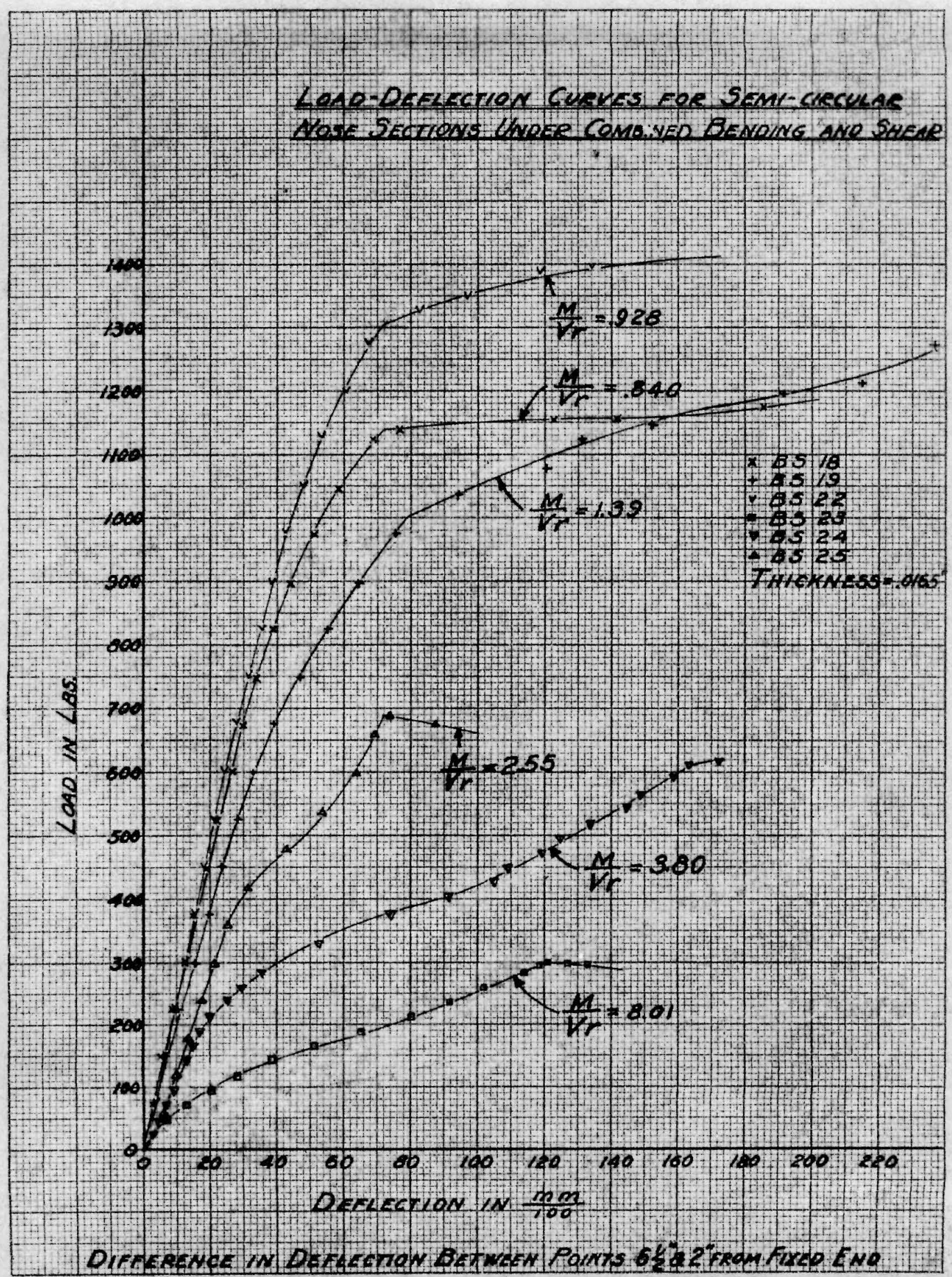
LOAD-DEFLECTION CURVES FOR SEMI-CIRCULAR NOSE SECTIONS UNDER COMBINED BENDING AND SHEAR
M/Vr = .928
M/Vr = .840
M/Vr = 1.39
M/Vr = 2.55
M/Vr = 3.80
M/Vr = 8.01
× B5 18
+ B5 19
▾ B5 22
■ B5 23
▼ B5 24
▲ B5 25
THICKNESS = .0165"
LOAD IN LBS.
0
100
200
300
400
500
600
700
800
900
1000
1100
1200
1300
1400
0
20
40
60
80
100
120
140
160
180
200
220
DEFLECTION IN mm/100
DIFFERENCE IN DEFLECTION BETWEEN POINTS 6½" & 2" FROM FIXED END

FIG. 51.

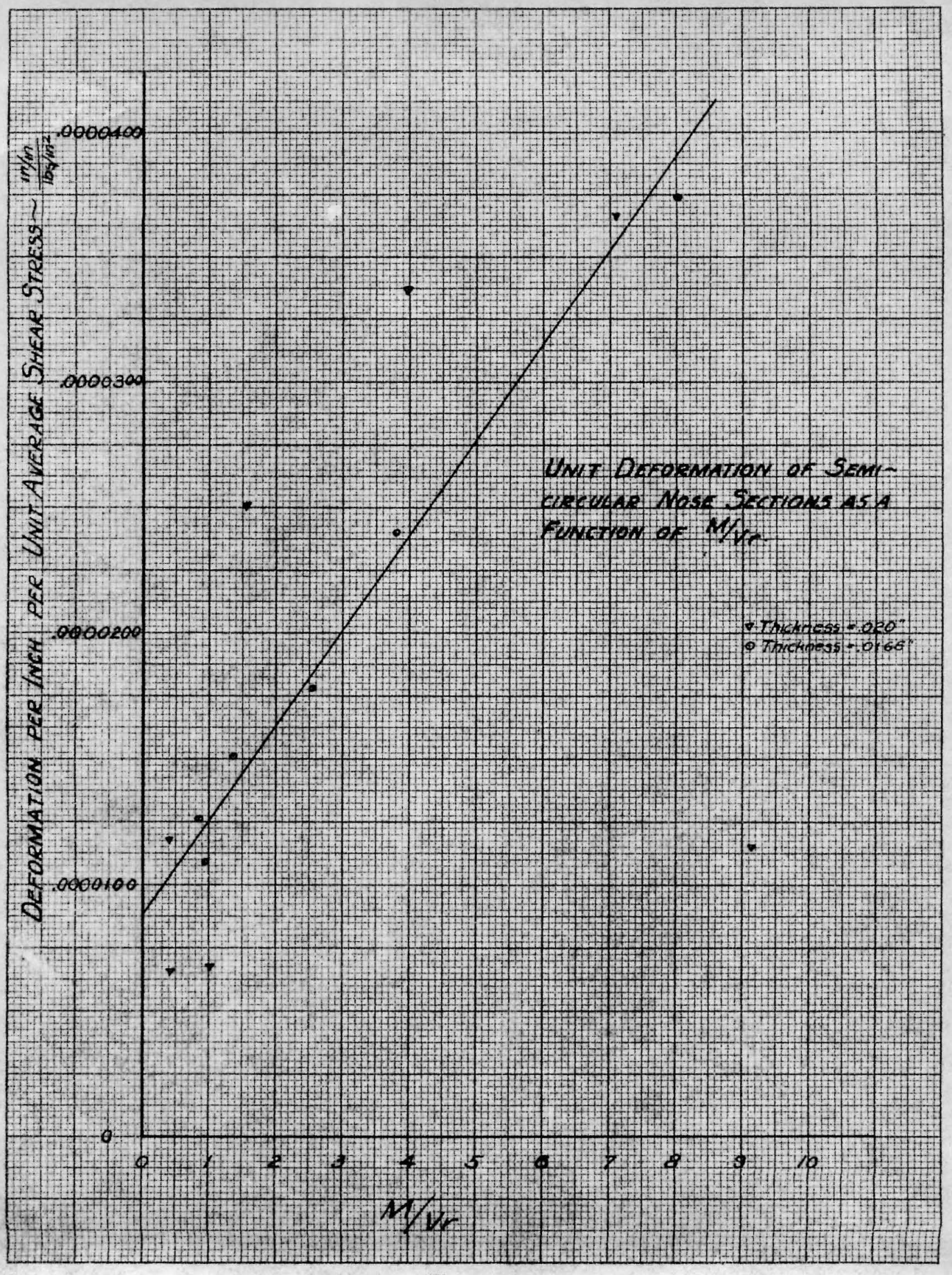
DEFORMATION PER INCH PER UNIT AVERAGE SHEAR STRESS ~ in/in / lbs/in²
.0000400
.0000300
.0000200
.0000100
0
0
1
2
3
4
5
6
7
8
9
10
M/Vr
UNIT DEFORMATION OF SEMI-CIRCULAR NOSE SECTIONS AS A FUNCTION OF M/Vr.
▼ Thickness = .020"
⊙ Thickness = .0166"

FIG. 52.

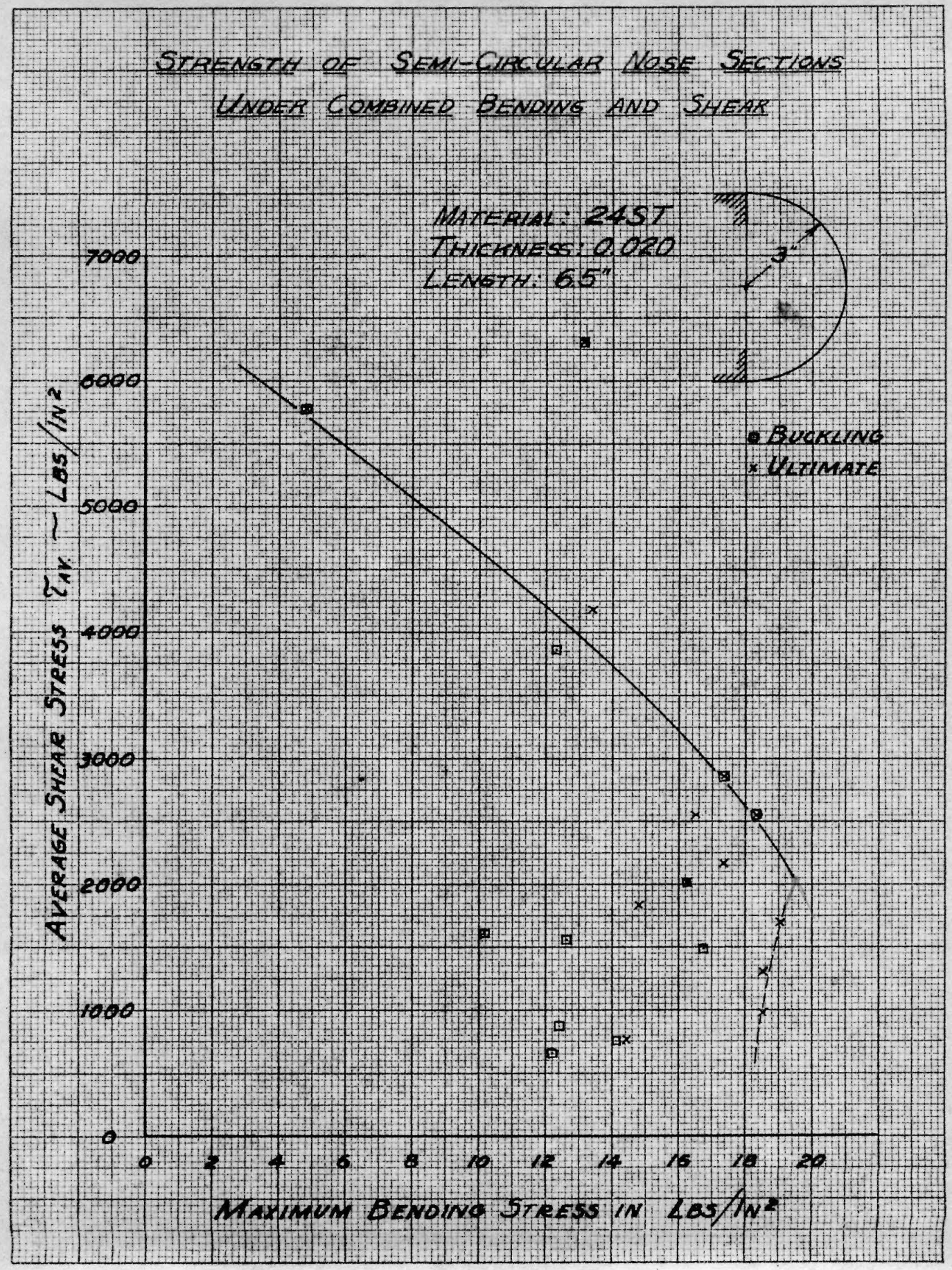
STRENGTH OF SEMI-CIRCULAR NOSE SECTIONS
UNDER COMBINED BENDING AND SHEAR
MATERIAL: 24ST
THICKNESS: 0.020
LENGTH: 6.5"
3"
BUCKLING
ULTIMATE
AVERAGE SHEAR STRESS $\tau_{AV.}$ — LBS/IN²
7000
6000
5000
4000
3000
2000
1000
0
0
2
4
6
8
10
12
14
16
18
20
MAXIMUM BENDING STRESS IN LBS/IN²

FIG. 53.

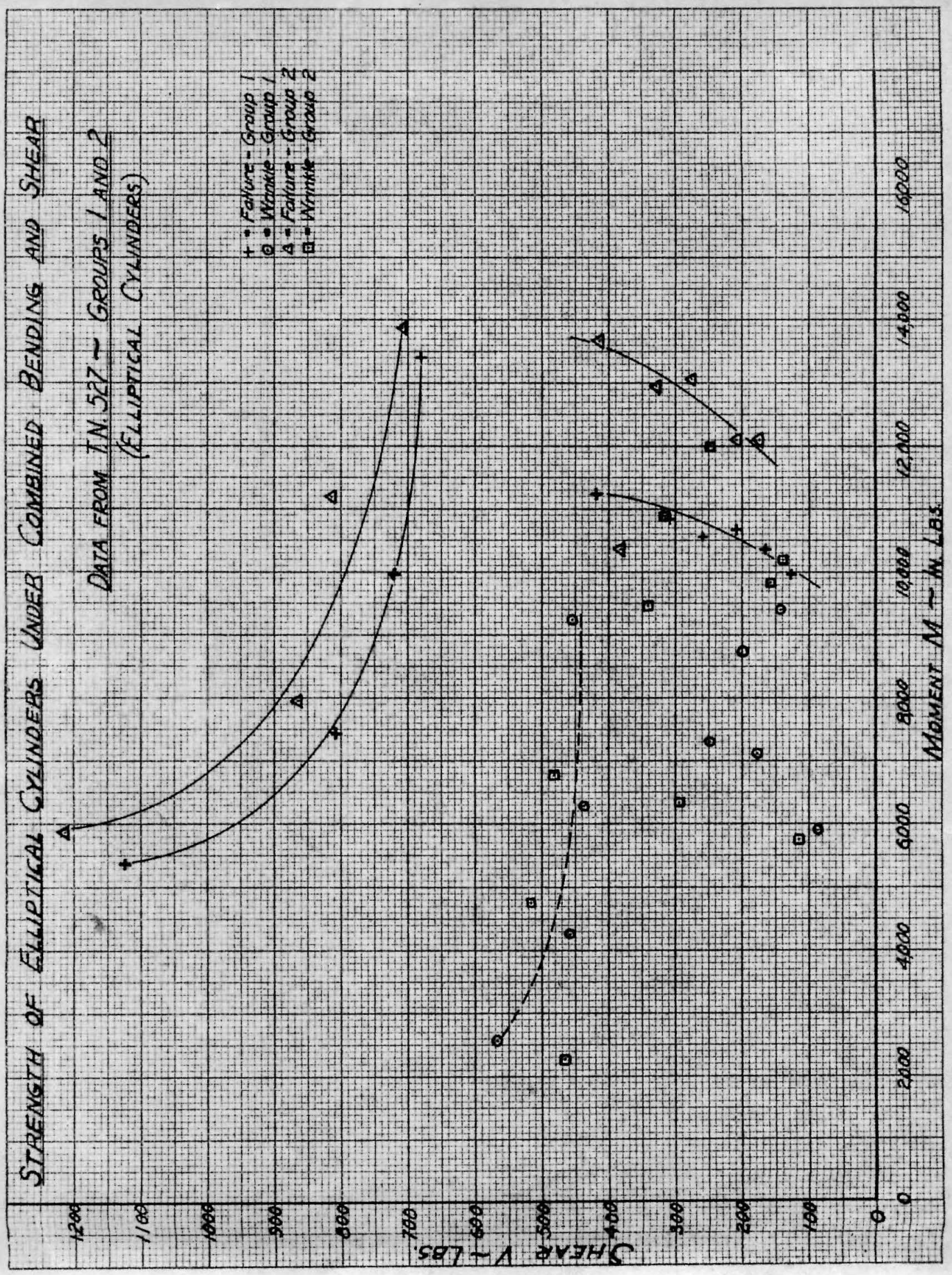
STRENGTH OF ELLIPTICAL CYLINDERS UNDER COMBINED BENDING AND SHEAR
DATA FROM T.N. 527 – GROUPS 1 AND 2
(ELLIPTICAL CYLINDERS)
+ = Failure - Group 1
⊙ = Wrinkle - Group 1
Δ = Failure - Group 2
□ = Wrinkle - Group 2
SHEAR V – LBS.
MOMENT M – IN. LBS.
0
100
200
300
400
500
600
700
800
900
1000
1100
1200
2000
4000
6000
8000
10000
12000
14000
16000

FIG 54

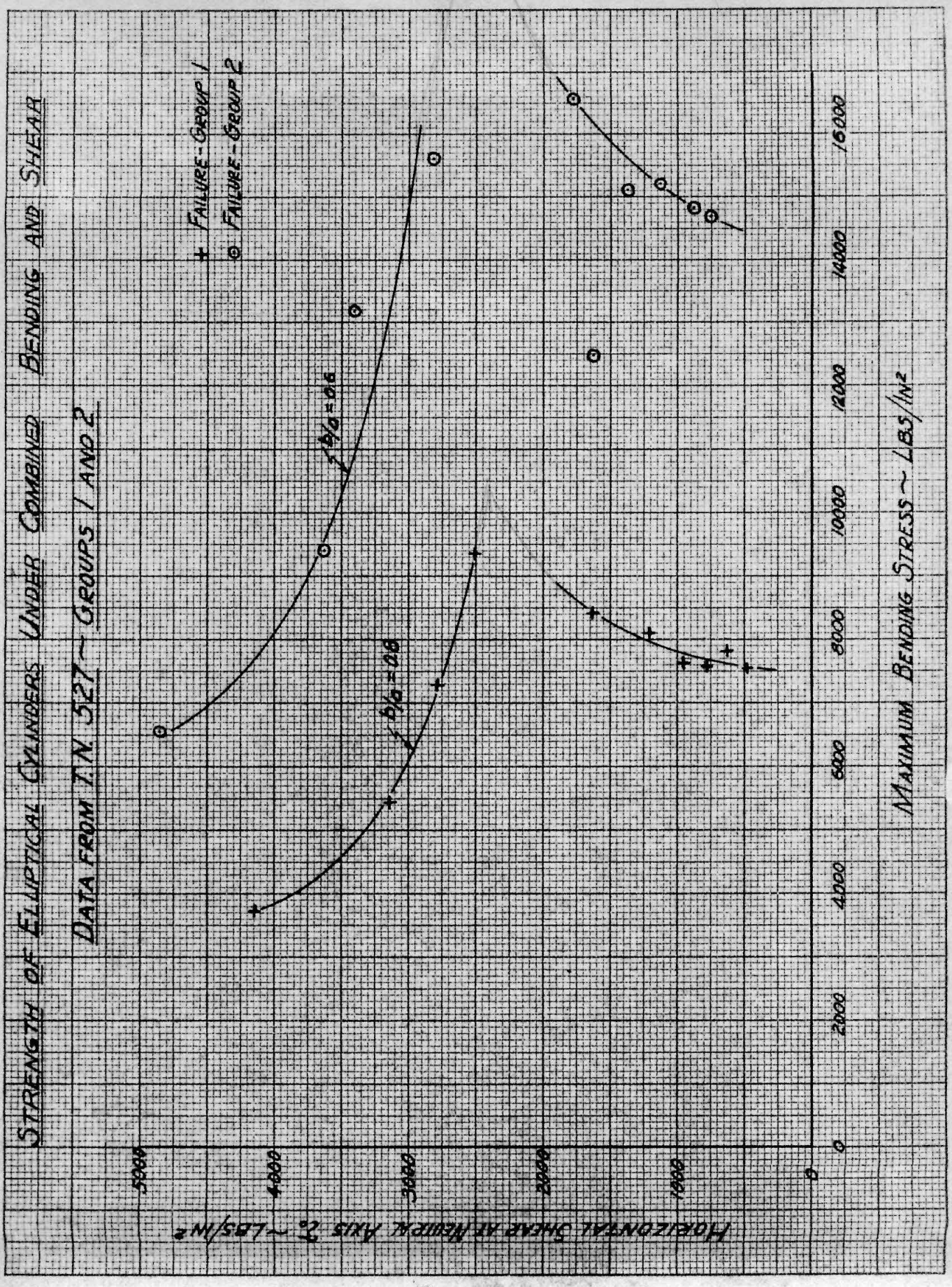
STRENGTH OF ELLIPTICAL CYLINDERS UNDER COMBINED BENDING AND SHEAR
DATA FROM T.N. 527 - GROUPS 1 AND 2
+ FAILURE - GROUP 1
⊙ FAILURE - GROUP 2
b/a = 0.6
b/a = 0.8
HORIZONTAL SHEAR AT MEDIUM AXIS S - LBS/IN²
MAXIMUM BENDING STRESS - LBS/IN²
5000
4000
3000
2000
1000
0
2000
4000
6000
8000
10000
12000
14000
16000

FIG. 55.

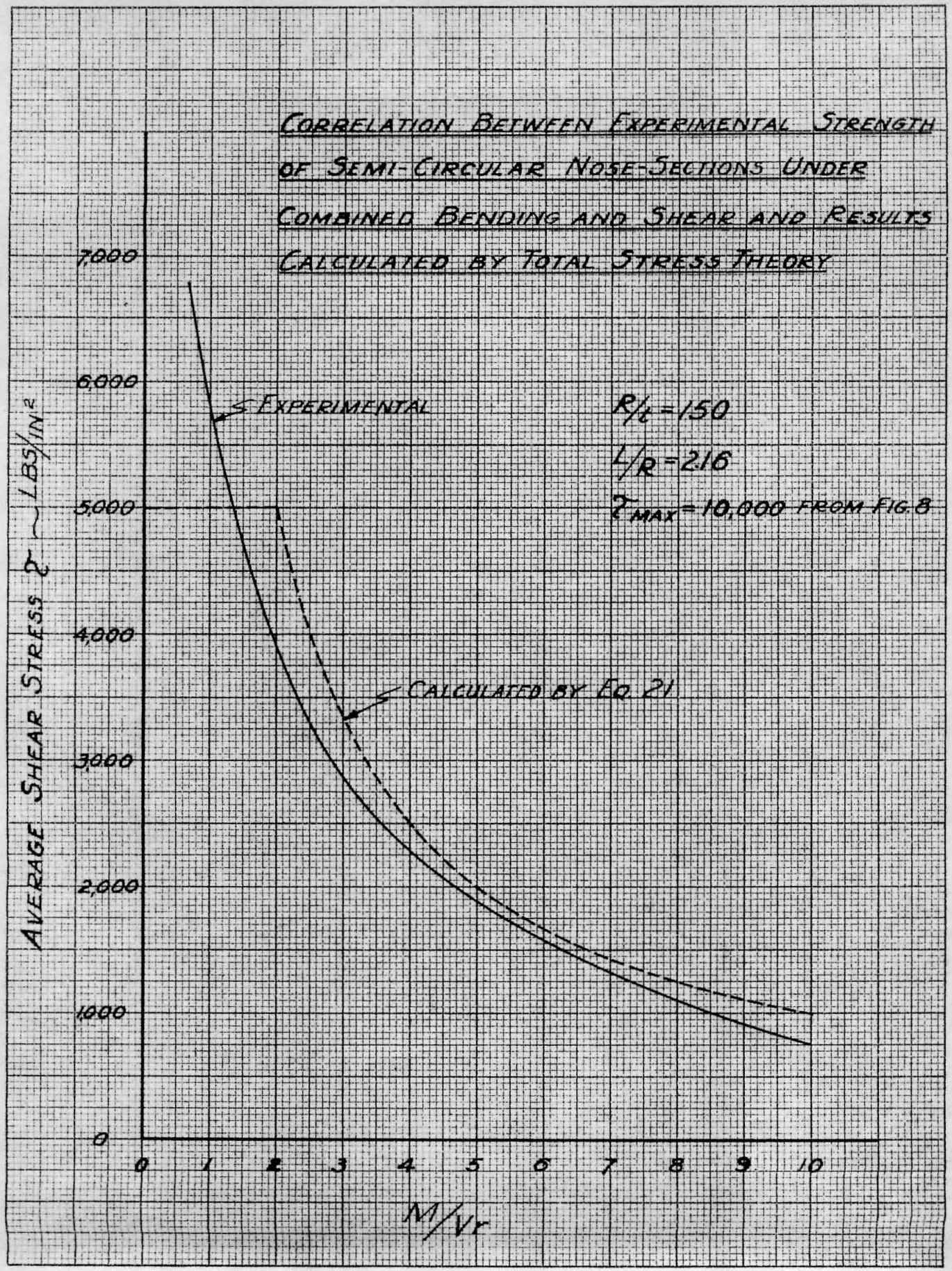
CORRELATION BETWEEN EXPERIMENTAL STRENGTH OF SEMI-CIRCULAR NOSE-SECTIONS UNDER COMBINED BENDING AND SHEAR AND RESULTS CALCULATED BY TOTAL STRESS THEORY
AVERAGE SHEAR STRESS τ ~ LBS/IN.²
7,000
6,000
5,000
4,000
3,000
2,000
1,000
0
EXPERIMENTAL
CALCULATED BY EQ. 21
R/t = 150
L/R = 2.16
τ MAX = 10,000 FROM FIG. 8
0
1
2
3
4
5
6
7
8
9
10
M/Vr

FIG. 56

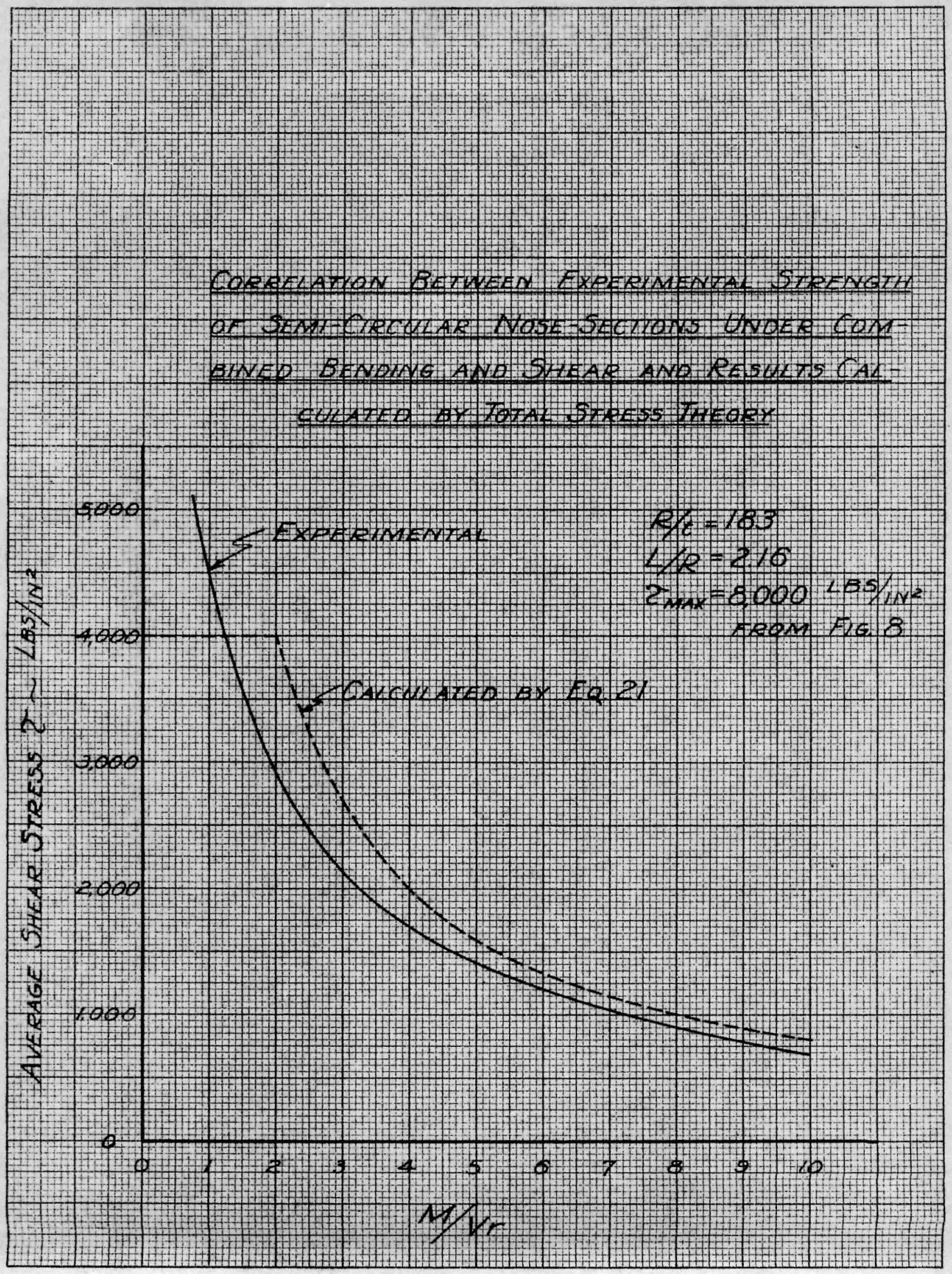
CORRELATION BETWEEN EXPERIMENTAL STRENGTH OF SEMI-CIRCULAR NOSE-SECTIONS UNDER COMBINED BENDING AND SHEAR AND RESULTS CALCULATED BY TOTAL STRESS THEORY
AVERAGE SHEAR STRESS τ ~ LBS/IN²
5,000
4,000
3,000
2,000
1,000
0
EXPERIMENTAL
CALCULATED BY EQ. 21
R/t = 183
L/R = 2.16
τ MAX = 8,000 LBS/IN² FROM FIG. 8
0 1 2 3 4 5 6 7 8 9 10
M/Vr

FIG 57

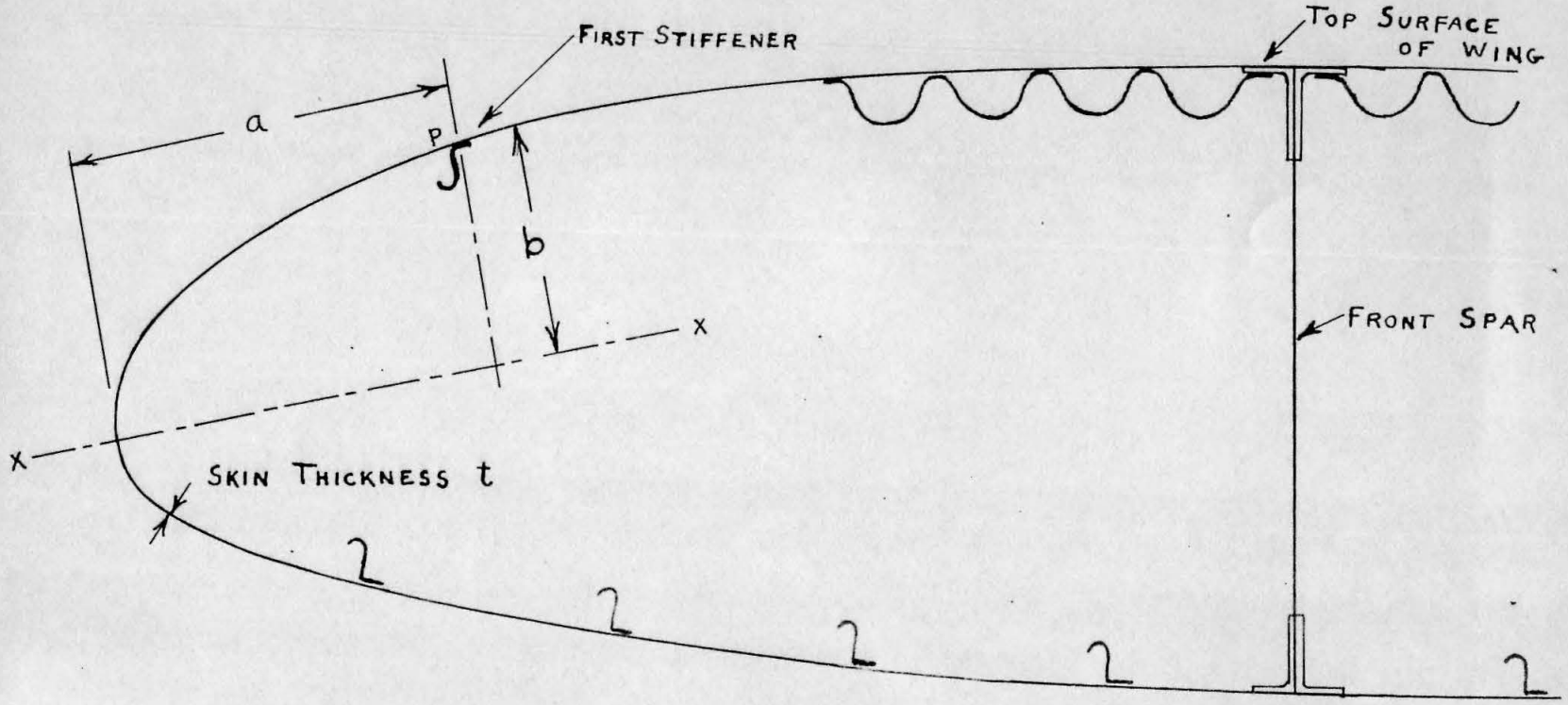

Fig. 58. Method of Determining the Amount of Ellipticity on Stiffened Wing Nose Sections

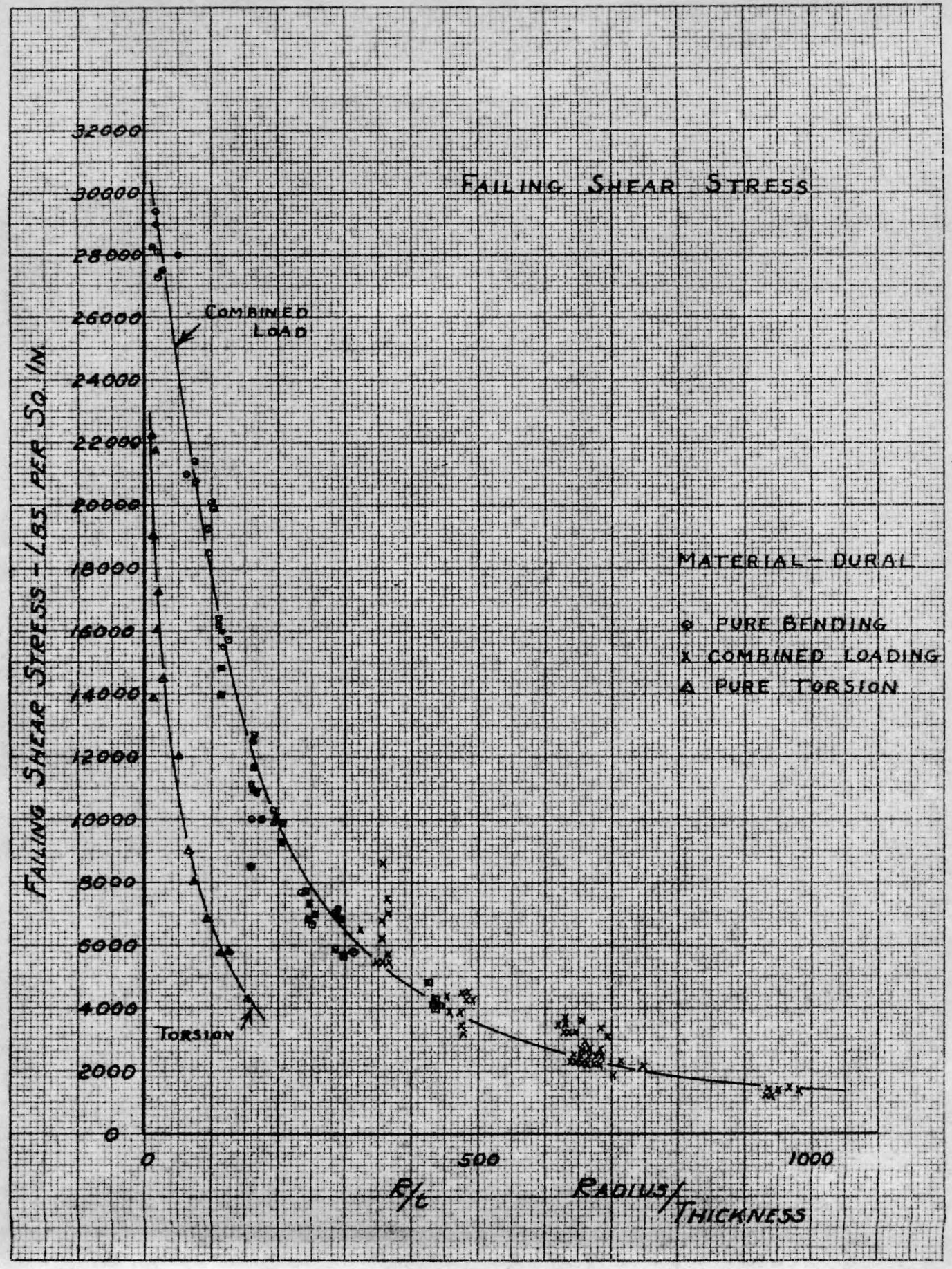
FAILING SHEAR STRESS
COMBINED LOAD
TORSION
MATERIAL – DURAL
⊙ PURE BENDING
x COMBINED LOADING
Δ PURE TORSION
FAILING SHEAR STRESS - LBS PER SQ. IN
32000
30000
28000
26000
24000
22000
20000
18000
16000
14000
12000
10000
8000
6000
4000
2000
0
0
500
1000
R/t
RADIUS/THICKNESS

FIG 59

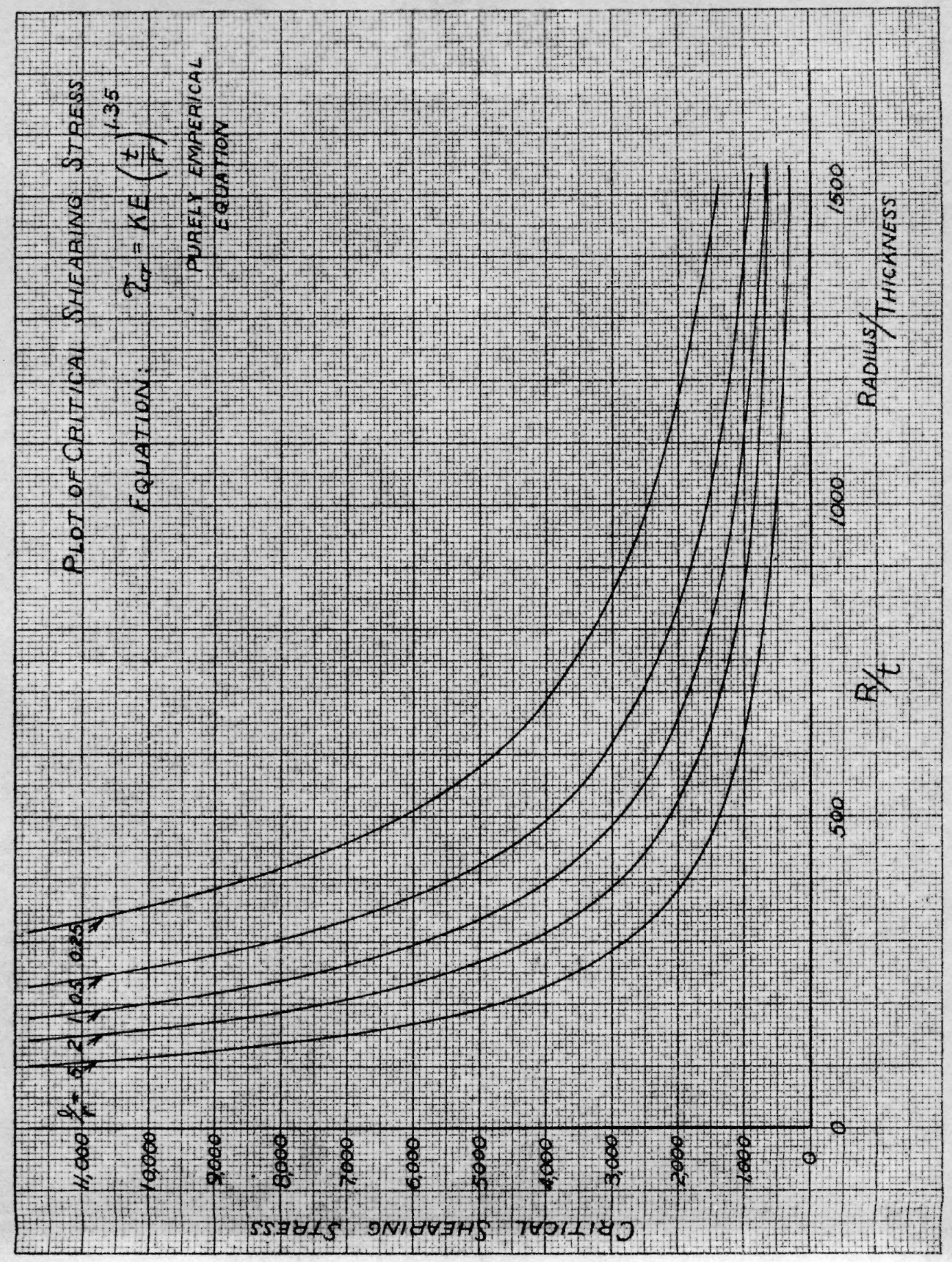
PLOT OF CRITICAL SHEARING STRESS
EQUATION: $\tau_{cr} = KE\left(\frac{t}{r}\right)^{1.35}$
PURELY EMPERICAL EQUATION
CRITICAL SHEARING STRESS
RADIUS/THICKNESS
R/t
0
500
1000
1500
1,000
2000
3,000
4000
5000
6,000
7000
8,000
9000
10,000
11,000
h/r = 0.2 0.15 0.25

FIG. 60.

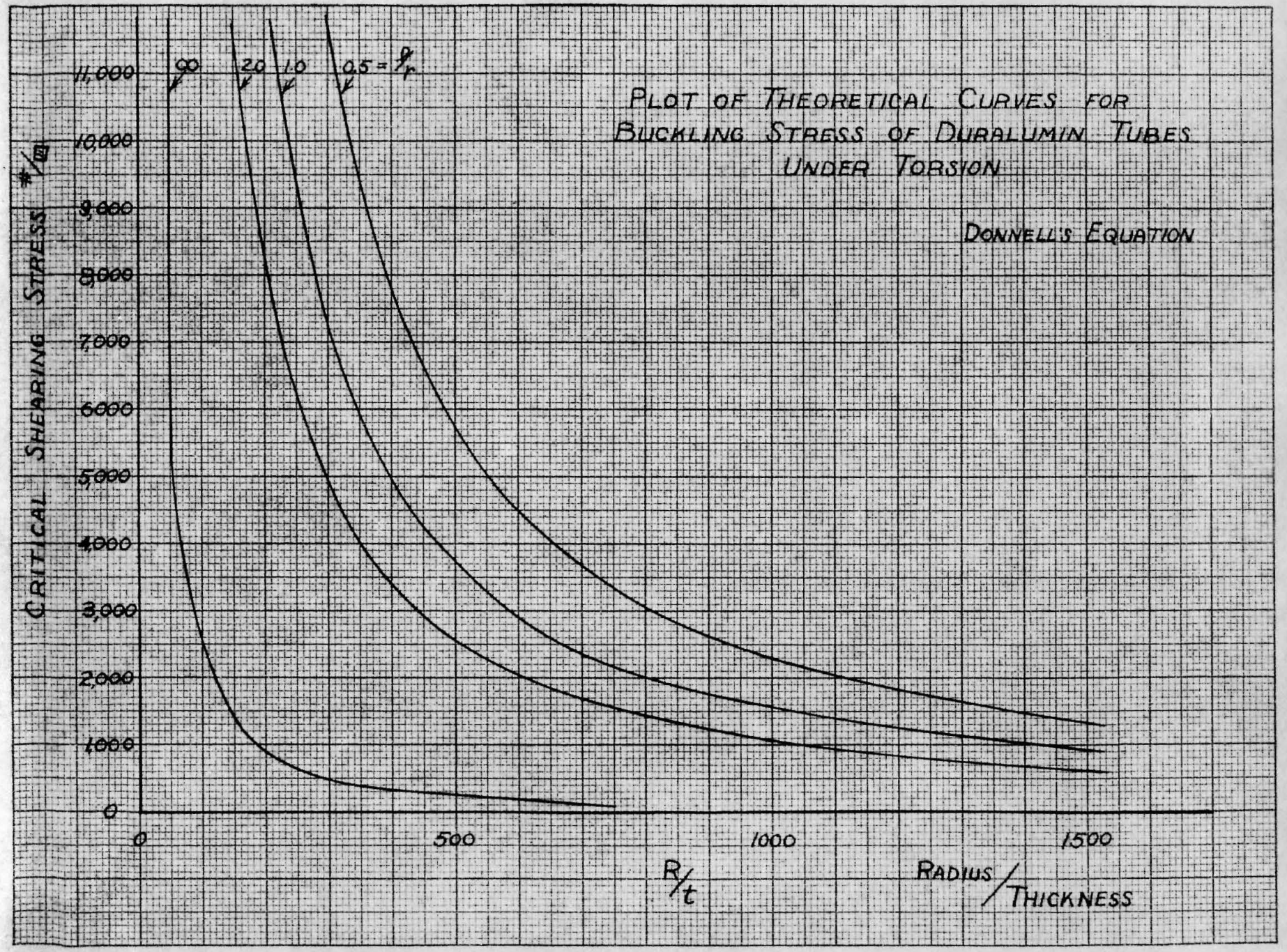
PLOT OF THEORETICAL CURVES FOR
BUCKLING STRESS OF DURALUMIN TUBES
UNDER TORSION
DONNELL'S EQUATION
CRITICAL SHEARING STRESS #/□
11,000
10,000
9,000
8,000
7,000
6000
5,000
4,000
3,000
2,000
1,000
0
∞
2.0
1.0
0.5 = l/r
0
500
1000
1500
R/t
RADIUS / THICKNESS

FIG 61.

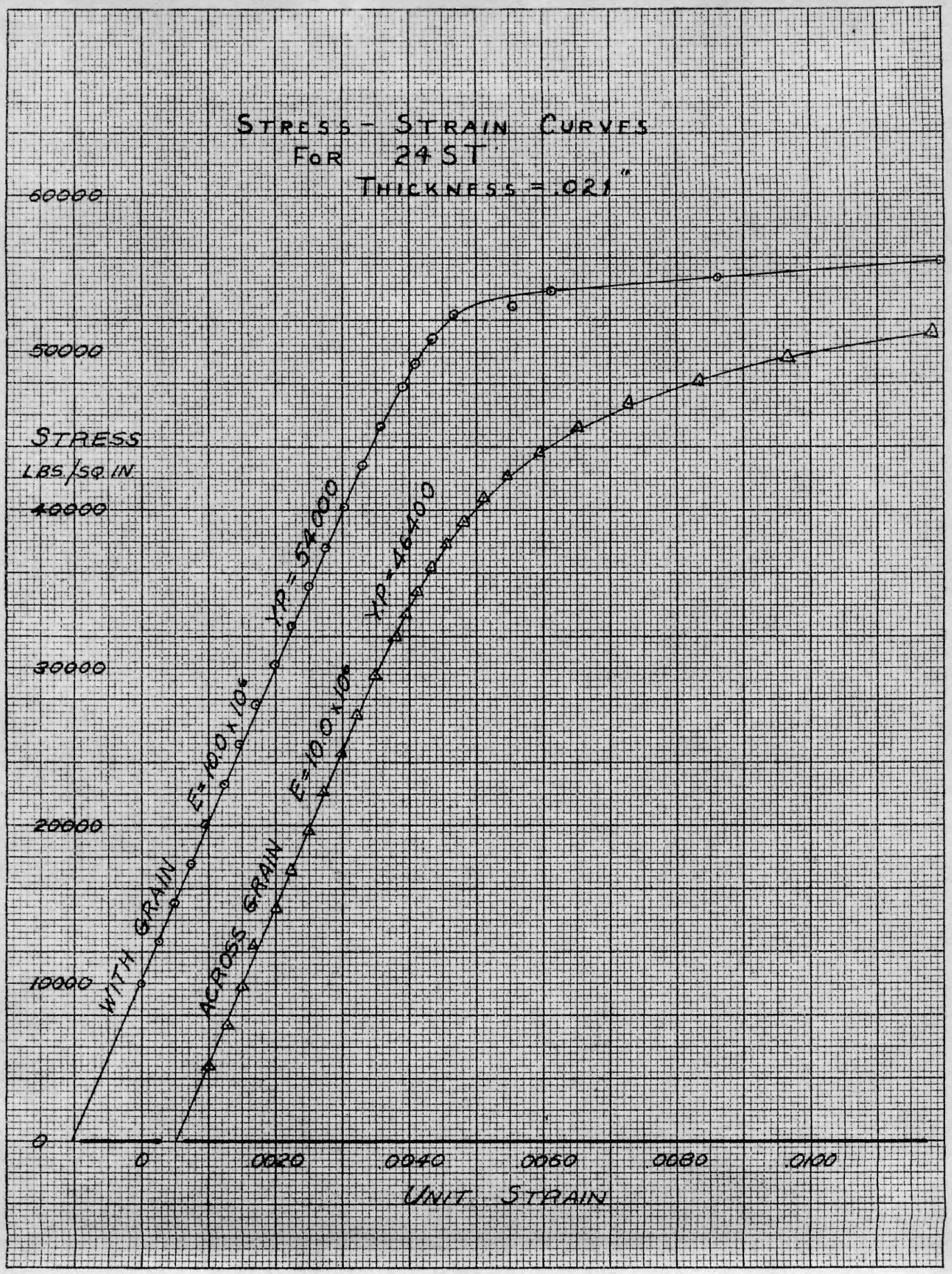
STRESS - STRAIN CURVES
FOR 24 ST
THICKNESS = .021"
60000
50000
40000
30000
20000
10000
0
STRESS
LBS/SQ IN
0
.0020
.0040
.0060
.0080
.0100
UNIT STRAIN
WITH GRAIN
ACROSS GRAIN
E = 10.0 x 10⁶
E = 10.0 x 10⁶
YP = 54000
YP = 46400

FIG 62

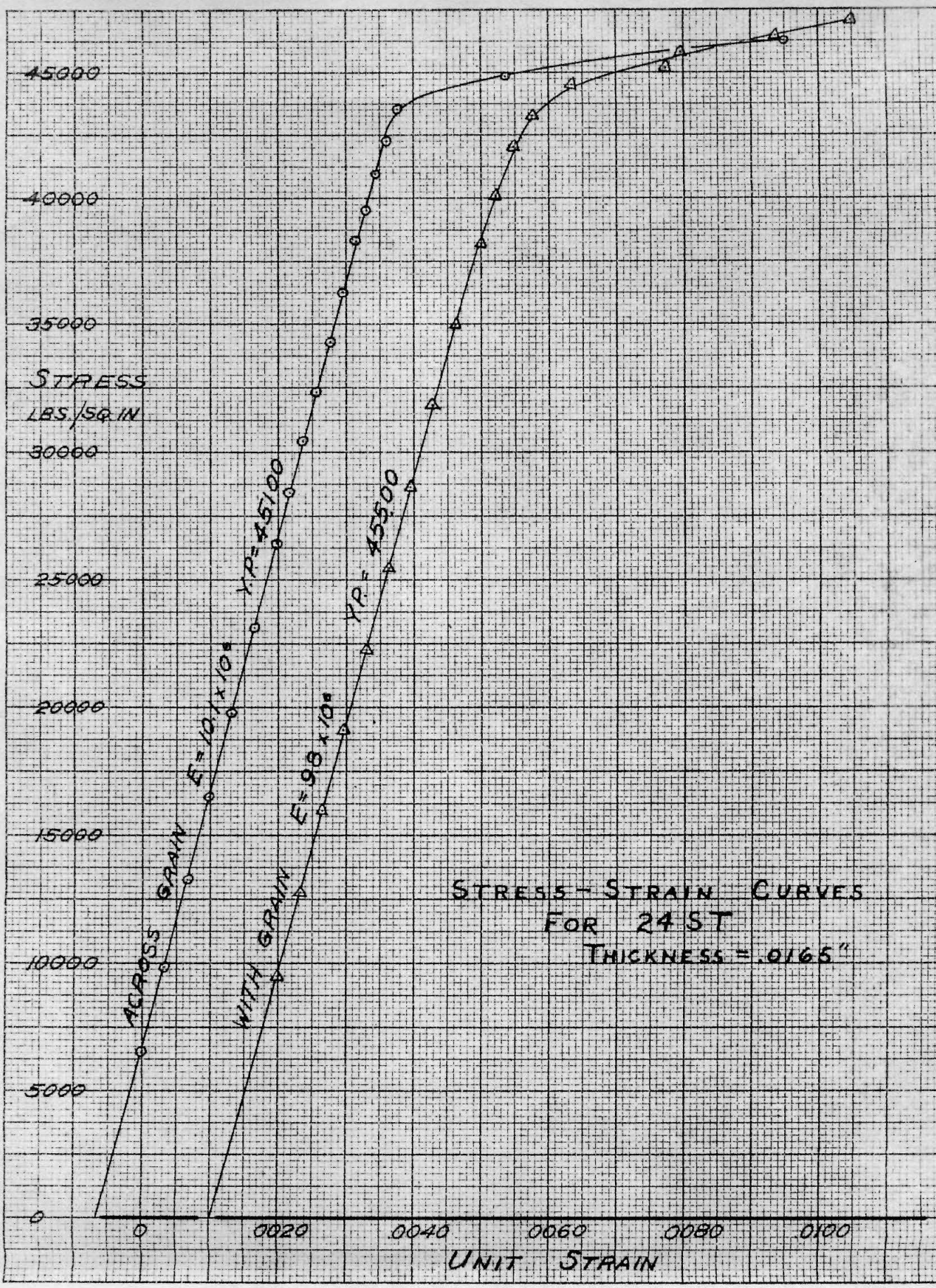
45000
40000
35000
STRESS
LBS./SQ.IN
30000
25000
20000
15000
10000
5000
0
0
.0020
.0040
.0060
.0080
.0100
UNIT STRAIN
ACROSS GRAIN
E = 10.1 x 10⁶
Y.P. = 45100
WITH GRAIN
E = 9.8 x 10⁶
Y.P. = 45500
STRESS - STRAIN CURVES
FOR 24 ST
THICKNESS = .0165"

FIG. 63.

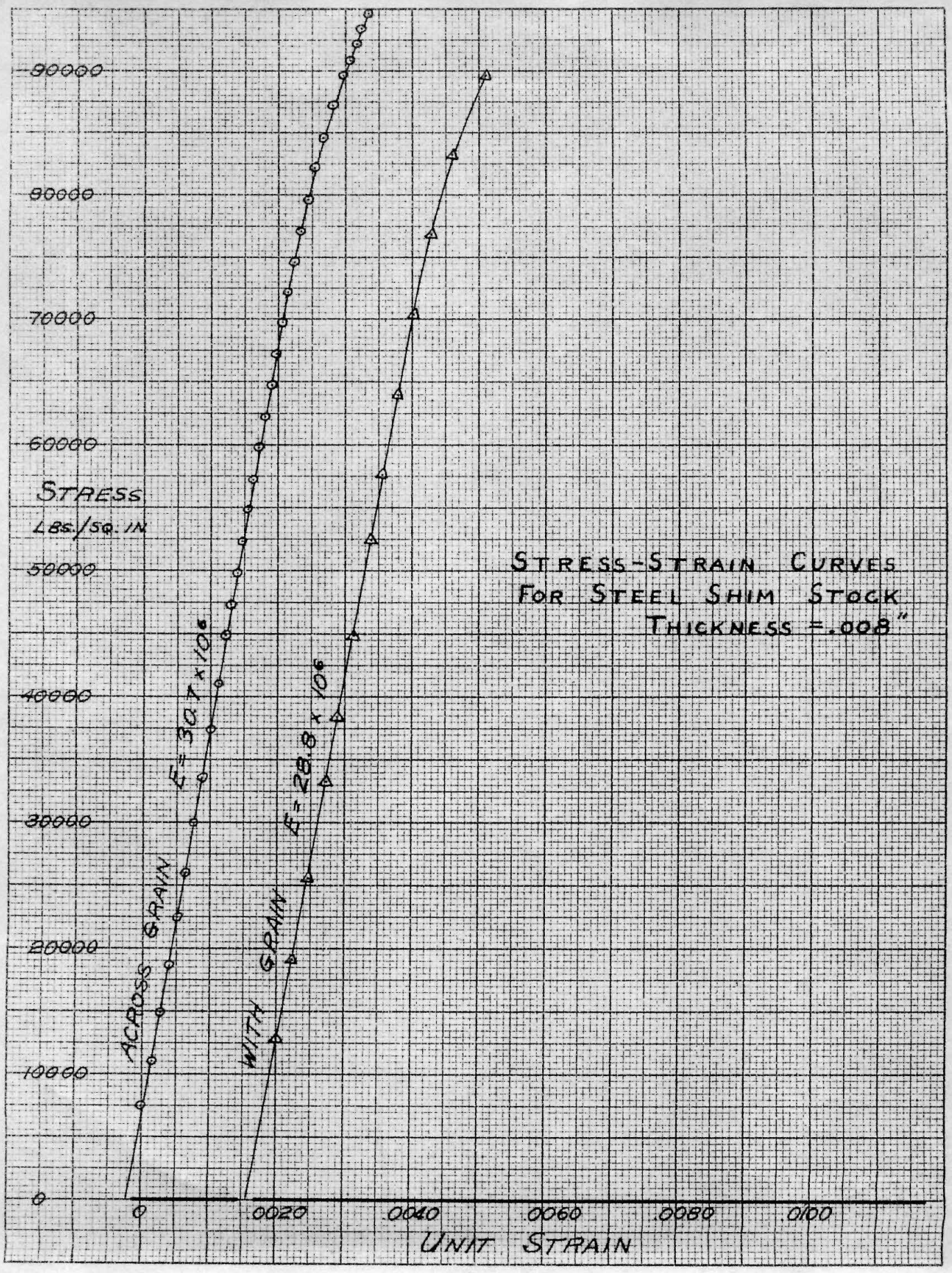
90000
80000
70000
60000
STRESS
LBS./SQ. IN
50000
40000
30000
20000
10000
0
0
.0020
.0040
.0060
.0080
.0100
UNIT STRAIN
STRESS-STRAIN CURVES
FOR STEEL SHIM STOCK
THICKNESS =.008"
E = 30.7 x 10⁶
ACROSS GRAIN
E = 28.8 x 10⁶
WITH GRAIN

FIG 64